CHALMERS

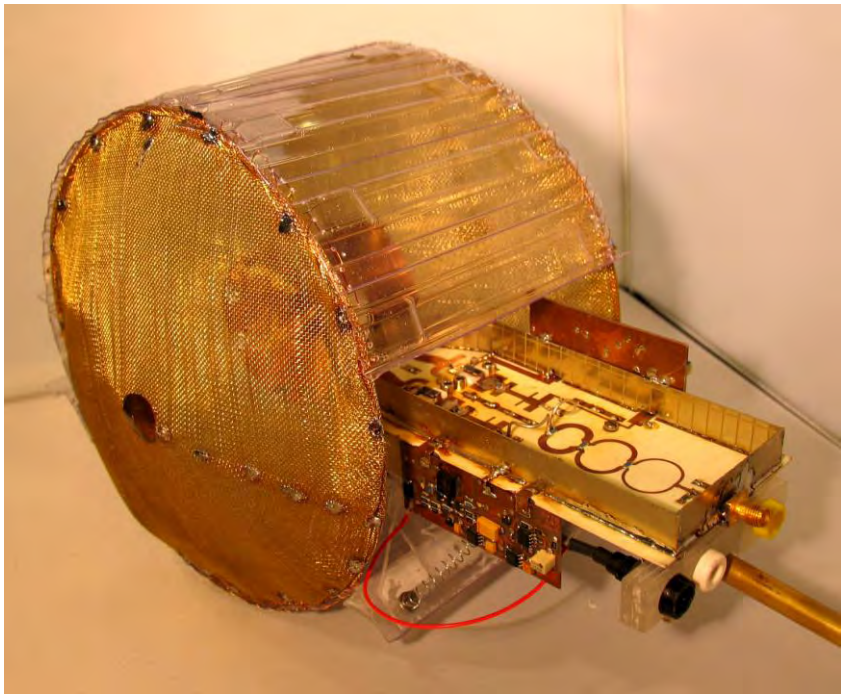

Co-Design and Integration of Wideband Push-Pull Power Amplifier and Omnidirectional Antenna

Master's thesis in Wireless, Photonics and Space Engineering

VIKTOR HALLMAN
ERIK SANFORD

Saab AB
Electronic Defence Systems
Department of Microwave, Antennas, and Laser
Gothenburg, Sweden, 2013

MASTER'S THESIS IN WIRELESS, PHOTONICS AND SPACE ENGINEERING

Co-Design and Integration of Wideband Push-Pull Power Amplifier and Omnidirectional Antenna

VIKTOR HALLMAN
ERIK SANFORD

Saab AB

Electronic Defence Systems

Department of Microwave, Antennas, and Laser

Gothenburg, Sweden, 2013

Co-Design and Integration of Wideband Push-Pull Power Amplifier and Omnidirectional Antenna

VIKTOR HALLMAN, ERIK SANFORD

Master's thesis
Saab AB
Electronic Defence Systems
Department of Microwave, Antennas and Laser
SE-412 89 Göteborg
Sweden
Telephone: +46 (0)31 794 90 00

Cover:
Complete antenna-amplifier system

Saab AB Linköping
Repro Center
Sweden 2013

Date 2013-06-18 | Issue A | Document ID 87/03631-1/FCK11507

Issued by
OEGPU Viktor Hallman, Erik Sanford

Classification Company Confidentially
COMPANY UNCLASSIFIED
Classification Export Control
NOT EXPORT CONTROLLED
Classification Defence Secrecy
ÖPPEN/UNCLASSIFIED

MASTER'S THESIS PROJECT

Co-Design and Integration of Wideband Push-Pull Power Amplifier and Omnidirectional Antenna

Viktor Hallman Erik Sanford

2013-06-18

Authorisation

Approved by	Date
OEGPUB (Ingvar Sundvall)	2013-06-27

Date 2013-06-18 | Issue A | Document ID 87/03631-1/FCK11507

Issued by
OEGPU Viktor Hallman, Erik Sanford

Classification Company Confidentially
COMPANY UNCLASSIFIED
Classification Export Control
NOT EXPORT CONTROLLED
Classification Defence Secrecy
ÖPPEN/UNCLASSIFIED

Abstract

A novel technique to co-design a push-pull power amplifier and a wideband omnidirectional antenna has been investigated. The goal was to cover the frequency range from 750 MHz to 3 GHz. A biconical antenna has been simulated in Ansys HFSS and the resulting parameters were exported to AWR Microwave Office, where the remaining part of the co-design was performed. The complete design resulted in simulated values of a total gain of 11 ± 1 dB and a PAE of 35% and a maximum output power of 47 dBm. The main focus of the project was to overcome the problems entailed with abandoning the standardised interface. Leaving to common interface required new, non-standardised, methods to conduct simulations.

Keywords: Integrated antenna, Push-pull, Wideband, Power amplifier, Omnidirectional, Biconical antenna

Date 2013-06-18 | Issue A | Document ID 87/03631-1/FCK11507

Issued by
OEGPU Viktor Hallman, Erik Sanford

Classification Company Confidentially
COMPANY UNCLASSIFIED
Classification Export Control
NOT EXPORT CONTROLLED
Classification Defence Secrecy
ÖPPEN/UNCLASSIFIED

Preface and Acknowledgements

This Master's thesis project has been carried out at Saab Electronic Defence Systems in Lackarebäck and Kallebäck, Gothenburg, during the first half of the year of 2013. It is the finalising part of our studies at the Master's Programme of *Wireless, Photonics and Space Engineering* and the Bachelor's Programme of *Engineering Physics* at Chalmers University of Technology.

First of all we would like to thank our supervisors during this project, Anders Bernland and Hannes Illipe. Hannes for his extensive input concerning the amplifier design and aid in all realisations of our simulations. Anders for his invaluable help with the antenna simulations and sharp eyes reviewing this report. We would also like to thank Per Aulin for showing great interest in our work and for supplying us with means to proceed with our undertakings. We would like to show our deepest gratitude to Lars Lygnebrandt and Hans Nordgren at the anechoic chamber for making the antenna measurements a reality despite a tight schedule. Our thanks goes also to Christian Fager at MC2, Chalmers, for his input and point of view along the course of the project. Finally we would like to thank Lovisa Björklund and Ingvar Sundvall, Managers at Saab EDS, for making it possible for us to conduct this Master's thesis project at their departments.

Gothenburg, 2013-06-10
Viktor Hallman and Erik Sanford

Date 2013-06-18 | Issue A | Document ID 87/03631-1/FCK11507
Issued by
OEGPU Viktor Hallman, Erik Sanford
Classification Company Confidentially
COMPANY UNCLASSIFIED
Classification Export Control
NOT EXPORT CONTROLLED
Classification Defence Secrecy
ÖPPEN/UNCLASSIFIED

Contents

Date 2013-06-18 | Issue A | Document ID 87/03631-1/FCK11507
Issued by
OEGPU Viktor Hallman, Erik Sanford
Classification Company Confidentially
COMPANY UNCLASSIFIED
Classification Export Control
NOT EXPORT CONTROLLED
Classification Defence Secrecy
ÖPPEN/UNCLASSIFIED

Date 2013-06-18 | Issue A | Document ID 87/03631-1/FCK11507
Issued by
OEGPU Viktor Hallman, Erik Sanford
Classification Company Confidentially
COMPANY UNCLASSIFIED
Classification Export Control
NOT EXPORT CONTROLLED
Classification Defence Secrecy
ÖPPEN/UNCLASSIFIED

1 Introduction

The 50 Ω interface is a well known concept to any high frequency engineer and researcher. Everything from amplifiers and attenuators to network analysers are all developed in order to be able to connect to this standardised environment without any impedance mismatch. This great advantage of universal connectability has also got some drawbacks. Suppose that two devices are to be connected to each other, both units having an preferred impedance of 10 Ω at the point of connection. According to present standards, both of them would have to be impedance transformed to the 50 Ω environment, which inevitably would entail loss in the system and limit the possible bandwidth compared to if they were just connected using a 10 Ω interface .

Another aspect of the 50 Ω measurement interface is that there is only one signal connector and one ground connector. If a half wave dipole antenna, which is balancedly fed, is going to be connected to the standardised unbalanced interface, there has got to be a network in between to convert from signal-ground to signal-signal, a so called balun.

The main goal of this thesis has been to investigate whether abandoning the unbalanced 50 Ω interface could be beneficial compared to the standard design procedure when developing an antenna-amplifier system. As depicted in Figure 1.1, the proposed design approach would yield a less complex system than conventionally. To design the system a couple of design goals, or restric-

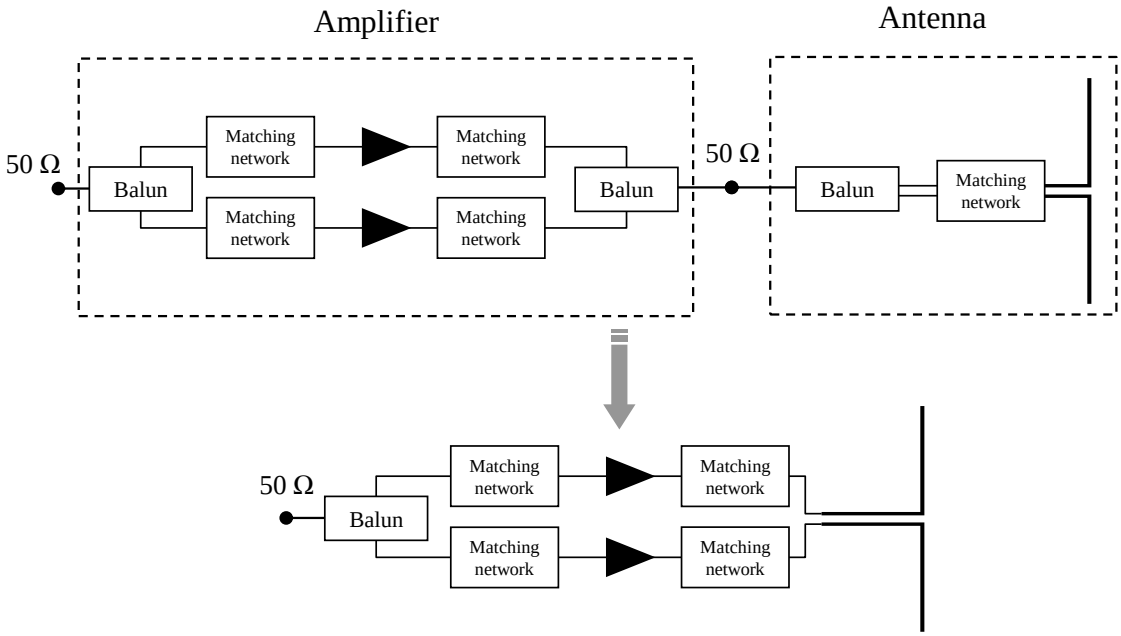

Figure 1.1: The goal of this thesis has been to investigate the possible advantages of integrating an antenna-amplifier system as shown in the lower flow chart instead of the conventional way shown in the upper flow chart

Date 2013-06-18 | Issue A | Document ID 87/03631-1/FCK11507
Issued by
OEGPU Viktor Hallman, Erik Sanford
Classification Company Confidentially
COMPANY UNCLASSIFIED
Classification Export Control
NOT EXPORT CONTROLLED
Classification Defence Secrecy
ÖPPEN/UNCLASSIFIED

tions, had to be set up. A bandwidth of a 1:4 ratio between the lowest and highest frequency of operation was chosen as the target frequency range of the system. In order to be able to perform in laboratory measurement with the antenna in a not too cumbersome manner, but also to be able to cover the whole frequency range in the anechoic measurement chamber, the specific frequency band of interest was set to be from 750 MHz to 3 GHz. With respect to the examining nature of the project, a specific goal of output power was not of great importance. Instead the choice of transistor, 35 W CREE GaN HEMT, was putting a limit to the output power. This specific transistor was mainly chosen due to its favourable characteristics in the frequency region of interest.

Another part of the investigation has also been to see if the integration could be made using a wideband omnidirectional antenna. Omnidirectional radiation is advantageously utilised in broadcasting scenarios, since the transmitting and receiving capabilities in this case essentially are independent of the orientation of the terminal [1]. If the advantages with the proposed design would be realised as previously stated along with an omnidirectional antenna with electrically small dimensions, the end result would be a compact low-loss wideband antenna-amplifier unit. Such a unit would be of great interest to any non-stationary transmitter or receiver.

Date 2013-06-18 | Issue A | Document ID 87/03631-1/FCK11507
Issued by
OEGPU Viktor Hallman, Erik Sanford
Classification Company Confidentially
COMPANY UNCLASSIFIED
Classification Export Control
NOT EXPORT CONTROLLED
Classification Defence Secrecy
ÖPPEN/UNCLASSIFIED

2 Theory

In this section, the theory used to justify the different design goals and techniques is described. First of all some general microwave theory will be dealt with, followed by two sections concerning the theory of amplifiers and antennas that are of interest to the proceeding report.

The mathematical typesetting used, not only in this section but in the whole thesis, is based on the article of Beccari [2]. Beccari bases his article on the ISO 31/XI standard for *"Mathematical sign and symbols for use in physical sciences and technology"*.

2.1 Microwave theory

This section will cover some basic concepts of microwave theory. Emphasis is given to the parts that are of significant interest to this thesis. The concepts in this section, albeit not the nomenclature, is inspired by the book of Pozar [3].

2.1.1 S-parameters

Scattering parameters, commonly know as *S-parameters*, are a very useful tool within microwave theory and practice. Basically the S-parameters are the elements of the matrix describing the relationship between incident and reflected voltage waves on an N-port circuit. This relationship can be written as

$$\begin{pmatrix} b_1 \\ \vdots \\ b_n \\ \vdots \\ b_N \end{pmatrix} = \begin{pmatrix} \mathrm{S}_{11} & \cdots & \mathrm{S}_{1n} & \cdots & \mathrm{S}_{1N} \\ \vdots & \ddots & & & \vdots \\ \mathrm{S}_{n1} & & \mathrm{S}_{nn} & & \mathrm{S}_{nN} \\ \vdots & & & \ddots & \vdots \\ \mathrm{S}_{N1} & \cdots & \mathrm{S}_{Nn} & \cdots & \mathrm{S}_{NN} \end{pmatrix} \begin{pmatrix} a_1 \\ \vdots \\ a_n \\ \vdots \\ a_N \end{pmatrix}, \tag{2.1}$$

where a_n is the incident wave at the nth port and b_n the reflected wave at the same port.

The case when N equals 2, referred to as a 2-port, is very common and can be seen in Figure 2.1.

Figure 2.1: The common 2-port. Incident waves are represented by a_1 and a_2. In the same manner outgoing waves are represented by b_1 and b_2.

Date 2013-06-18 | Issue A | Document ID 87/03631-1/FCK11507
Issued by
OEGPU Viktor Hallman, Erik Sanford
Classification Company Confidentially
COMPANY UNCLASSIFIED
Classification Export Control
NOT EXPORT CONTROLLED
Classification Defence Secrecy
ÖPPEN/UNCLASSIFIED

The expression 2.1 is then reduced to

$$\begin{pmatrix} b_1 \\ b_2 \end{pmatrix} = \begin{pmatrix} \mathrm{S}_{11} & \mathrm{S}_{12} \\ \mathrm{S}_{21} & \mathrm{S}_{22} \end{pmatrix} \begin{pmatrix} a_1 \\ a_2 \end{pmatrix},$$

where S_{11} and S_{22} are the coefficients describing the reflection at the ports. S_{12} and S_{21} are the coefficients describing the gain between the ports in both directions.

2.1.2 Mismatch

High frequency signals reflect in the boundary between two impedances. In reality this reflection is mostly undesirable since it will result in power loss when part of the signal is reflected back to the source. The reflection between two impedances is expressed by the coefficient Γ_L,

$$\Gamma_\mathrm{L} = \frac{V_-}{V_+} = \frac{Z_\mathrm{L} - Z_0}{Z_\mathrm{L} + Z_0},$$

where V_+ and V_- are the phasor of the in- and outgoing wave. The impedance Z_L is the load impedance and Z_0 is the standard 50 Ω impedance according to Figure 2.2.

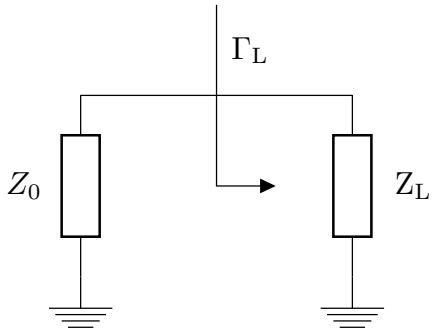

Figure 2.2: Γ_L marked in the boundary between two impedances. The arrow is always pointing towards the impedance considered as load.

Another frequently used way to describe mismatch is the *Standing Wave Ratio*, SWR. A standing wave occurs when the ingoing wave and the reflected wave are added before the mismatch and the ratio is taken of the highest and lowest amplitude of the standing wave.

The maximum amplitude of the standing wave will occur at the position where the waves are added constructively and the resulting amplitude is $V_\mathrm{max} = |V_+| + |V_-|$. The minimum of the standing wave will in an opposite way occur at the position where the two waves are added in a destructive way which will correspond to an amplitude of $V_\mathrm{min} = |V_+| - |V_-|$ for a passive load. The SWR is computed as the ratio between V_max and V_min,

Date 2013-06-18 | Issue A | Document ID 87/03631-1/FCK11507
Issued by
OEGPU Viktor Hallman, Erik Sanford
Classification Company Confidentially
COMPANY UNCLASSIFIED
Classification Export Control
NOT EXPORT CONTROLLED
Classification Defence Secrecy
ÖPPEN/UNCLASSIFIED

$$\text{SWR} = \frac{|V_+| + |V_-|}{|V_+| - |V_-|} = \frac{|V_+|\,(1 + |\Gamma_\text{L}|)}{|V_+|\,(1 - |\Gamma_\text{L}|)} = \frac{1 + |\Gamma_\text{L}|}{1 - |\Gamma_\text{L}|}.$$

2.1.3 Transmission lines

The purpose of transmission lines is to transfer signals over a distance. For high frequency techniques different types of transmission lines are used and realised in different ways. A transmission line is characterised by its characteristic impedance Z_c which depends on the physical dimensions of the transmission line. In this section two different types of transmission lines will be explained. The first one is the microstrip which is seen as the technically more flexible alternative since it can be realised in different shapes depending of the application. The other one is the coaxial cable which consists of a core surrounded by a shield. The coaxial cable is technically not flexible since the characteristic impedance is fixed along the cable. However, the physical flexibility is much better and therefore used to transfer signals far distances between devices.

2.1.3.1 Microstrip Microstrips are widely used as conducting paths in all kinds of high frequency circuits. A microstrip consists of a conductor and a ground plane which are separated by a dielectric medium of a certain height. The wavelength of a wave traveling through the microstrip for a given frequency is depending on the relative permittivity ϵ_r of the substrate. High relative permittivity gives a short physical wavelength.

Microstrips of certain shapes can be used to replace lumped components like inductors and capacitors. The lengths of a transmission line is often specified by the electrical length θ, which is an angle corresponding to a phase at a given angular frequency ω:

$$\theta = \beta l = \frac{2\pi}{\lambda} l = \frac{\omega}{v_\text{p}} l, \tag{2.2}$$

where v_p is the velocity of propagation, λ is the corresponding wavelength and β is the wavenumber defined as $2\pi/\lambda$. A general expression of the input impedance of a transmission line of electric length θ and characteristic impedance Z_0 loaded with Z_L is

$$Z_\text{in} = Z_0 \frac{Z_\text{L} + \text{j} Z_0 \tan\theta}{Z_0 + \text{j} Z_\text{L} \tan\theta}. \tag{2.3}$$

For a shorted piece of transmission line ($Z_\text{L} = 0$) the expression is

$$Z_\text{in} = Z_0 \text{j} \tan\theta, \tag{2.4}$$

which can be compared with the reactance of an inductor

$$Z_{\text{ind}} = \mathrm{j}\omega L = \mathrm{j}X_{\text{ind}}. \tag{2.5}$$

Combining (2.4) and (2.5) the following expression for X_{ind} can be derived:

$$X_{\text{ind}} = Z_0 \tan\theta. \tag{2.6}$$

For small values of the electric length, $\tan\theta \approx \theta$. Combining (2.6) and (2.2) the expression for X_{ind} can be written as

$$X_{\text{ind}} = Z_0\theta = Z_0\frac{\omega l}{v_{\text{p}}},$$

which shows that the reactance X_{ind} of a narrow transmission line is proportional to frequency and length and the inductance is given by

$$L = Z_0\frac{l}{v_{\text{p}}}.$$

In the same way the reactance X_{cap} of an open stub can be derived using (2.3) having $Z_{\text{L}} = \infty$, which leads to the expression

$$X_{\text{cap}} = -Z_0 \cot\theta$$

and for small θ the approximate value of the resulting capacitance is

$$C = \frac{l}{Z_0 v_{\text{p}}}. \tag{2.7}$$

Summing up, the inductor is realised by a narrow piece of microstrip (high Z_0) and the inductance is proportional the the length. According to (2.7) a large capacitance is achieved by having a long piece of stub with a low characteristic impedance Z_0. A low characteristic impedance corresponds to a wide conductor. Note that the assumption of having $\tan\theta \approx \theta$ should always be considered and is only valid for small values of θ.

2.1.3.2 Coaxial cable Coaxial cables are often used to transfer signals over long distances ($l \gg \lambda$). Connecting an arbitrary frequency dependent load $Z_{\text{L}}(\omega)$ to a coaxial cable of characteristic impedance Z_0 the input-impedance is

$$Z_{\text{in}}(\omega) = Z_0\frac{Z_{\text{L}}(\omega) + \mathrm{j}Z_0\tan\theta}{Z_0 + \mathrm{j}Z_{\text{L}}(\omega)\tan\theta}.$$

Date 2013-06-18 | Issue A | Document ID 87/03631-1/FCK11507
Issued by
OEGPU Viktor Hallman, Erik Sanford
Classification Company Confidentially
COMPANY UNCLASSIFIED
Classification Export Control
NOT EXPORT CONTROLLED
Classification Defence Secrecy
ÖPPEN/UNCLASSIFIED

The input impedance Z_{in} could be expressed in terms of Γ_{L}, where Γ_{L} is calculated relative the characteristic impedance Z_0, which gives:

$$\Gamma_{\text{IN}}(\omega) = \Gamma_{\text{L}}(\omega)\text{e}^{-2\text{j}\beta l} = \Gamma_{\text{L}}(\omega)\text{e}^{-2\text{j}l\omega/v_{\text{p}}}. \tag{2.8}$$

The extra term $\text{e}^{-2\text{j}l\omega/v_{\text{p}}}$ is a rotation of Γ_{IN} in the Smith chart by an angle of $-2l\omega/v_{\text{p}}$ radians. A frequency shift of $\Delta\omega$ will therefore cause a rotation of gamma equal to $-2l\Delta\omega/v_{\text{p}}$, which is proportional to the length of the transmission line. That means the length l of a transmission line emphasizes the rotation of Γ_{IN} which is equivalent to a variation in Z_{in}.

2.1.4 Balun

In order to transform an unbalanced signal to a balanced signal a balun is used. An unbalanced signal is always measured towards ground. For a balanced signal, ground is not present and the signal is seen as the potential difference between two conductors. In Figure 2.3, a balun is realised using a quarter wavelength transmission line. The core of the transmission line will be isolated from ground on both sides. According to (2.3), a grounded termination will be transformed into open circuit at a distance $\lambda/4$ (90°) and therefore the shield of the transmission line in Figure 2.3 can be considered as isolated from ground at a distance $\lambda/4$ from the ground. Both the shield and the core of the transmission line will be seen as isolated from ground at the right side and hence the output is balanced.

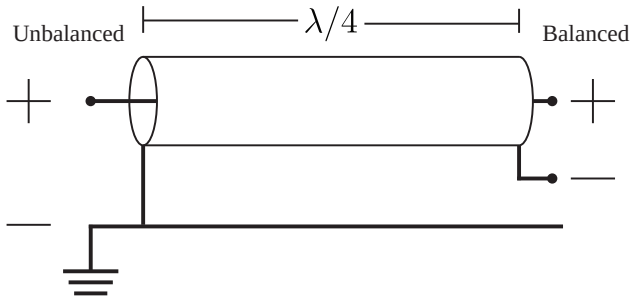

Figure 2.3: Unbalanced to balanced using a quarter wavelength coaxial cable

The problem of using coaxial baluns is the bandwidth. The requirement of having the length $\lambda/4$ will be valid for one and only one frequency and therefore hard to design for a broadband application. In section 3.2.1 other alternatives will be discussed.

Date 2013-06-18 | Issue A | Document ID 87/03631-1/FCK11507
Issued by
OEGPU Viktor Hallman, Erik Sanford
Classification Company Confidentially
COMPANY UNCLASSIFIED
Classification Export Control
NOT EXPORT CONTROLLED
Classification Defence Secrecy
ÖPPEN/UNCLASSIFIED

2.2 Antenna theory

In this section a couple of antenna parameters are defined, in order to evaluate the proceeding design. Also, the theory behind wideband antennas in general will be briefly described. The theory of two antennas under consideration, the TASH antenna and the biconical antenna, is also presented here.

2.2.1 Antenna characteristics

There are a lot of parameters that can be used to characterise an antenna. The parameters can roughly be divided into two categories: parameters describing the amount of energy radiated from the antenna element and parameters describing in which direction the energy is radiated. Most of the definitions in this section are taken from the book of Balanis [4] and the chapter on *Fundamental Parameters of Antennas*, which is partly built upon IEEE standards [5] from the year of 1983. Some guidance has also been taken from the more recent standards of 1993 [6].

2.2.1.1 Antenna input impedance The input impedance of an antenna is defined as the ratio of the voltage to current at the antenna port and can be written as

$$Z_{\mathrm{A}} = R_{\mathrm{A}} + \mathrm{j}X_{\mathrm{A}},$$

where Z_{A} is the antenna impedance, R_{A} the antenna resistance and X_{A} the antenna reactance. R_{A} is generally considered to consist of two parts as

$$R_{\mathrm{A}} = R_{\mathrm{rad}} + R_{\mathrm{loss}},$$

where R_{rad} is the *radiation resistance* of the antenna and R_{loss} is resistance caused by losses in the material of the antenna. Radiation resistance could be thought of as the constant that relates the power in the radiated field to the square of the current put into the port of the antenna. If the internal impedance of the generator feeding the antenna is assumed to be on the form

$$Z_{\mathrm{g}} = R_{\mathrm{g}} + \mathrm{j}X_{\mathrm{g}},$$

the instance of maximum power delivered to the antenna will occur when the impedance of the antenna and the impedance of the generator are the conjugate of each other. This means that

$$\begin{aligned} R_{\mathrm{rad}} + R_{\mathrm{loss}} &= R_{\mathrm{g}} \\ X_{\mathrm{A}} &= -X_{\mathrm{g}}. \end{aligned}$$

Furthermore, since it is only R_{rad} that is useful, it is desired that R_{loss} and X_{A} are close to or equal to zero.

Date 2013-06-18 | Issue A | Document ID 87/03631-1/FCK11507
Issued by
OEGPU Viktor Hallman, Erik Sanford
Classification Company Confidentially
COMPANY UNCLASSIFIED
Classification Export Control
NOT EXPORT CONTROLLED
Classification Defence Secrecy
ÖPPEN/UNCLASSIFIED

2.2.1.2 $|S_{11}|$ and SWR As described earlier in the chapter, the relationship between incident and reflected waves on an N-port can be described using S-parameters. This way of seeing things also applies to antennas. In case of a purely transmitting antenna, $|S_{11}|$ will show how well matched the antenna is to its environment. It is clear that $|S_{11}|$ should have a value as close to zero as possible. If $|S_{11}|$ is unity, the antenna is completely useless, since all power will be reflected back to the source. Often, $|S_{11}|$ is expressed in terms of decibel (dB). What an acceptable value of $|S_{11}|$ is varies between applications, but a commonly used standard is that the level of $|S_{11}|$ should not be higher than -10 dB [7] [1], which means that no more than 10 % of the incident power should be reflected back to the generator. Another common measure of reflection or mismatch is the SWR, also known as *Voltage Standing Wave Ratio*, VSWR. The common practice with SWR is that it should not be higher than 2:1 [7] [1], which corresponds to $|S_{11}|$ being approximately -10 dB.

2.2.1.3 Bandwidth An important parameter for characterisation of an antenna is the *bandwidth*. The bandwidth is defined as the range of frequency within which a specific criterion holds true. One criterion could be $|S_{11}| < -10$ dB. The bandwidth that can be expected varies between different types of antennas. For some antennas with a narrow band of operation, a couple of percent of the center frequency could be acceptable. For antennas with a wideband field of operation, several multiples of the lowest operational frequency could be the goal. A common practice when specifying a bandwidth is that for narrow band antennas, the bandwidth is given in percent of the center frequency. For wideband antennas, the bandwidth is often given as a ratio between the highest and the lowest frequency of operation.

2.2.1.4 Antenna efficiency *Antenna efficiency* is often defined as the efficiency in the antenna with respect to mismatch at the feeding point and losses, both conductive and dielectric. According to Balanis, the total efficiency η_0 can be expressed as

$$\eta_0 = \eta_\mathrm{r}\eta_\mathrm{c}\eta_\mathrm{d},$$

where η_r is the reflection efficiency, η_c is the conduction efficiency and η_d is the dielectric efficiency. The reflection efficiency is defined as $\eta_\mathrm{r} = (1 - |\Gamma|^2)$, where Γ is the reflection coefficient for the intersection between the antenna and the transmission line which is feeding it. Often it is very difficult to obtain values for η_c and η_d numerically. Therefore it is common practice to determine them by measurements and group them into one parameter, $\eta_\mathrm{cd} = \eta_\mathrm{c}\eta_\mathrm{d}$.

2.2.1.5 Directivity The *directivity* of an antenna in a certain direction is defined as the ratio of the radiation intensity in a certain direction δ to the mean radiation intensity. Since the radiated power is 4π times the mean radiation intensity, the directivity D_δ can be written as

$$D_\delta = \frac{I_\delta}{I_0} = \frac{4\pi I_\delta}{P_\mathrm{rad}},$$

Date 2013-06-18 | Issue A | Document ID 87/03631-1/FCK11507
Issued by
OEGPU Viktor Hallman, Erik Sanford
Classification Company Confidentially
COMPANY UNCLASSIFIED
Classification Export Control
NOT EXPORT CONTROLLED
Classification Defence Secrecy
ÖPPEN/UNCLASSIFIED

where I_δ is the radiation intensity, I_0 is the mean radiation intensity and P_{rad} is the radiated power. Often one is interested in the directivity in the direction of the maximum radiation. The expression is then turned into

$$D_{\text{max}} = \frac{I_{\text{max}}}{I_0} = \frac{4\pi I_{\text{max}}}{P_{\text{rad}}}.$$

2.2.1.6 Gain A parameter similar to the directivity is the *gain*. The only thing separating the two is that the gain takes into account the accepted input power,

$$P_{\text{acc}} = (1 - |\Gamma|^2)P_{\text{avs}},$$

in contrast to the radiated power in the case of directivity. Here, P_{avs} is the power available from the source. The relationship between the accepted and radiated power can be written as

$$P_{\text{rad}} = \eta_{\text{cd}} P_{\text{acc}},$$

where η_{cd} is defined as in section 2.2.1.4. This yields the relationship between directivity and gain G as

$$G = \eta_{\text{cd}} D.$$

Occasionally it is useful to talk about something called *realised gain*, which is the reduced gain of an antenna, taken into account the mismatch at the input of the antenna. The power considered when dealing with realised gain is P_{avs}, which leads to that the realised gain G_{R} can be written as

$$G_{\text{R}} = (1 - |\Gamma|^2)\eta_{\text{cd}} D.$$

2.2.1.7 Radiation pattern To show the spatial radiation characteristics it is common to use a plot of the *radiation pattern*. The radiation pattern is defined as the representation of radiation characteristics as a function of spatial coordinates. A property of interest can for example be the directivity of an antenna. In Figure 2.4 the spatial definitions along with a typical radiation pattern of a half-wave dipole antenna is depicted.

In Figure 2.4a, r is defined as the radial distance from the center point, φ is defined as the angular distance from the x axis and θ is defined as the angular distance from the z axis. Another name for φ is *azimuth angle* and another name for θ is *elevation angle*.

Radiation region separation In most cases when mentioning the radiation pattern this is understood to be at a distance

$$r \geq \frac{2D^2}{\lambda} \tag{2.9}$$

away from the antenna center point. Here, D is the diameter of the smallest sphere encapsulating the antenna. The regime where (2.9) holds true is called *far-field region* or *Fraunhofer region*. The region where (2.9) does not hold true is called the *near-field region*. The near-field region is divided into the *radiating near-field region*, also called the *Fresnel region*, and the *reactive near-field region*.

Date 2013-06-18 | Issue A | Document ID 87/03631-1/FCK11507
Issued by
OEGPU Viktor Hallman, Erik Sanford
Classification Company Confidentially
COMPANY UNCLASSIFIED
Classification Export Control
NOT EXPORT CONTROLLED
Classification Defence Secrecy
ÖPPEN/UNCLASSIFIED

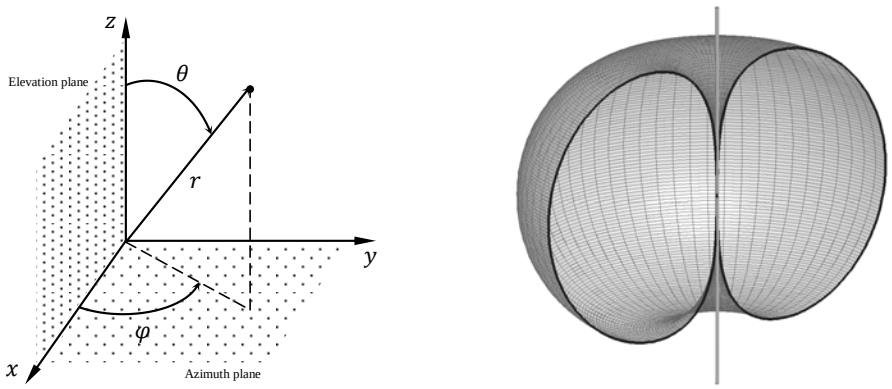

(a) **(b)**

Figure 2.4: (a) Commonly used spatial definitions and (b) radiation pattern of the half-wave dipole antenna directivity in logarithmic scale

2.2.1.8 Phase center

The Fraunhofer region field components of an antenna can be written as

$$\mathbf{E}_u = \hat{\mathbf{u}} E(\theta, \varphi) e^{\mathrm{j}\psi(\theta,\varphi)} \frac{e^{-\mathrm{j}\beta r}}{r},$$

where $\hat{\mathbf{u}}$ is a unit vector that describes field polarisation, $E(\theta, \varphi)$ represents the amplitude variation in space and $\psi(\theta, \varphi)$ represent the phase variation in space. In many aviation systems, such as navigation and tracking, it is often of interest to assign the antenna to one radiating point in space. In order to do this, $\psi(\theta, \varphi)$ has got to be constant for a given frequency. The reference point in space that yield the independence of θ and φ is called the *phase center* of the antenna. The waves occurring on a sphere surrounding the phase center should have the same phase. Insignificant variations in the position of the phase center will call upon the use of the term *apparent phase center*.

2.2.2 Wideband antennas

In many RF products, such as mobile phones and in radar applications, wideband antennas are of great interest since it reduces the number of antennas needed when utilising several frequency bands. The wideband behaviour is also favorable when doing measurements of waves with unknown frequency. In theory some antennas can be designed to show infinite wideband behaviour if their geometry is extended to infinity. These antennas are called *Frequency Independent* (FI) antennas. In reality however, practical limitations make true FI antennas an impossibility, whereas their realisable projections in wideband antennas are an important asset to the antenna engineer.

There are different ways to theoretically approach the FI antennas. An antenna designed for a specific frequency can be redesigned for an arbitrary frequency by scaling its linear dimensions [8].

Date 2013-06-18 | Issue A | Document ID 87/03631-1/FCK11507
Issued by
OEGPU Viktor Hallman, Erik Sanford
Classification Company Confidentially
COMPANY UNCLASSIFIED
Classification Export Control
NOT EXPORT CONTROLLED
Classification Defence Secrecy
ÖPPEN/UNCLASSIFIED

Therefore an antenna with a structure that is invariant under linear scaling is also going to show the same characteristics independent of frequency. One way a structure like this can be imagined is by thinking of the geometry of the FI antenna as a combination of adjacent cells where the ratio of the dimensions of one cell to its neighbour is constant throughout the whole structure as depicted in Figure 2.5 [9].

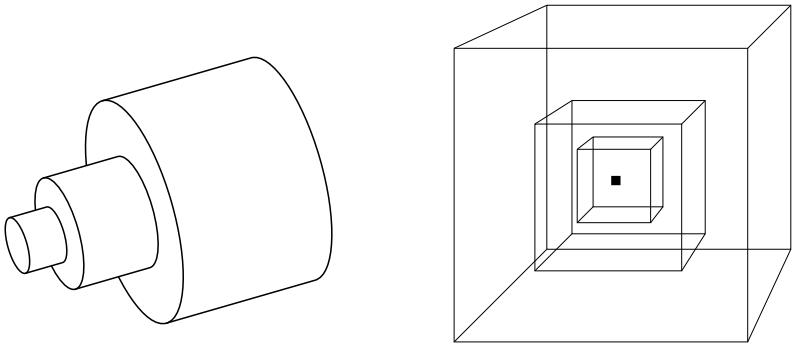

(a) **(b)**

Figure 2.5: Example of geometries where the adjecent cells are (a) simply connected and (b) multiply connected

If D_n is some dimension of the nth cell, this constant ratio can be written on the form

$$\frac{D_n}{D_{n+1}} = \tau, \tag{2.10}$$

where $\tau < 1$ if $n = 0$ is the index of the smallest cell. When $n = 0$ the cell should in theory be represented as a point. In the same manner, when n goes towards infinity, also the dimensions of the cell goes towards infinity. In theory, this kind of geometry has to be of infinite extension and of infinite precision in order to represent all cells. In practice though, an infinitely large structure is rather impractical and the precision of construction has got an upper limit. Hence, truncation of the structure needs to be done. The smallest cell defines the upper working frequency in the same way as the largest cell defines the lowest working frequency. To make the impact of the lower frequency truncation as negligible as possible the antenna must be designed so that no, or little, current flow is cut off. The current should be attenuated at the point of truncation [10].

Victor H. Rumsey started to investigate FI antennas in the early 1950s since he got curious about an observation in 1949. The conclusion of the observation stated that planar self-complementary antennas have got an impedance of half the intrinsic impedance of vacuum, for all frequencies. After some investigation of his own, Rumsey came up with the conclusion that the impedance and pattern properties of an antenna are going to be independent of frequency, given that the antenna geometry can be described only in terms of angles. This conclusion is sometimes referred to as "Rumsey's principle" [10].

Even if true FI antennas can not be realised, there are many wideband antennas of interest. The biconical, the helical and the spiral antennas, depicted in Figure 2.6, are three common types of wideband antennas. All three types are suitable for detection of signals of unknown frequency. Especially the biconical antenna is used for testing of Electromagnetic Compatibility (EMC) due

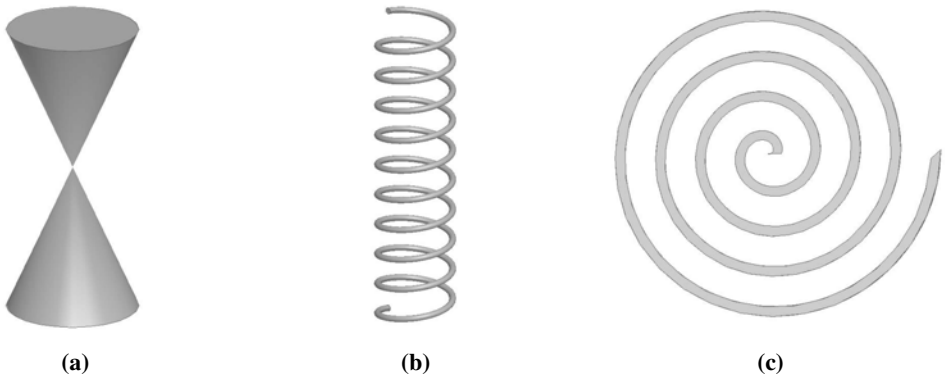

(a) **(b)** **(c)**

Figure 2.6: Three common wideband antennas: (a) the biconical, (b) the helical and (c) the spiral antenna.

to its high bandwidth and omnidirectional behaviour [11]. The helical and the spiral antennas are mostly used in communication applications, such as satellite communication, due to their circular polarisation of the electromagnetic field [12].

In the subsequent sections, two types of wideband antennas, the TASH antenna and the biconical antenna, will be described more thoroughly. These antennas were chosen due to their wideband behaviour and their exhibition of omnidirectional radiation pattern. An antenna also having these characteristics is the planar spiral antenna. The reason why the spiral antenna was not considered was that the electrical size of the antenna is larger than the TASH and the biconical antenna [4][13].

2.2.3 The biconical antenna

A popular antenna, especially for measurements, is the biconical antenna due to its wide frequency range and near frequency independent radiation pattern [14]. In the following sections, the infinite and finite biconical antennas along with their impedances will be dealt with.

2.2.3.1 The infinite case A popular way to describe the biconical antenna is by making analogies to the theory of transmission lines [12][4]. As depicted in Figure 2.7, the bicone acts as a guide for spherical waves in the same manner as the transmission line is a guide for plane waves.

Also, in analogy to the infinite transmission line, in the case of a biconical antenna with infinite extension only outgoing waves have to be considered. Given that the geometry of the infinite

Date 2013-06-18 | Issue A | Document ID 87/03631-1/FCK11507
Issued by
OEGPU Viktor Hallman, Erik Sanford
Classification Company Confidentially
COMPANY UNCLASSIFIED
Classification Export Control
NOT EXPORT CONTROLLED
Classification Defence Secrecy
ÖPPEN/UNCLASSIFIED

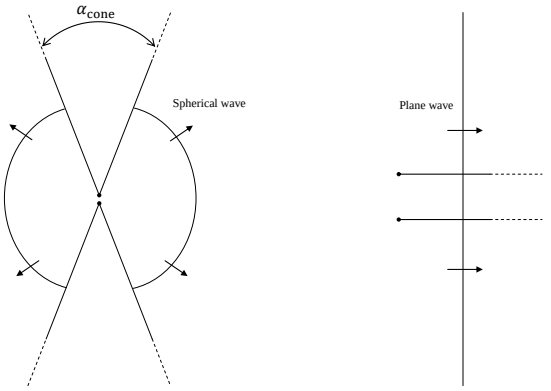

Figure 2.7: The analogy between an (a) infinite biconical antenna and an (b) infinite uniform transmission line

biconical antenna is completely determined by spatial angles, using Faraday's law and Ampere's law, it is found that [4, equation 9-12a] the characteristic impedance of the antenna, Z_{c}, is constant with respect to frequency and expressed as

$$Z_{\text{c}} = 120 \ln \left[\cot \left(\frac{\alpha_{\text{cone}}}{4} \right) \right] \Omega, \tag{2.11}$$

where α_{cone} is the cone angle as shown in Figure 2.7a. The variation of Z_{c} as a function of α_{cone} is depicted in Figure 2.8.

If one of the cones is replaced by an infinite ground plane, the amplitude of the emitted field above the ground plane is the same as with two cones. Therefore, the total power emitted is going to be half of the one emitted by the bicone, but with the same current fed to the antenna. By the law of $\text{P} = \text{RI}^2$ this implies that the characteristic impedance of the single cone antenna will be half of the biconical one.

2.2.3.2 The finite case One way to approach the finite biconical antenna was suggested in the year of 1943 by Schelkunoff [15]. Schelkunoff's idea is to assume that most of the energy propagating along the surfaces of the cones is reflected back towards the input. The energy propagating parallel to the mirror plane of the two cones on the other hand, is almost completely radiated into free space. This is depicted in Figure 2.9.

By taking the idea one step further, the reflected energy can be thought of as a result of that the ends of the cones are being terminated with a certain load impedance, Z_{L}. By altering Z_{L} and the length l of the cone side one can alter the input impedance of the biconical antenna in a similar

Date 2013-06-18 | Issue A | Document ID 87/03631-1/FCK11507
Issued by
OEGPU Viktor Hallman, Erik Sanford
Classification Company Confidentially
COMPANY UNCLASSIFIED
Classification Export Control
NOT EXPORT CONTROLLED
Classification Defence Secrecy
ÖPPEN/UNCLASSIFIED

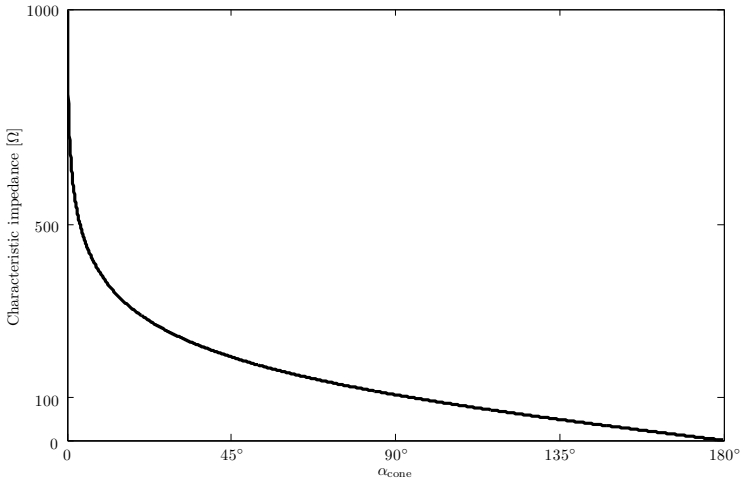

Figure 2.8: The characteristic impedance of a infinite biconical antenna as a function of cone angle α_{cone} according to equation (2.11)

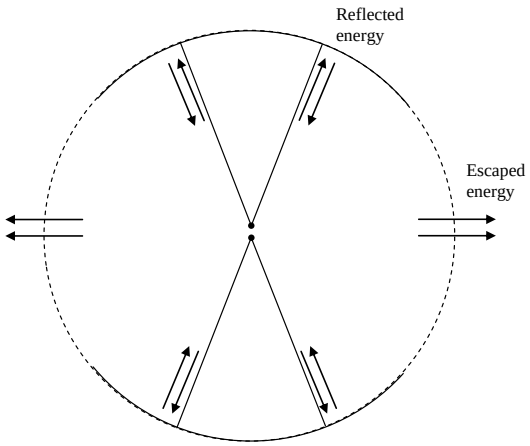

Figure 2.9: Energy traveling towards the poles of the sphere encapsulating the antenna is reflected back. Energy travelling towards the equator of the sphere is escaping into free space.

way as with a transmission line with characteristic impedance Z_{c} and length l being terminated with a load Z_{L}, see Figure 2.10.

In analogy with the transmission line the input impedance Z_{i} of the biconical antenna is related to the characteristic impedance Z_{c} of the cones, the slant height l of the cone and the termination impedance Z_{L}. This relationship can be written as

$$Z_{\text{i}} = Z_{\text{c}} \frac{Z_{\text{L}} + \text{j}Z_{\text{c}} \tan \beta l}{Z_{\text{c}} + \text{j}Z_{\text{L}} \tan \beta l},$$

Date 2013-06-18 | Issue A | Document ID 87/03631-1/FCK11507
Issued by
OEGPU Viktor Hallman, Erik Sanford
Classification Company Confidentially
COMPANY UNCLASSIFIED
Classification Export Control
NOT EXPORT CONTROLLED
Classification Defence Secrecy
ÖPPEN/UNCLASSIFIED

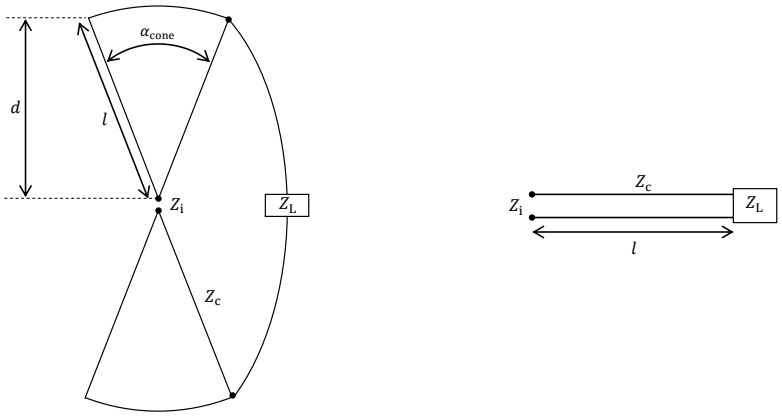

Figure 2.10: The finite biconical antenna can be seen upon as a transmission line with a characteristic impedance, Z_{c}, that is terminated with a certain load, Z_{L}. This results in an input impedance Z_{i}.

where β is the wavenumber. The theoretical impedance of the finite bicone for some specific cases is presented by Kraus [12, section 8-4]. One important observation that he calls upon is that the variation in impedance is decreasing when the angle of the cone is increased.

Occasionally in the literature the lowest operational frequency of the biconical antenna is being related to the distance d rather than the slant height l of the cone [16][17]. In accordance with the transmission line analogy this holds for small angles, since $d = l \cos \frac{\alpha_{\text{cone}}}{2}$, but for larger angles $l \gg d$ and it would be less relevant to relate the lowest operating frequency to d.

2.2.4 The TASH antenna

In September 2001, Thomas J. Warnagiris proposed a novel type of wideband antenna in Microwave Journal [18]. He called it Tapered Area Small Helix (TASH) antenna. The easiest way to describe the TASH geometry is maybe to describe it as a triangle that has been rolled up from one of its bases into a cylinder shaped object, see Figure 2.11, with a feeding point and a grounding point at the base spiral.

In the second article of Warnagiris there are some quite precise design recommendations to follow [19]. The design parameters are stated in Table 1 and their descriptions are illustrated in Figure 2.12.

Warnagiris also states a couple of advantages over traditional antennas. For example, albeit that the log-periodic antenna easily exhibits wideband characteristics, its phase center varies with frequency, its largest physical dimension is quite large compared to the lowest operating frequency and the antenna is highly directional. These, in some cases, inconveniences would according to Warnagiris be overcome using the TASH. In comparison with the biconical antenna the main stated advantage would be that the TASH is far less bulky.

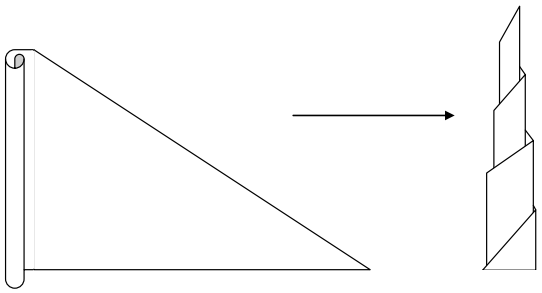

Figure 2.11: The Tapered Area Small Helix (TASH) antenna is essentially a triangle that has rolled up from one of its bases into a cylinder shaped geometry.

Table 1: The design parameters given in the article by Warnagiris [19]

Parameter	Designation	Value
TASH height	Y	0.2 λ
Base length	X	0.32 λ
Ground spacing	S	0.004 λ
Feed point	F_1	at the innermost point
Shorting point	F_2	0.08 λ in from the tip
TASH diameter	D	0.1 λ

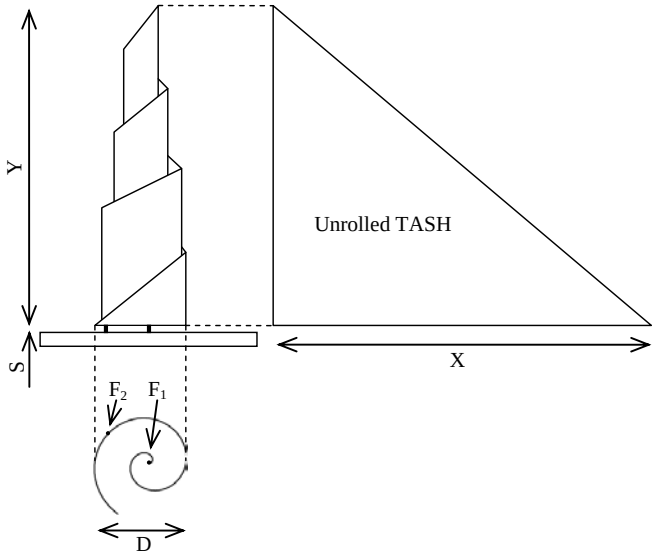

Figure 2.12: The definitions of the TASH parameters to be considered

In order to explain the radiating behavior of the TASH one can think of the antenna as a superposition of a monopole antenna, a transmission line antenna and a helical antenna [19], where the

Date 2013-06-18 | Issue A | Document ID 87/03631-1/FCK11507
Issued by
OEGPU Viktor Hallman, Erik Sanford
Classification Company Confidentially
COMPANY UNCLASSIFIED
Classification Export Control
NOT EXPORT CONTROLLED
Classification Defence Secrecy
ÖPPEN/UNCLASSIFIED

radiation modes of the different antennas would sum up to the total radiation. This is illustrated in Figure 2.13.

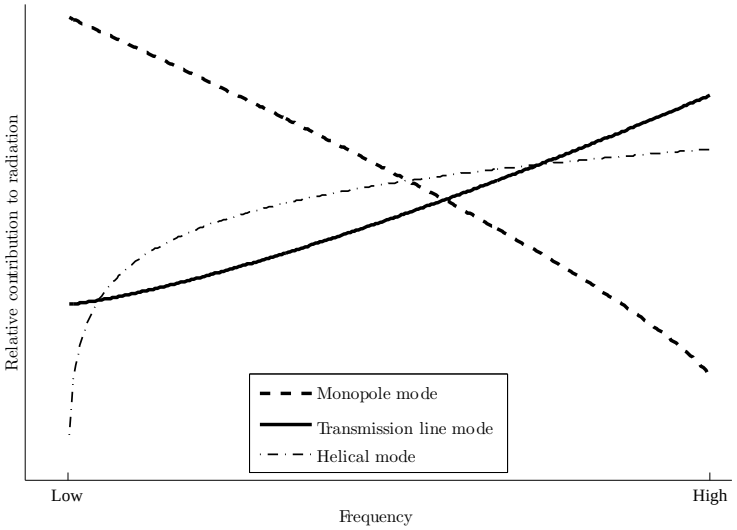

Figure 2.13: The relative radiation contribution from each one of the TASH radiation modes with respect to frequency

Another way to consider the antenna is to think of the base spiral as a transmission line that feed an infinite amount of radiating elements that are perpendicular to the transmission line. Almost like a log-periodic antenna that has been splitted in the direction of the main lobe and rolled up into a cylinder.

In his two articles about the TASH, Warnagiris is rather specific when it comes to the design parameters of the antenna, defining for instance the diameter of the rolled element to be $\lambda/8$. However, in the patent of the TASH antenna, Warnagiris is widely extending the spectrum of what can be considered to be a TASH antenna[20]:

> *"Although the present invention has been described in detail, it should be understood that various changes, substitutions, and alterations can be made hereto without departing from the spirit and scope of the invention..."*

2.3 Amplifier theory

Depending on the area of use for the amplifier, different parameters are studied. For receivers the noise performance is more important. For power amplifiers the maximum output power and *Power Added Efficiency* (PAE) are more taken under consideration. In this section some of the important measures for power amplifiers will be explained together with the theory of stability. Some different classes of amplifier will also be explained.

2.3.1 Amplifier characteristics

To determine the performance of an amplifier a number of different measures can be used. In this section the ones important for power amplifiers will be explained.

2.3.1.1 Power Added Efficiency In general, the efficiency of an amplifier is important for two main reasons. First of all it reduces the power consumption and second it prevents the amplifier from overheating. The importance of the power consumption aspect grows with the number of amplifiers produced and is therefore a well discussed topic within the area of large telecom networks [21]. The PAE is the ratio between the added RF-power divided by the total power consumption:

$$\text{PAE} = \frac{P_{\text{out}} - P_{\text{in}}}{P_{\text{DC}}}.$$

Referring to the conservation of energy the heat generated by the amplifier is

$$P_{\text{heat}} = P_{\text{in}} - P_{\text{out}} + P_{\text{DC}} = P_{\text{DC}}(1 - \text{PAE}).$$

2.3.1.2 Return loss An important specification when designing an input matching network is the achieved *return loss* (RL). The RL of a device shows the amount of reflected power and is often given in dB. The goal is to have a small amount of reflected power. Given the S-parameters of a circuit the RL in dB can be calculated using

$$\text{RL} = 20\log_{10}\left|\text{S}_{11}\right|. \tag{2.12}$$

The S-parameters are calculated for an N-port having all ports terminated to 50 Ω which means (2.12) is only valid having all other ports terminated to 50 Ω.

2.3.1.3 Gain The total gain of the amplifier is dependent of the impedance seen at the input and output of the transistor. The optimal impedances are more or less frequency dependent and in order to get an understanding of how the source and load impedances affect the gain, a load and pull measurement can be performed which sweeps through all possible loads and sources and retrieve the resulting gain. More details about this in a later section.

2.3.1.4 Stability The following theory analyzing the stability of a linear 2-port system will be based on theory provided by [22]. Seeing the amplifier as a 2-port circuit including a matching network with corresponding S-parameters the stability can be derived depending on the S-parameters and the terminations. Instability occurs when the total reflection in any interface is greater than 1. For the 2-port network there are four reflections that need to be considered according to Figure 2.14. For $|\Gamma_{\mathrm{S}}| < 1$ and $|\Gamma_{\mathrm{L}}| < 1$ the only requirement is that the Re $Z_{\mathrm{L}} > 0$ and Re $Z_{\mathrm{S}} > 0$ which is always true for passive terminations which will be assumed. Hence only Γ_{IN} and Γ_{OUT} remains to be considered.

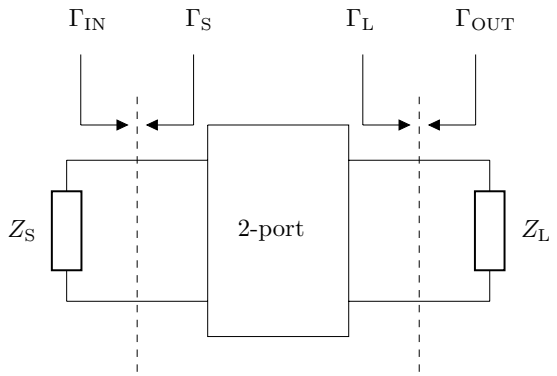

Figure 2.14: All possible reflections in a 2-port which needs to be considered for stability estimations.

The input reflection coefficient Γ_{IN} can be seen as a sum of infinitely many reflections. The first reflection is S_{11}. The second reflection goes through the 2-port and reflects against the load and back again. That gives a contribution of $\mathrm{S}_{21}\Gamma_{\mathrm{L}}\mathrm{S}_{12}$. The third reflection bounces one additional time between the load and the 2-port, which gives an extra contribution of a factor of $\mathrm{S}_{21}\Gamma_{\mathrm{L}}\mathrm{S}_{22}\Gamma_{\mathrm{L}}\mathrm{S}_{12}$. The total expression can be written using a trigonometric sum

$$\begin{aligned}\Gamma_{\mathrm{IN}} &= \mathrm{S}_{11} \\ &+ \mathrm{S}_{21}\Gamma_{\mathrm{L}}\mathrm{S}_{12} \\ &+ \mathrm{S}_{21}\Gamma_{\mathrm{L}}\mathrm{S}_{22}\Gamma_{\mathrm{L}}\mathrm{S}_{12} \\ &+ \mathrm{S}_{21}(\Gamma_{\mathrm{L}}\mathrm{S}_{22})^2\Gamma_{\mathrm{L}}\mathrm{S}_{12} \\ &+ \mathrm{S}_{21}(\Gamma_{\mathrm{L}}\mathrm{S}_{22})^3\Gamma_{\mathrm{L}}\mathrm{S}_{12} + ... \\ &= \mathrm{S}_{11} + \tfrac{\mathrm{S}_{21}\Gamma_{\mathrm{L}}\mathrm{S}_{12}}{1-\Gamma_{\mathrm{L}}\mathrm{S}_{22}},\end{aligned}$$

$$\text{for } |\Gamma_{\mathrm{L}}\mathrm{S}_{22}| < 1.$$

This shows the importance of keeping Γ_{L}, S_{12} and S_{22} as low as possible in order to prevent instability. This also shows the relationship between stability and gain expressed as S_{21}. In the same way an expression for Γ_{OUT} can be derived by just changing S_{11} to S_{22} and Γ_{L} to Γ_{S}. The complete set of inequalities to ensure stability will be:

$$\begin{aligned}|\Gamma_{\mathrm{S}}| &< 1 \\ |\Gamma_{\mathrm{L}}| &< 1 \\ |\Gamma_{\mathrm{IN}}| &= \left|\mathrm{S}_{11} + \tfrac{\mathrm{S}_{21}\Gamma_{\mathrm{L}}\mathrm{S}_{12}}{1-\Gamma_{\mathrm{L}}\mathrm{S}_{22}}\right| < 1 \\ |\Gamma_{\mathrm{OUT}}| &= \left|\mathrm{S}_{22} + \tfrac{\mathrm{S}_{21}\Gamma_{\mathrm{S}}\mathrm{S}_{12}}{1-\Gamma_{\mathrm{S}}\mathrm{S}_{11}}\right| < 1.\end{aligned}$$

The inequalities $|\Gamma_{\mathrm{IN}}| < 1$ and $|\Gamma_{\mathrm{OUT}}| < 1$ can be transformed into a forbidden region for Γ_{L} and Γ_{S} respectively. The inequality $|\Gamma_{\mathrm{IN}}| < 1$ will result in a forbidden region of Γ_{L} given by

$$\left|\Gamma_{\mathrm{L}} - C_{\mathrm{p}}\right| < R,$$

where

$$\begin{aligned}C_{\mathrm{p}} &= \tfrac{(\mathrm{S}_{22}-\mathrm{S}_{11}^{*}\Delta)^{*}}{|\mathrm{S}_{22}|^2-|\Delta|^2} \\ R &= \left|\tfrac{\mathrm{S}_{12}\mathrm{S}_{21}}{|\mathrm{S}_{22}|^2-|\Delta|^2}\right| \\ \Delta &= \mathrm{S}_{11}\mathrm{S}_{22} - \mathrm{S}_{12}\mathrm{S}_{21},\end{aligned}$$

which can be seen as a circle in the Smith chart with center point C_{p} and radius R according to Figure 2.15. In an analog way the forbidden region for Γ_{S} can be derived.

Date 2013-06-18 | Issue A | Document ID 87/03631-1/FCK11507
Issued by
OEGPU Viktor Hallman, Erik Sanford
Classification Company Confidentially
COMPANY UNCLASSIFIED
Classification Export Control
NOT EXPORT CONTROLLED
Classification Defence Secrecy
ÖPPEN/UNCLASSIFIED

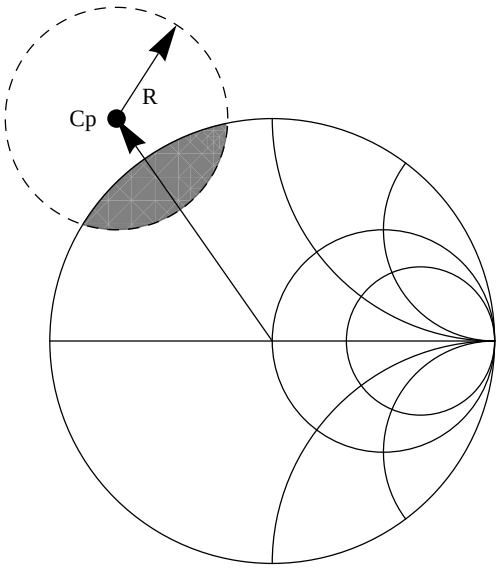

Figure 2.15: Forbidden region for Γ_{L} assuming passive termination ($|\Gamma_{\mathrm{L}}| < 1$)

All criteria above can be expressed using one criterion called the K factor,

$$\begin{aligned} \mathrm{K} &= \frac{1-|\mathrm{S}_{11}|^2-|\mathrm{S}_{22}|^2+|\Delta|^2}{2|\mathrm{S}_{21}\mathrm{S}_{12}|} \\ \Delta &= \mathrm{S}_{11}\mathrm{S}_{22} - \mathrm{S}_{12}\mathrm{S}_{21}. \end{aligned}$$

In order to ensure stability another stability measure B1 is used. B1 is also called the auxiliary stability factor and is defined as

$$\begin{aligned} \mathrm{B1} &= 1 + |\mathrm{S}_{11}|^2 - |\mathrm{S}_{22}|^2 - |\Delta|^2 \\ \Delta &= \mathrm{S}_{11}\mathrm{S}_{22} - \mathrm{S}_{12}\mathrm{S}_{21}. \end{aligned}$$

In general, stability can be categorised into one of the following groups:

- Unstable $\mathrm{K} < 1$ and $\mathrm{B1} < 0$
- Conditionally stable $\mathrm{K} < 1$ and $\mathrm{B1} > 0$
- Unconditionally stable $\mathrm{K} > 1$ and $\mathrm{B1} > 0$

where the state conditionally stable means the stability is dependent on the load.

2.3.2 Classes of amplifiers

There are many different types of amplifiers and it is of great importance to know the advantages and disadvantages of the main types before starting the design. Amplifiers are divided into different classes based on the conduction angle θ_c when a sinusoidal signal is considered. The conduction angle describes how many degrees of a cycle the transistor is conducting.

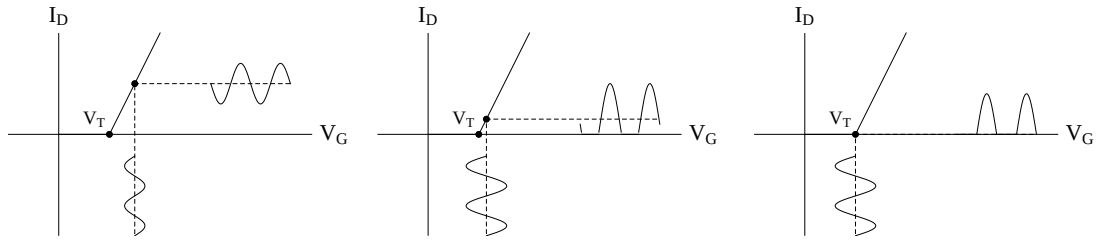

(a) Class A bias having a conduction angle of 360°

(b) Class AB bias having a conduction angle of $180^\circ < \theta_c < 360^\circ$

(c) Class B bias having a conduction angle of 180°

Figure 2.16: Different amplifier configurations

2.3.2.1 Class A A class A amplifier has a conduction angle of 360° and is therefore conducting through the whole cycle and the resulting output will theoretically be a pure sinusoidal wave according to Figure 2.16a. That is accomplished by choosing the gate bias point V_{GS} large enough to fulfill $(V_{GS} - V_{gs}) > V_T$ where V_{gs} is the amplitude of the input signal at the gate and V_T is the transistor voltage threshold.

2.3.2.2 Class AB As the name implies class AB amplifier can be seen as a hybrid of a class A and a class B amplifier with a conduction angle $180^\circ < \theta_c < 360^\circ$. The amount of harmonics are lower than a class B amplifier since the output is more like a pure sinusoidal signal and the efficiency is better than class A amplifier.

2.3.2.3 Class B In a class B amplifier the transistor is switched off during half the cycle. This is achieved by choosing the gate bias to V_T where V_T is the threshold voltage which defines the threshold where the transistor enters the conducting state, illustrated in Figure 2.16c. A single transistor biased in class B will produce an output shown in Figure 2.16c.

By using two transistors biased in class B together in a push-pull configuration, shown in Figure 2.17, the nonlinearity will be compensated. Each transistor will be conducting half a period and in that way cover the whole period. The total output will be the difference of the two outputs.

One great advantage using a class B amplifier in a push-pull configuration is the fact that the second harmonic will be canceled out due to the way the output is composed. The output from

Date 2013-06-18 | Issue A | Document ID 87/03631-1/FCK11507
Issued by
OEGPU Viktor Hallman, Erik Sanford
Classification Company Confidentially
COMPANY UNCLASSIFIED
Classification Export Control
NOT EXPORT CONTROLLED
Classification Defence Secrecy
ÖPPEN/UNCLASSIFIED

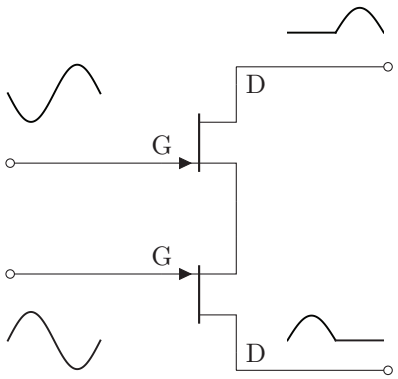

Figure 2.17: Push-pull amplifier biased in class B having two inputs phase separated by 180°. The resulting output is seen as the difference of the two outputs.

each transistor will have a 180° phase difference at the output at the fundamental. At the second harmonic this phase shift will correspond to a 360° phase shift since the frequency is doubled. That means the second harmonic of the outputs will be in phase and therefore not contribute to the total differential output. Instead the second harmonic will contribute to the common mode output where the signals are driven in phase instead. In a similar way the third harmonics ($f = 3f_0$) of the two branches will have a phase shift of $3 \cdot 180°$ and are therefore out of phase which means they will contribute to the differential mode in the same way the fundamental frequency does.

In case the conduction angle is less than 180° the total output will be distorted according to Figure 2.18, where part of the period none of the transistors are conducting[23].

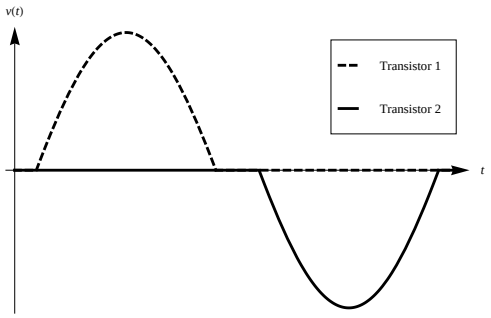

Figure 2.18: Showing the contribution of each transistor to the total output in a push-pull amplifier when the conduction angle is less than 180°. Part of the cycle no transistor will be conducting and the distortion is called crossover distortion.

Date 2013-06-18 | Issue A | Document ID 87/03631-1/FCK11507
Issued by
OEGPU Viktor Hallman, Erik Sanford
Classification Company Confidentially
COMPANY UNCLASSIFIED
Classification Export Control
NOT EXPORT CONTROLLED
Classification Defence Secrecy
ÖPPEN/UNCLASSIFIED

3 Design

In this section the design of the antenna-amplifier system under investigation will be described. First of all, the antenna design will be presented. The antenna simulations and measurements resulted in impedance parameters that was then used in the amplifier design for optimisation. The antenna simulations were carried out in *Ansys HFSS* and the amplifier simulations were carried out in *AWR Microwave Office*. All prototypes of the antenna as well as all the amplifier parts were built and measured at the Saab AB facility in Lackarebäck, Sweden.

3.1 Design of antenna

In this section the design of a TASH antenna and a biconical antenna will presented. The first antenna to be designed was the TASH. Despite initial promising results from simulations and prototyping, the TASH was left behind in order to avoid any potential patent intrusion. Then a biconical antenna was designed. The biconical antenna is such a fundamental antenna element that patent intrusion is out of the question.

Throughout all simulations the overall goal has been to design a wideband omnidirectional antenna that should be easy to match from the amplifier's point of view, which led to the pursuit of an antenna input impedance of low variation. Since the impedance of the antenna element and its feeding later was going to be used as an end load for the optimisation of the amplifier, a short distance between the antenna and amplifier was desired in order to reduce the error in the matching network, as described in section 2.1.3.2. That the antenna should be electrically small has also been kept in mind, in order to result in a compact final solution. The investigation of the input impedance as well as the behaviour of reflection coefficients was made as a measure of goodness concerning the capabilities of matching. That the antenna reactance should be close to zero was also taken into account, since the reactance does not contribute to any radiation in the far-field.

Along the design process many antennas have been simulated in *Ansys HFSS*, built and eventually measured to confirm the simulated data. Most of the data post processing has been carried out using *MATLAB*, but also with the built in computational framework of *HFSS*.

3.1.1 Design of the TASH antenna

The behaviour of S_{11} at the TASH feeding that is presented in the second article of Warnagiris [19], is shown in Figure 3.1.

As an initial investigation the design from the article was followed, with the deviation that the lowest frequency of operation being 400 MHz instead of 225 MHz, in favor of size reduction. In

Date 2013-06-18 | Issue A | Document ID 87/03631-1/FCK11507
Issued by
OEGPU Viktor Hallman, Erik Sanford
Classification Company Confidentially
COMPANY UNCLASSIFIED
Classification Export Control
NOT EXPORT CONTROLLED
Classification Defence Secrecy
ÖPPEN/UNCLASSIFIED

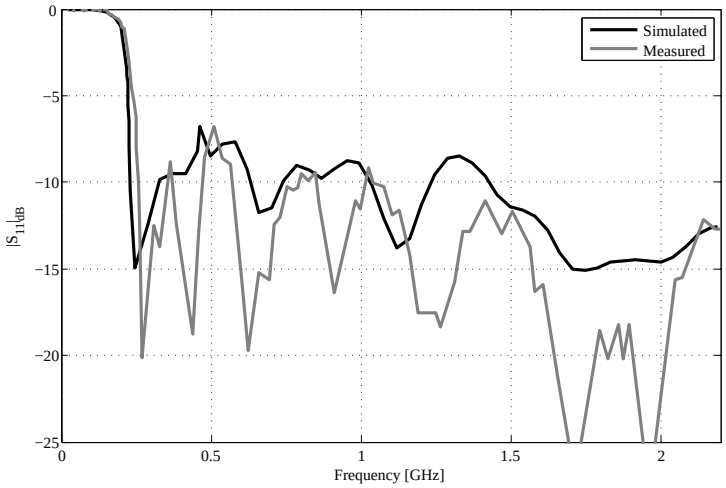

Figure 3.1: Simulated and measured $|S_{11}|$ frequency response presented in [18]

Figure 3.2 the simulated and measured S_{11} values of the designed TASH are shown. The simulated model and its reality counterpart are shown in Figure 3.3.

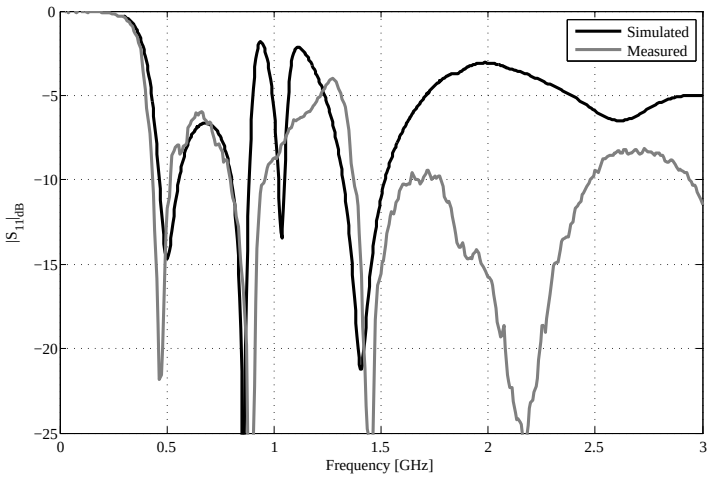

Figure 3.2: Simulated and measured $|S_{11}|$ frequency response of the designed TASH antenna

As with the data presented in the article, the overall resemblance between simulated and measured curves is acceptable with the exception of some resonances. If one compare the data in Figure 3.1 and 3.2 there are actually significant differences. The level of $|S_{11}|$ is higher for the TASH of this project than in the article, both simulated and measured. Also the shape of the curves in Figure 3.1 and 3.2 differs. That the differences in the data are greater between the two

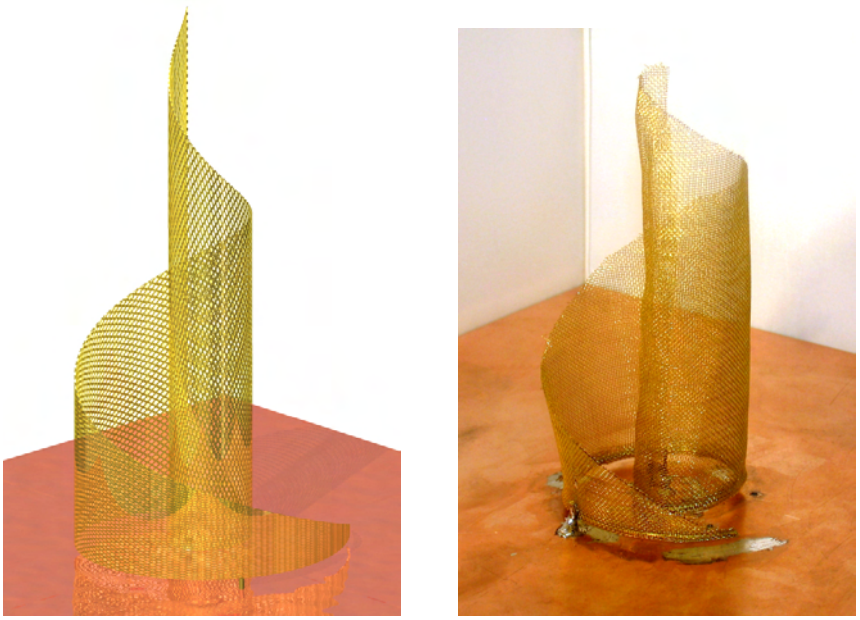

(a) **(b)**

Figure 3.3: (a) The simulated antenna model and (b) the manufactured counterpart. The rendering of the model has been made in *Autodesk Inventor*.

TASH antennas than the difference between simulated and measured data belonging to them respectively, could be a sign of the antennas not being completely coinciding in their designs. The difference between simulated and measured data of this project is most likely due to that the overall behaviour of the TASH antenna is quite sensitive to any change of parameters. Since the TASH construction was not done with exceptional precision, the risk of behavioural alteration was prominent. The goal of the realisation though was merely to roughly verify the simulations, which was the reason why not too much time was spent on constructing the antenna perfectly.

To further enhance the TASH for the purpose of the project, some parametric sweeps and optimisation with *HFSS* were made. In his article, Warnagiris is stating that one of the most relevant parameter when it comes to altering the antenna impedance, is the position of the feeding point and the grounding point. Therefore, the positions of the two points were swept and the standard deviation of the impedance in the interval 400 MHz to 1.6 GHz was analysed. In Figure 3.4 the standard deviation is shown as a function of the different combinations of feeding and grounding points. The plot is based on interpolations from 56 simulated values.

The blank diagonal area in the plot represents the case of feeding and grounding point being too close to each other, which would yield short circuit and no radiation. To set up a condition for what is "too close" was in this case somewhat arbitrary and should perhaps be investigated more carefully. The boundaries of the short circuit region should therefore merely be looked upon as

Date 2013-06-18 | Issue A | Document ID 87/03631-1/FCK11507
Issued by
OEGPU Viktor Hallman, Erik Sanford
Classification Company Confidentially
COMPANY UNCLASSIFIED
Classification Export Control
NOT EXPORT CONTROLLED
Classification Defence Secrecy
ÖPPEN/UNCLASSIFIED

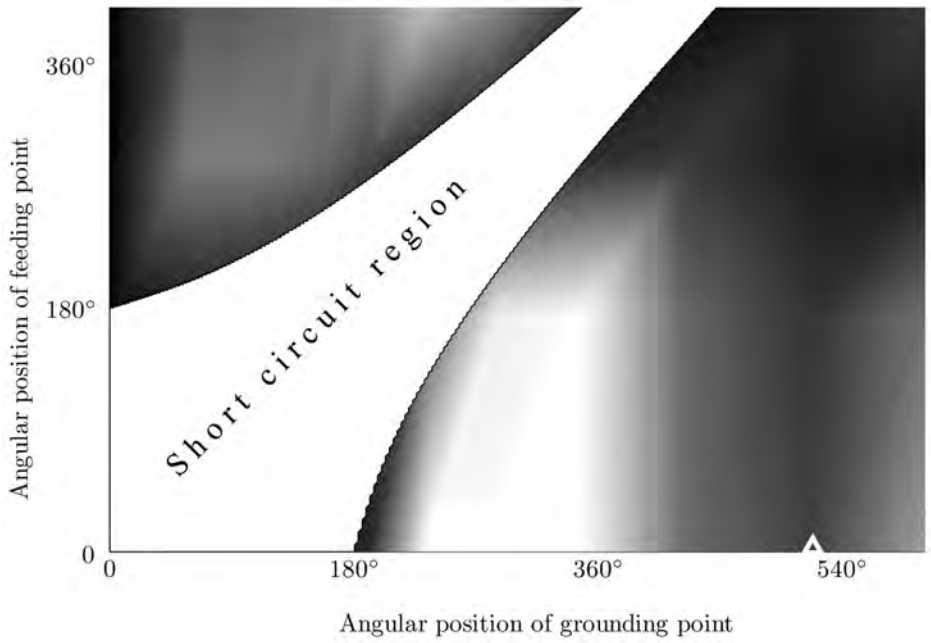

Figure 3.4: Standard deviation as a function of the angular position of the feeding and grounding wires on the TASH base spiral. White indicates a high standard deviation, whereas black indicates low standard deviation. The combination of positions given by the article is marked by a white triangle in the plot. The blank region indicates the angular positions that yield too short distance between the feeding and grounding point. A too short distance will result in short circuit and no radiation.

guidelines for the appearance of the area. The point marked with a triangle shows the design positions proposed in the article. The regime of low standard deviation above the triangle was chosen as a starting guess for the *HFSS* simulations aiming to optimise the feeding and grounding positions. In addition to low standard deviation, a mean input impedance of 20 Ω was put as an optimisation goal. The reason for choosing 20 Ω was primarily that it would be closer to the impedance that the transistors wanted to see than the conventional 50 Ω, which would then yield a less complex matching network at the amplifier side. On the other hand, if the impedance goal was set too low, there was a risk of making the optimiser favorise conditions similar to short circuit.

In Figure 3.5, the Smith chart representation of the normalised antenna impedance of the original TASH and the improved one are shown. The position of the feeding pin is 355° from the center point and 470° for the grounding pin. As can be seen, the length of the trace as well as its spreading over the chart is substantially smaller for the improved antenna, which would yield an easier matching of the antenna.

Despite the initial promising results of the improved TASH antenna, the decision to abandon it was taken due to uncertainty concerning the legal aspect of patent intrusion that could have been

Date 2013-06-18 | Issue A | Document ID 87/03631-1/FCK11507
Issued by
OEGPU Viktor Hallman, Erik Sanford
Classification Company Confidentially
COMPANY UNCLASSIFIED
Classification Export Control
NOT EXPORT CONTROLLED
Classification Defence Secrecy
ÖPPEN/UNCLASSIFIED

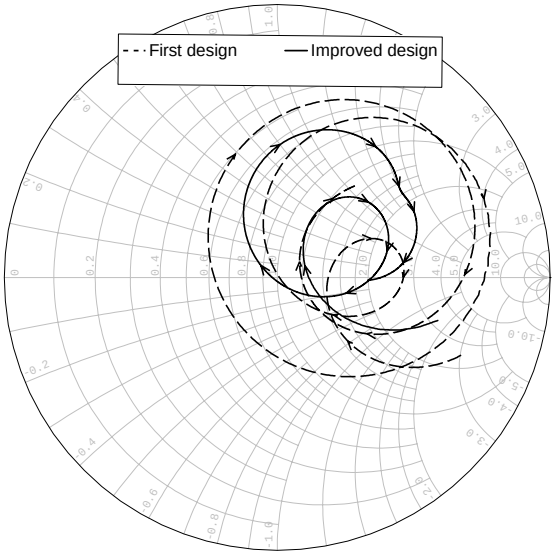

Figure 3.5: The normalised antenna impedance of the original TASH and the improved one

a matter of attention if the TASH was put into production.

3.1.2 Design of the biconical antenna

When the TASH was left behind the antenna focus was shifted to another omnidirectional antenna, the biconical antenna. Since the biconical antenna is such a fundamental and well investigated antenna, there is no reason to fear any patent intrusion.

The final aim of the simulations was always to investigate the biconical antenna with a balanced feeding. However, in order to make in process measurements, the initial design was made with a monocone placed over a conducting ground plane. The gain of doing so was not only to enable measurements in the familiar 50 Ω environment, but the problem for *HFSS* to solve was reduced by a factor of two compared to the biconical case.

To make sure that a cone could be simulated and built with matching results, a solid shell cone with cone angle α_{cone} being 45° and top cone angle α_{top} being 90° was investigated. According to Kraus [12], these design parameters are typical ones for biconical antennas. In Figure 3.6 the simulated and the built cone is shown.

At the first instance the antenna feeding was modeled with a lumped port in *HFSS*. When doing the measurements it became clear that something was not modeled correctly enough according to what was actually built. It was soon to be discovered that a more accurate modeling of the point of feeding was needed in order to get acceptable resemblance between simulated and measured data. The solution was to use the concept of wave port excitation instead of lumped port when

Date 2013-06-18 | Issue A | Document ID 87/03631-1/FCK11507
Issued by
OEGPU Viktor Hallman, Erik Sanford
Classification Company Confidentially
COMPANY UNCLASSIFIED
Classification Export Control
NOT EXPORT CONTROLLED
Classification Defence Secrecy
ÖPPEN/UNCLASSIFIED

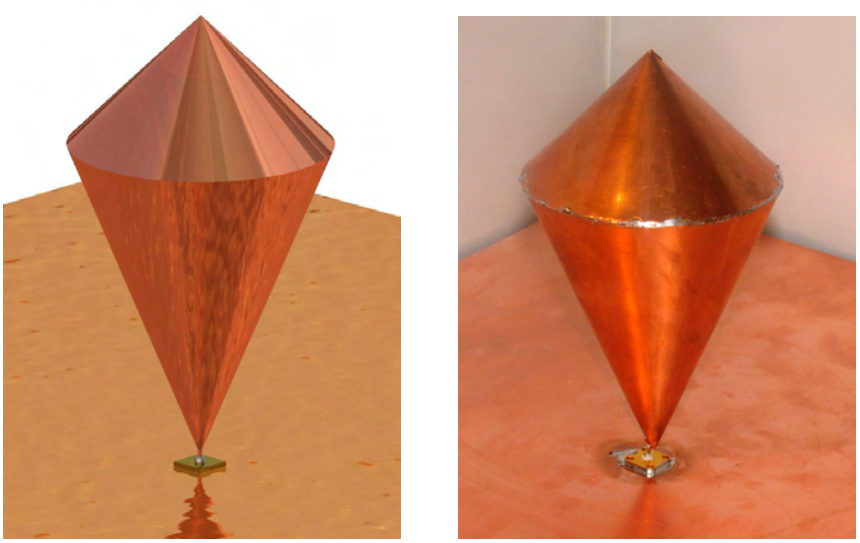

(a) **(b)**

Figure 3.6: (a) The simulated antenna model and (b) the manufactured counterpart. The rendering of the model has been made in *Autodesk Inventor*.

modeling. The difference can be seen in Figure 3.7. More on how to model the feeding excitation can be found in Appendix A.

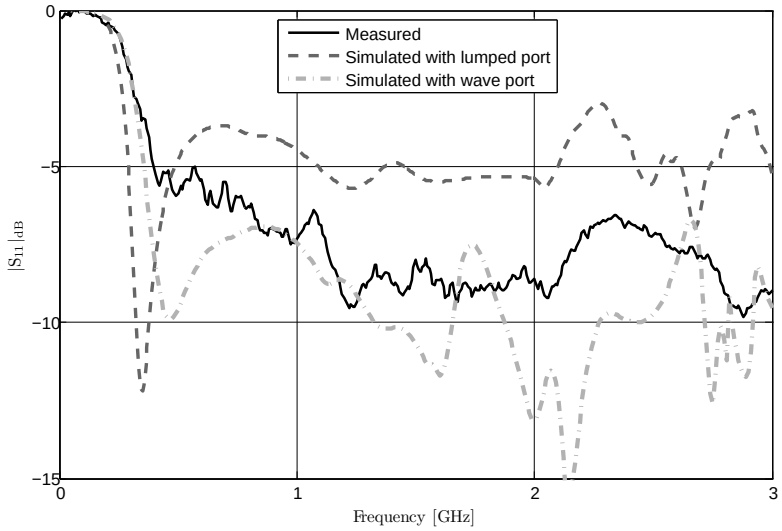

Figure 3.7: Simulated $|S_{11}|$ with lumped port and wave port excitation along with the measured data

From theory it is clear that the standard deviation of the biconical antenna input impedance is decreasing when α_{cone} is increasing. As previously stated, an impedance with low standard deviation

and a value close to around 20 Ω instead of the traditional 50 Ω would reduce the complexity of the matching network needed between the antenna and the amplifier. In order to combine these two desired features of the antenna impedance into one variable to analyse, it is convenient to define a reflection coefficient Γ_{A} for the antenna as

$$\Gamma_{\mathrm{A}} = \frac{Z_{\mathrm{A}} - Z_{\mathrm{d}}}{Z_{\mathrm{A}} + Z_{\mathrm{d}}},$$

where Z_{A} is the impedance of the antenna and Z_{d} is the desired goal impedance, which in this case is 20 Ω. Three primary measures of goodness concerning Γ_{A} was used during the simulations: the length Λ and spreading ς of the Γ_{A} curve in the Smith chart and the mean magnitude of Γ_{A}, defined as

$$\overline{|\Gamma_{\mathrm{A}}|} = \frac{1}{N} \sum_{f=f_{\min}}^{f_{\max}} |\Gamma_{\mathrm{A}(f)}|,$$

where N is the number of sampling points in the frequency interval $[f_{\min}, f_{\max}]$. The spreading ς is defined as

$$\varsigma = (\max \mathrm{Re}\,\Gamma_{\mathrm{A}} - \min \mathrm{Re}\,\Gamma_{\mathrm{A}}) \cdot (\max \mathrm{Im}\,\Gamma_{\mathrm{A}} - \min \mathrm{Im}\,\Gamma_{\mathrm{A}}).$$

One way of looking upon ς is simply as the area of the rectangle enclosing Γ_{A} in the Smith chart. The reason why ς is of interest is that it complements Λ in the way that even if Λ would be infinitely large, a Γ_{A} that is concentrated to one point in the Smith chart would turn out to be of interest according to ς. An illustration of the parameters Λ, ς and $\Gamma_{\mathrm{A},f}$ is shown in Figure 3.8.

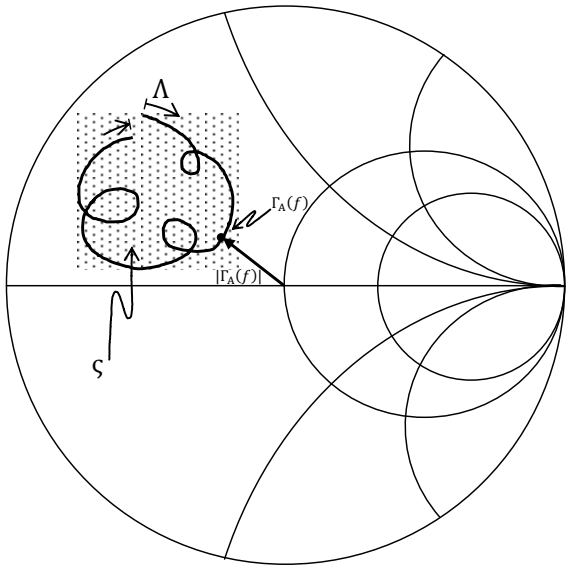

Figure 3.8: The parameters used during the antenna simulation. The area ς of the square is enclosing the curve consisting of the points $\Gamma_{\mathrm{A},f}$ having a length of Λ.

Date 2013-06-18 | Issue A | Document ID 87/03631-1/FCK11507
Issued by
OEGPU Viktor Hallman, Erik Sanford
Classification Company Confidentially
COMPANY UNCLASSIFIED
Classification Export Control
NOT EXPORT CONTROLLED
Classification Defence Secrecy
ÖPPEN/UNCLASSIFIED

To investigate the impact of different α_{cone} on the behaviour of the antenna, model variations with α_{cone} between 10° and 145° was simulated. During the simulations the slant height l, defined as in the theory chapter, was kept constant. The frequency interval of interest was 750 MHz to 3 GHz during all biconical investigations.

In literature, the guidelines for how to choose α_{top} are very vague. To determine the influence of α_{top}, every cone angle simulation was carried out with α_{top} being 90°, 110°, 130° and 150°. In Figure 3.9, Λ as a function of α_{cone} is presented. As can be observed, Λ is decreasing up to the point where $\alpha_{\text{cone}} \approx 110°$, but then rapidly increases.

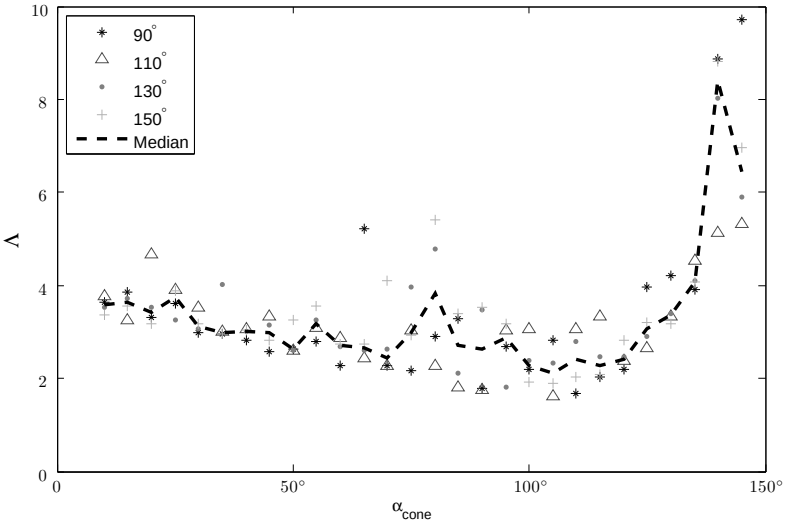

Figure 3.9: The length Λ of the curve of Γ_{A} when it is represented in the Smith chart as a function of α_{cone}

The spreading ς, plotted in Figure 3.10, also shows similar behaviour to Λ with a minimum between $\alpha_{\text{cone}} = 105°$ and $\alpha_{\text{cone}} = 135°$.

When it comes to the mean magnitude of Γ_{A}, which primarily serves as a measure of how close the antenna impedance and goal impedance are to each other, the relationship to α_{cone} is quite trivial as can be seen in Figure 3.11. The mean magnitude of Γ_{A} is monotonically decreasing when α_{cone} is increasing.

Another parameter that had to be taken into account was the degree of which the antenna was presenting an omnidirectional radiation pattern. To analyse this, the mean directivity $\overline{D}$ in the φ-plane with θ being 45° and 90° was plotted as a function of α_{cone}, as depicted in Figure 3.12.

As can be seen in the figure, $\overline{D}$ approaches a value of around 3.5 when α_{cone} is close to 0 and θ is 90°. This is not exactly what is expected since D_{max} for a $\lambda/4$ monopole over a ground plane is 3.2 theoretically. The reason for this difference in directivity could be that the small angled cone is not uniformly thick as a true monopole is. The two curves presented in the figure show how the density of the directivity is somewhat shifted from the azimuth plane towards a higher elevation

Date 2013-06-18 | Issue A | Document ID 87/03631-1/FCK11507
Issued by
OEGPU Viktor Hallman, Erik Sanford
Classification Company Confidentially
COMPANY UNCLASSIFIED
Classification Export Control
NOT EXPORT CONTROLLED
Classification Defence Secrecy
ÖPPEN/UNCLASSIFIED

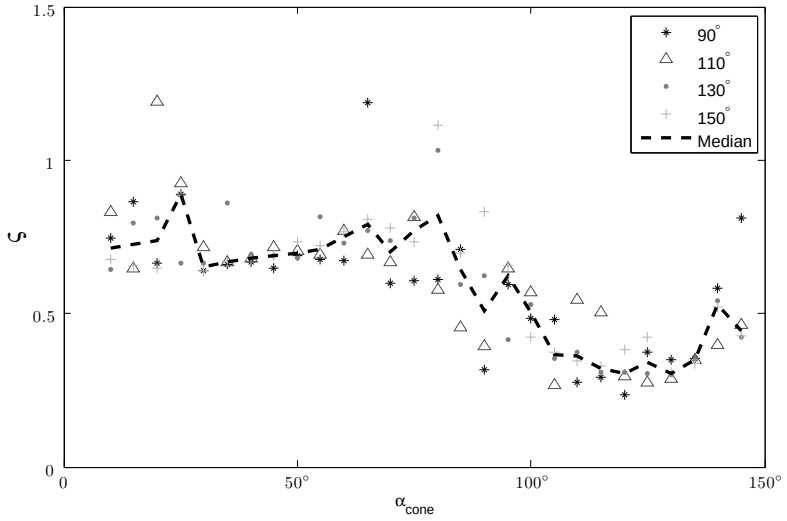

Figure 3.10: The spreading ς of the curve of Γ_A when it is represented in the Smith chart as a function of α_{cone}

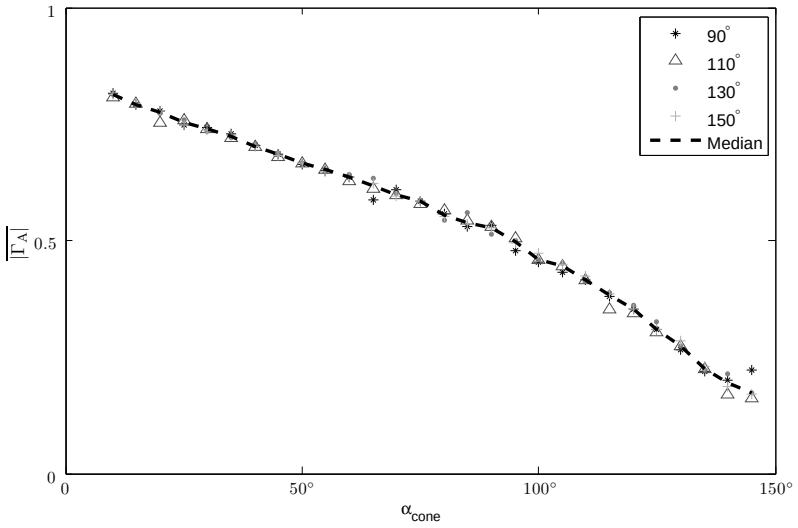

Figure 3.11: The mean magnitude of Γ_A as a function of α_{cone}

angle. For the purpose of this project, this change in directivity was not severe enough for any further considerations with respect to α_{cone} to be taken.

From the data presented in Figure 3.9, 3.10 and 3.11, it was clear that an α_{cone} of 110° would be suitable for the continued design. The data also gives a hint of that the chosen value of α_{top} is rather uncorrelated to the behavior of the antenna characteristics. Primarily, in order to keep the

Date 2013-06-18 | Issue A | Document ID 87/03631-1/FCK11507
Issued by
OEGPU Viktor Hallman, Erik Sanford
Classification Company Confidentially
COMPANY UNCLASSIFIED
Classification Export Control
NOT EXPORT CONTROLLED
Classification Defence Secrecy
ÖPPEN/UNCLASSIFIED

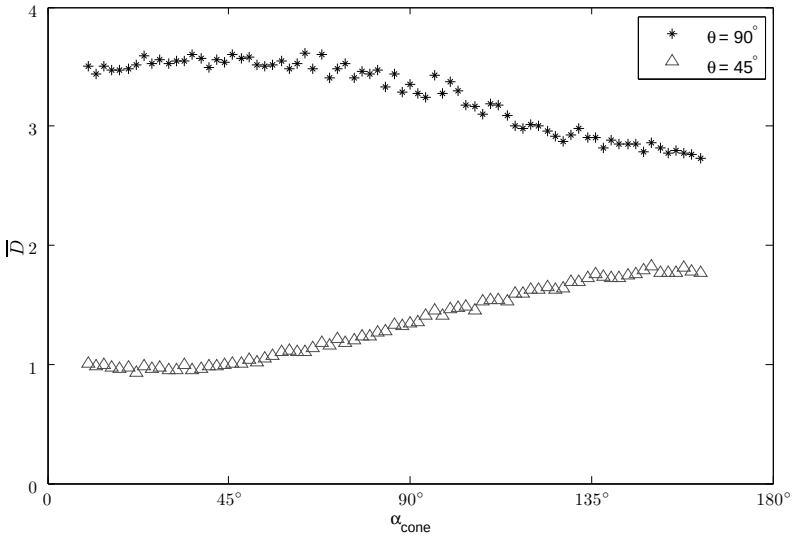

Figure 3.12: The mean directivity of the simulated monocone in the φ-plane as a function of α_{cone}

antenna size down, α_{top} was chosen to be 140°. More data to support the choice of α_{cone} and α_{top} is to be found in Appendix C.1.

Since the overall aim of the project was to closely integrate the antenna with the amplifier, it was clear that a lightweight antenna would reduce mechanical stress on the microstrip connecting the amplifier to the antenna. Therefore the approach of cones built up by wires was investigated. First of all, an eight wire cone with the previously deduced angles was simulated and built as depicted in Figure 3.13.

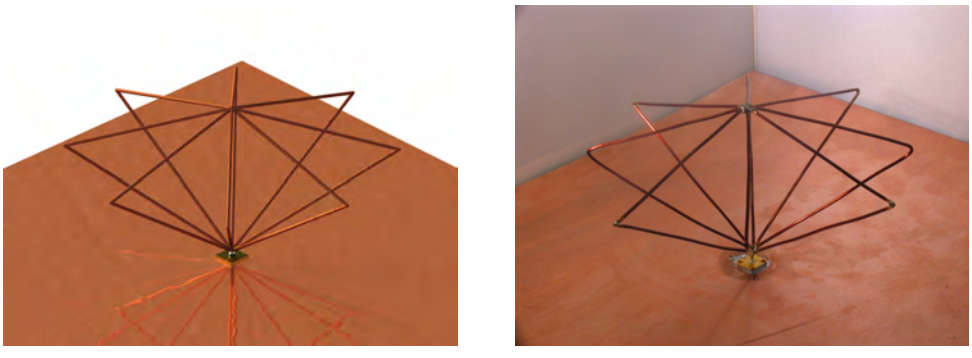

(a) **(b)**

Figure 3.13: (a) The simulated wire cone model and (b) the constructed counterpart. The rendering of the model has been made in *Autodesk Inventor*.

The $|S_{11}|$ frequency response of the simulated and the manufactured wire cone, along with the

Date 2013-06-18 | Issue A | Document ID 87/03631-1/FCK11507
Issued by
OEGPU Viktor Hallman, Erik Sanford
Classification Company Confidentially
COMPANY UNCLASSIFIED
Classification Export Control
NOT EXPORT CONTROLLED
Classification Defence Secrecy
ÖPPEN/UNCLASSIFIED

simulated solid cone, is shown in Figure 3.14. As can be seen in the figure, there is a resonance

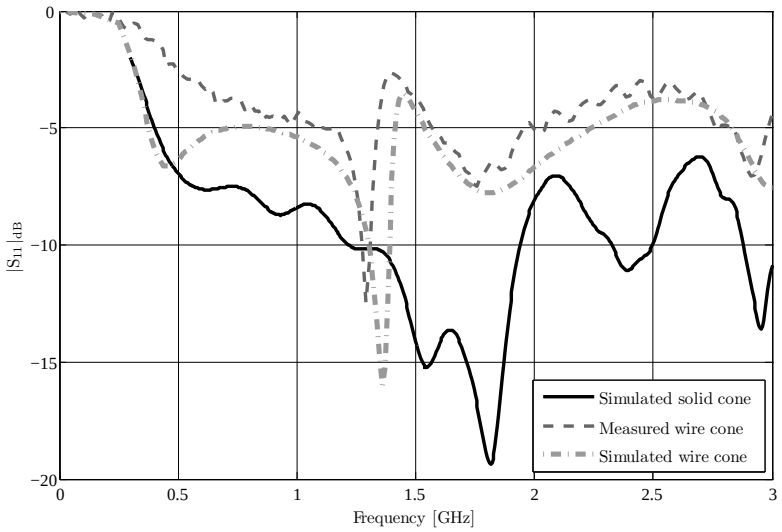

Figure 3.14: The $|S_{11}|$ frequency response of the simulated wire cone, the manufactured wire cone and the simulated solid cone

at 1.3 GHz with the wire cone that was not to be seen in the solid cone case. To analyse this more thoroughly, simulations were made with a solid cone and a wire cone at α_{cone} being 45° and 110° respectively. The simulation result of the resistance of each antenna is depicted in Figure 3.15.

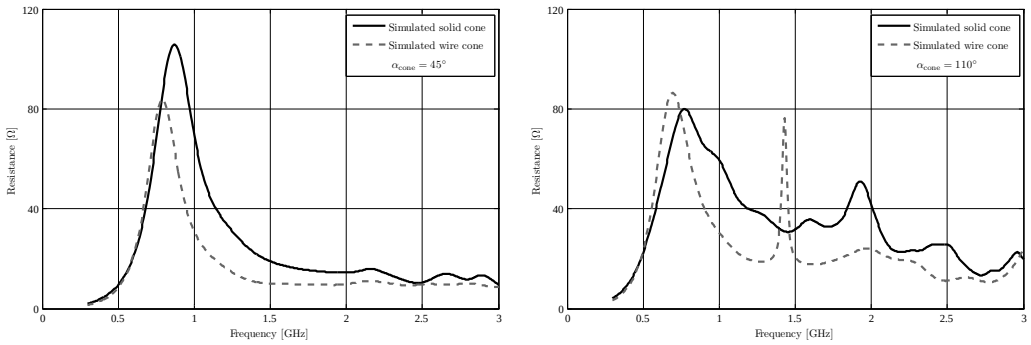

(a) **(b)**

Figure 3.15: The simulated antenna input resistance of the eight wire cone versus the solid cone for when α_{cone} is (a) 45° and (b) 110°

In the graphs it can be observed that the eight wire cone is a good approximation of the solid cone in the small angle case, but for the cone with large angle the wire approximation introduce an unwanted resonance as previously stated. A guess of why this behaviour arose is that the density

Date 2013-06-18 | Issue A | Document ID 87/03631-1/FCK11507
Issued by
OEGPU Viktor Hallman, Erik Sanford
Classification Company Confidentially
COMPANY UNCLASSIFIED
Classification Export Control
NOT EXPORT CONTROLLED
Classification Defence Secrecy
ÖPPEN/UNCLASSIFIED

of wires in the cone decreased when the cone angle increased, given that the number of wires was kept constant. In Figure 3.16 the results from simulations aiming to verify this guess is presented. In the figure, the input resistance at the antenna is shown as a function of frequency and the amount

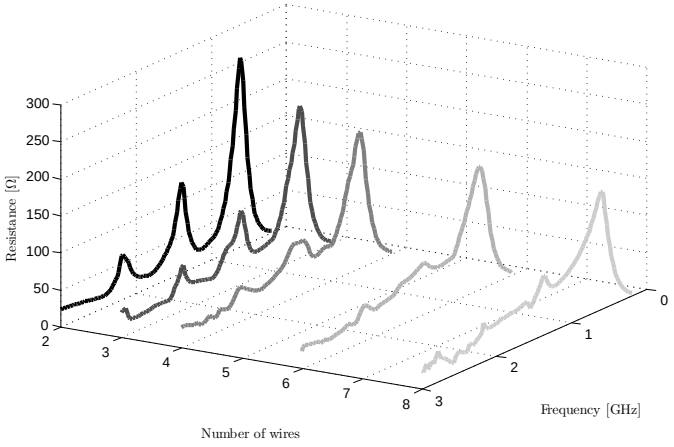

Figure 3.16: The results from simulating the 110° wire cone with different amount of wires

of wires in the model. From the data it is clear that a greater number of wires will even out the unwanted resonances. This is in line with that the solid cone, that in this case represents the case when the amount of wires goes towards infinity, is free from these resonances.

The idea of using wires instead of a solid construction was eventually left behind due to several reasons, the most prominent maybe being the resonances as previously explained. That the computational effort in *HFSS* was increased when wires were used also contributed to the degradation of the wire alternative. The insight of that the same net material used for the TASH antenna also could be used for the cone, made the lightweight argument not so strong. Another advantage of using the net was that the construction of the cone became much easier.

The next thing that had to be done was to design and simulate the transition between both of the antenna cones and the matching network of the amplifier. Both the fact that any element of metallic properties close to the antenna changes the antenna characteristics, and the fact that a short transition from the antenna to the amplifier reduces the matching complexity and loss of the system, had to be accounted for when determining the design.

In order to determine the widths and thereby the impedances of the transmission lines, the input impedance of the antenna when fed by a copper pad had to be known. To find this out, a simple model with an antenna and a feeding transmission line with a pad was simulated and built as shown in Figure 3.17.

The data obtained was from the interface with the SMA connector, meaning in this case 10 cm away from the antenna. The strip was made to be 10 cm away from the antenna in order to enable measurements without interfering with the antenna too much. As can be seen in the Smith chart

Date 2013-06-18 | Issue A | Document ID 87/03631-1/FCK11507
Issued by
OEGPU Viktor Hallman, Erik Sanford
Classification Company Confidentially
COMPANY UNCLASSIFIED
Classification Export Control
NOT EXPORT CONTROLLED
Classification Defence Secrecy
ÖPPEN/UNCLASSIFIED

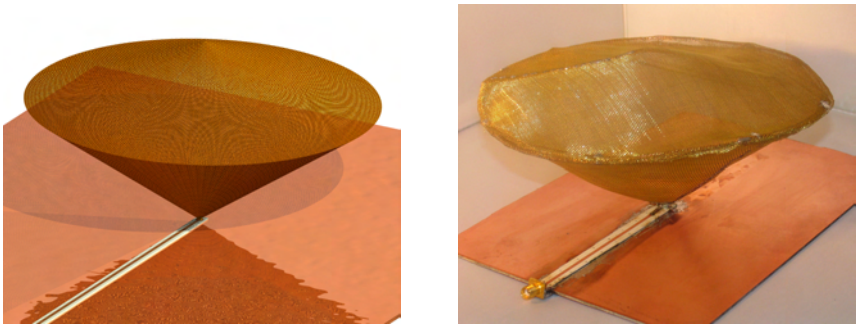

(a) (b)

Figure 3.17: The net cone antenna, (a) simulated and (b) constructed in order to determine the input impedance the antenna had when fed by a copper strip. The rendering of the model has been made in *Autodesk Inventor*.

of Figure 3.18, the impedance is circulating a point corresponding to approximately 40 Ω. From this the decision was taken to design the transmission line between the antenna and the amplifier matching network to present an impedance of 40 Ω.

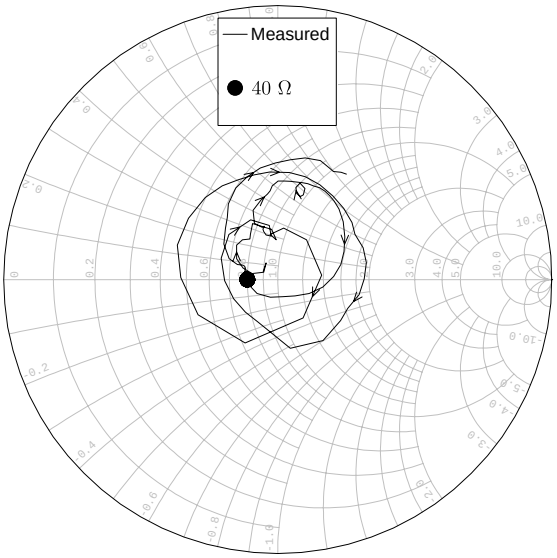

Figure 3.18: The impedance of the copper pad fed antenna at the SMA intersection

The idea of the transition was to let two separate transmission lines, coming from individual transistors, both climb upon a substrate perpendicular to the amplifier substrate and there start to couple to each other instead of to a ground plane. When at perpendicular substrate the two lines would feed one antenna cone each, as can be seen in the final design at page 44. The thickness of the perpendicular substrate was also a somewhat delicate matter. From simulations and theory it

Date 2013-06-18 | Issue A | Document ID 87/03631-1/FCK11507
Issued by
OEGPU Viktor Hallman, Erik Sanford
Classification Company Confidentially
COMPANY UNCLASSIFIED
Classification Export Control
NOT EXPORT CONTROLLED
Classification Defence Secrecy
ÖPPEN/UNCLASSIFIED

was clear that that the separation of the two antenna cones should be as small as possible. On the other hand, when the two couple strip lines are put closer together their widths must be decreased in order to present the same impedance. When decreasing the width, the power delivery capability will decrease, as will be described in Section 3.2.6 on page 62. This is highly undesirable in a high power system. Also, when having a thin substrate the mechanical stability will not be as prominent. The simple solution to this dilemma was to use the same substrate thickness as with the amplifier itself, which minimised the manufacturing effort. In Figure 3.19 the design of the transition is shown. The widths of the transmission lines was calculated using *AWR Microwave Office*.

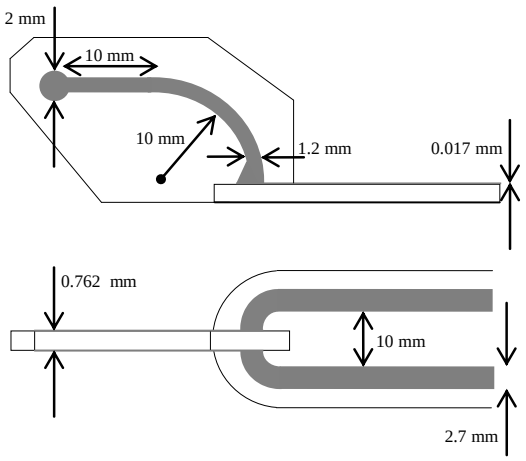

Figure 3.19: The design of the transition between the antenna and the amplifier

When the design of the transition was determined, the complete antenna-transition part with the amplifier shielding box and cooling block had to be simulated, in order to obtain an accurate antenna impedance as possible with respect to the surrounding environment. Also the radiation pattern would be affected by the presence of the metallic objects.

Since harmonics of the fundamental frequency was considered on the amplifier side, the simulated feeding of the antenna had to be done in both differential and common mode. The difference between the two modes is that the transmission lines are fed in phase during common mode and out of phase in differential mode. The simulated model is depicted in Figure 3.20 and the resulating common and differential mode impedance is plotted in the Smith chart of Figure 3.21.

Date 2013-06-18 | Issue A | Document ID 87/03631-1/FCK11507
Issued by
OEGPU Viktor Hallman, Erik Sanford
Classification Company Confidentially
COMPANY UNCLASSIFIED
Classification Export Control
NOT EXPORT CONTROLLED
Classification Defence Secrecy
ÖPPEN/UNCLASSIFIED

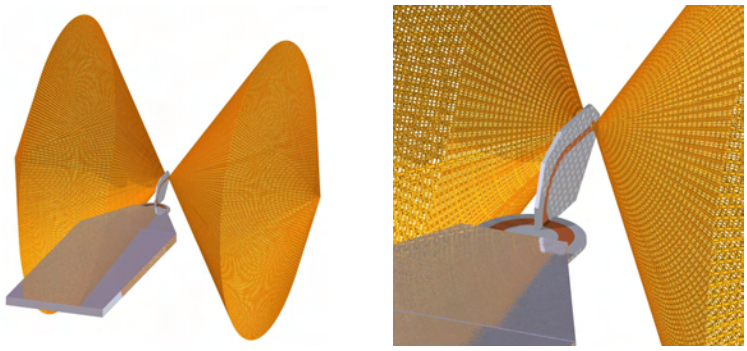

(a) (b)

Figure 3.20: The final model simulated in *HFSS* from a distance and zoomed in. The rendering of the model has been made in *Autodesk Inventor*.

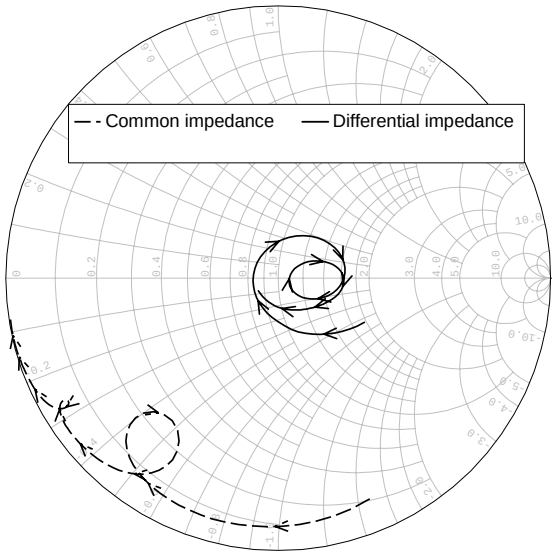

Figure 3.21: The common and differential mode impedance of the antenna with transition and the amplifier shielding box in the vicinity

3.2 Design of amplifier

Besides undesirable coupling, there is only one interface between the amplifier and the antenna. Therefore, technically the co-design will all be about that interface and to find out what impedance that is suitable for the amplifier and what impedances that is possible to achieve with the antenna.

In practice, the amplifier part of the co-design also includes the physical dimension of the amplifier. Since the antenna is supposed to be mounted directly at the output of the amplifier there are restrictions on the dimensions of the amplifier in order to make the mounting possible. The design will be based on two 35 W CREE GaN HEMT transistors in a push-pull configuration and all simulations will be performed in *AWR Microwave office*. The frequency range is from 750 MHz to 3 GHz and some main topic in the amplifier design chapter will be:

Unbalanced to balanced The push-pull configuration requires a signal splitter having a phase separation of 180°. Three different techniques to accomplish this have been studied during this project.

Impedance transformation In order to have the optimal impedance at the input and output of the transistors impedance transformation networks are used which could be constructed in many different ways using many different techniques.

Antenna representation The design is based on the simulated impedances of the antenna. Therefore, the impedances play an important role in the co-design process.

3.2.1 Unbalanced to balanced

In a push-pull design the input signal is divided into two branches having a phase difference of 180°. To split the signal into the branches a balun is used and during this project three different types of baluns have been investigated. The first one is described in [24] where coaxial cables together with ferrite beads are used to transform an unbalanced 50 Ω input to a balanced 12.5 Ω output. The second one is a Marchand balun using coplanar waveguides [25] and the third one is a balun based on a Wilkinson power divider plus a phase shifter of 180° discussed in [26].

3.2.1.1 Coaxial transformer In [24] a coaxial balun and a 4:1 coaxial transformer are simulated and implemented as an input network to a balanced push-pull class B amplifier. The coaxial transformer transforms an unbalanced 50 Ω signal to a balanced 12.5 Ω signal according to Figure 3.22. Since the amplifier is balanced the input to each transistor will be half of the total balanced output from the transformer described in Figure 3.23.

Date 2013-06-18 | Issue A | Document ID 87/03631-1/FCK11507
Issued by
OEGPU Viktor Hallman, Erik Sanford
Classification Company Confidentially
COMPANY UNCLASSIFIED
Classification Export Control
NOT EXPORT CONTROLLED
Classification Defence Secrecy
ÖPPEN/UNCLASSIFIED

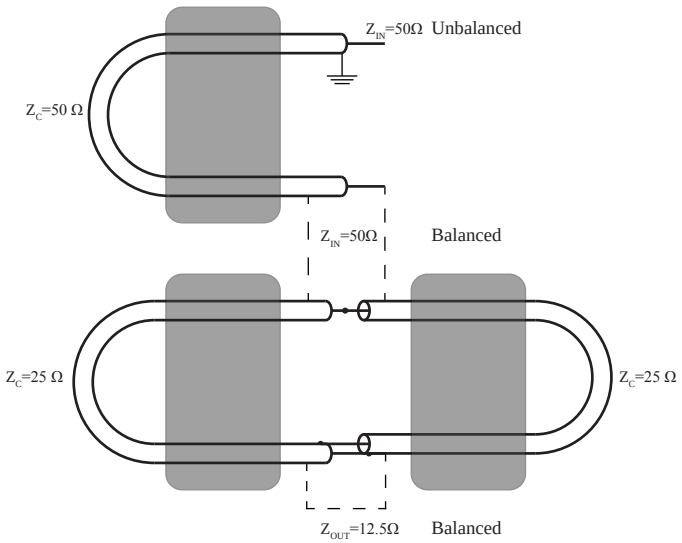

Figure 3.22: Schematic over the coaxial transformer. At the first stage the signal is transformed from 50 Ω unbalanced to 50 Ω balanced using a coaxial balun together with a ferrite bead. At the next section the two 25 Ω coaxial cables are connected in series and at the output the cables are connected in parallel which enables the 4:1 transformation. The grey boxes are ferrite beads which increases the parallel inductances along the core and the shield as shown in Figure 3.24

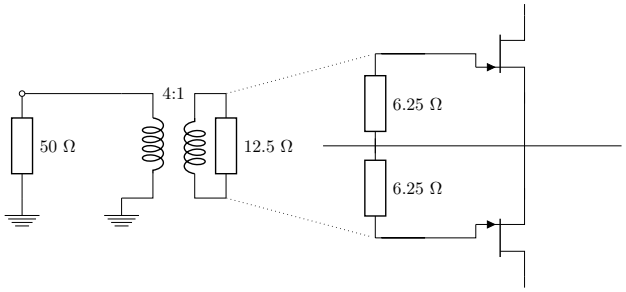

Figure 3.23: One of the benefit of balanced amplifier is the impedance halving of the balanced input which simplifies the impedance transformation when transforming to lower impedances

To be able to simulate the performance of the coaxial transformer a model of a coaxial cable through a ferrite bead is needed. A model provided by [24] has been used and shown in Figure 3.24 but instead of using ideal inductors the extra inductors have been measured and included as 2-port elements in order to make the model more realistic.

The inductors in the model represents the presence of the ferrite bead. A complete model of the coax transformer and more details about the model are presented in section C.2 on page 90. The measured return loss together with the simulated return loss for the coaxial transformer are shown in Figure 3.25. The matching of the model is well correlated to measured result from 40 MHz to

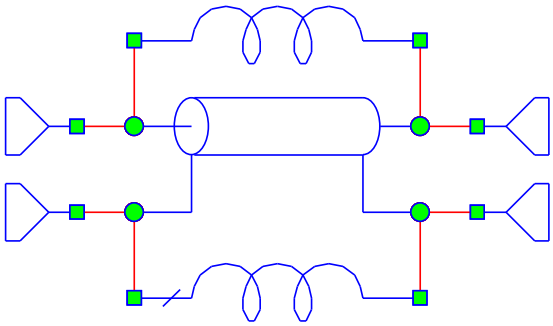

Figure 3.24: Model of coaxial cable through a ferrite bead

1 GHz. Because of difficulties to measure a balanced 12.5 Ω output, no measured data involving the output has been performed for the coaxial transformer. The phase balance and the amplitude balance were measured for the model and is shown in Figure 3.26 and 3.27 respectively.

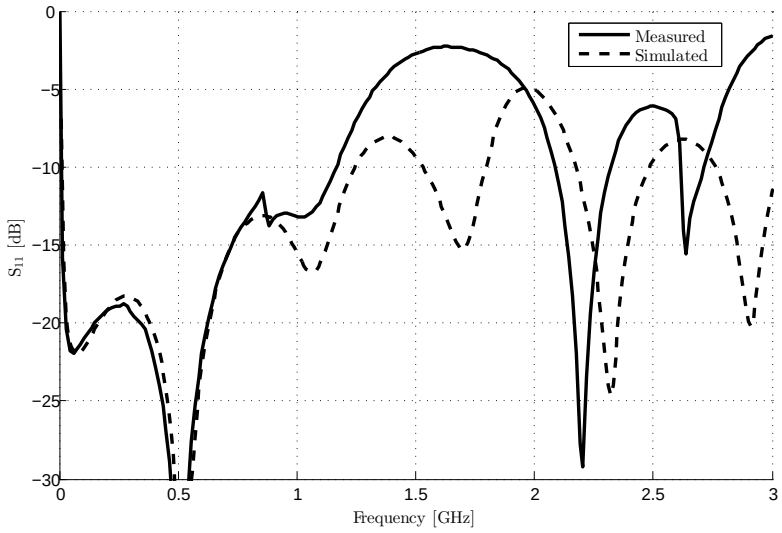

Figure 3.25: Both measured and simulated results for return loss of the coaxial transformer

This type of design is suited for frequencies up to 1 GHz. To cover the bandwidth from 750 MHz to 3 GHz using this type of design was shown to be too difficult. No further investigations were made.

Date 2013-06-18 | Issue A | Document ID 87/03631-1/FCK11507
Issued by
OEGPU Viktor Hallman, Erik Sanford
Classification Company Confidentially
COMPANY UNCLASSIFIED
Classification Export Control
NOT EXPORT CONTROLLED
Classification Defence Secrecy
ÖPPEN/UNCLASSIFIED

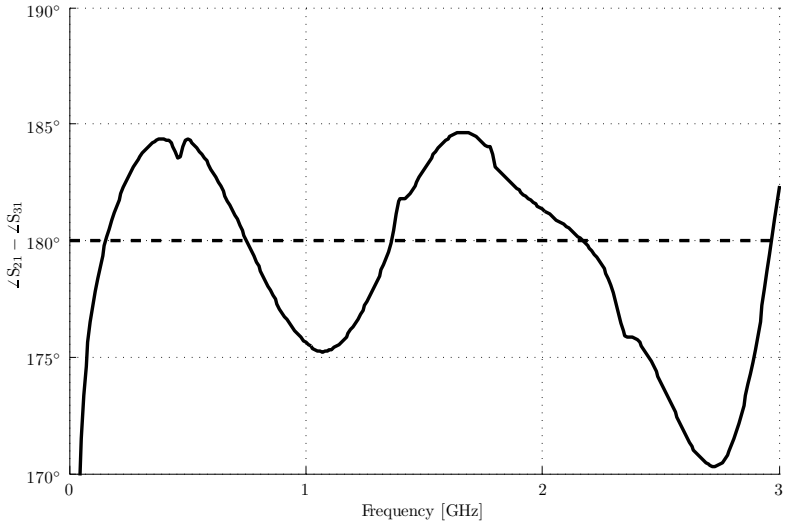

Figure 3.26: Phase balance for the model of the coaxial transformer

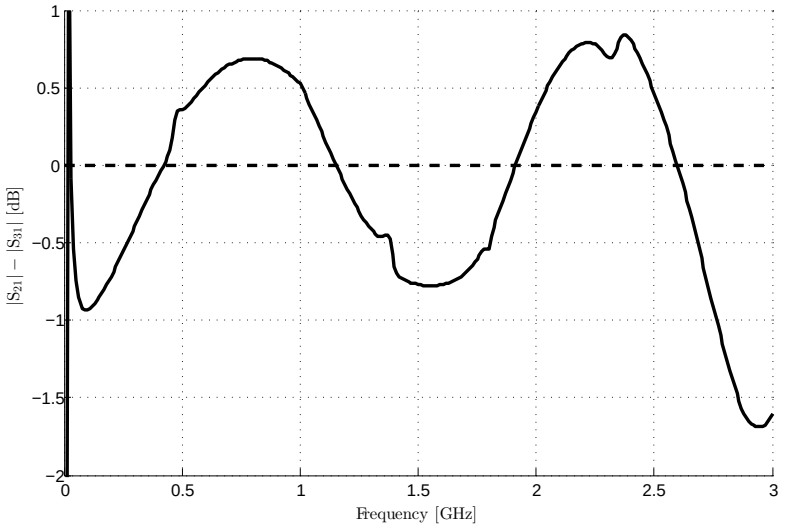

Figure 3.27: Amplitude balance for the model of the coaxial transformer

Date 2013-06-18 | Issue A | Document ID 87/03631-1/FCK11507
Issued by
OEGPU Viktor Hallman, Erik Sanford
Classification Company Confidentially
COMPANY UNCLASSIFIED
Classification Export Control
NOT EXPORT CONTROLLED
Classification Defence Secrecy
ÖPPEN/UNCLASSIFIED

3.2.1.2 Marchand balun An interesting design of a balun is the Marchand balun which is investigated in [25]. A Marchand balun can be design in different ways and one example of design is shown in Figure 3.28 where the center conductor is having a total length of $\lambda/2$.

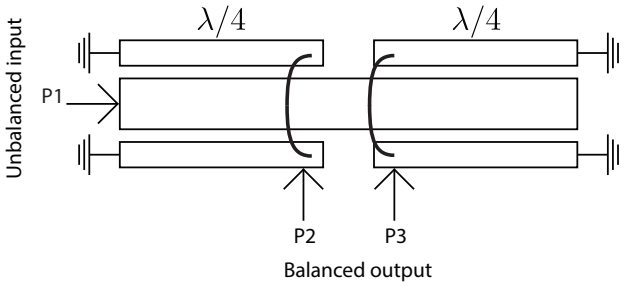

Figure 3.28: Marchand balun built up by coplanar waveguides and is used to convert an unbalanced input at port 1 to balanced output at port 2 and 3. The Marchand balun is named after Nathan Marchand who presented the solution in the year of 1944.

This setup will not be possible with the presence of a ground plane. A ground plane will decrease the possible amount of coupling between the conductors to a level which is not enough. Since the rest of the amplifier will be designed with the presence of a ground plane one solution could be to mount the balun perpendicular to the ground plane and in that way remove the coupling to ground. The need of absence of a ground plane is one disadvantage since the mounting will be more complicated.

The frequency range of the amplifier is from 750 MHz to 3 GHz with a ratio between f_1 and f_2 of 4, where f_1 and f_2 are the minimum and maximum frequency respectively. That means the wavelength λ will vary by a factor 4. Since the design of the Marchand balun will be based on the wavelength a good compromise would be to base the design on the geometrical mean f_c of f_1 and f_2 defined as

$$f_c = \sqrt{f_1 f_2}. \tag{3.1}$$

By designing the balun based on the geometrical mean frequency f_c defined by (3.1), length l of the middle conductor is given by

$$\begin{aligned} l &= \lambda_c/2 \\ &= \lambda_1/4 \\ &= \lambda_2, \end{aligned} \tag{3.2}$$

where $\lambda_{1,2}$ corresponds to the wavelength of $f_{1,2}$. Equation (3.2) shows the difficulties of designing a wideband balun using a layout which is based on the wavelength. For the high frequencies the middle conductor will not be $\lambda/2$ but rather λ and for the low frequencies the length will be

$\lambda/4$. Referring to the theory section, the input impedance of a transmission line will be highly dependent of the electrical length of the transmission line.

3.2.1.3 Multiple stage Wilkinson power divider Another design for a wideband balun that has been investigated during the design process is a topology based on a multiple stage Wilkinson power divider [26]. The principle behind this design is to split the signal into two branches using a Wilkinson power divider and then switch the phase on one channel $180°$. In order to reach the desired bandwidth a multiple stage Wilkinson power divider is used. Whether this really is a balun or not has been discussed during the project. There is no balanced signal in this setup so calling it balun would not be correct, but the function of producing two off-phase signals makes it equivalent to a balun so for the rest of this thesis it will be called balun.

A single stage Wilkinson power divider consists of a microstrip of characteristic impedance Z_0 which is divided into two lines each having characteristic impedance of $\sqrt{2}Z_0$. At a distance of $\lambda/4$ from the split the two branches are connected with a resistance of $2Z_0$ as in Figure 3.29.

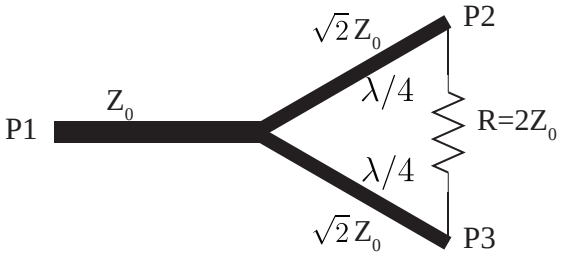

Figure 3.29: Single stage Wilkinson power divider. First time published by Ernest J. Wilkinson in 1960.

The bandwidth of a single stage Wilkinson power divider will not be wide enough and in order to increase the bandwidth a multiple stage technique is used. The bandwidth of power divider for different number of stages has been simulated in *AWR* and the resulting return loss is shown in Figure 3.30. The result shows a requirement of at least three stages in order to cover the whole bandwidth.

At a first level the design can be implemented in *AWR* using closed-form simulations, see Figure 3.31, which does not take any coupling between conductors into account.

The design goal is to cover the whole frequency interval from 750 MHz to 3 GHz with as low return loss as possible. In order to simplify the matching to the transistors in the next stage there will also be an impedance transformation to 25 Ω at the two outputs of the balun. Since the optimum input impedance of the transistors will be as low as a few ohms, the matching between balun and transistor will be much easier having a low impedance at the output. Based on Figure 3.30 three stages will be used in the design in order to reach the desired bandwidth and the complete design is shown in Figure 3.32.

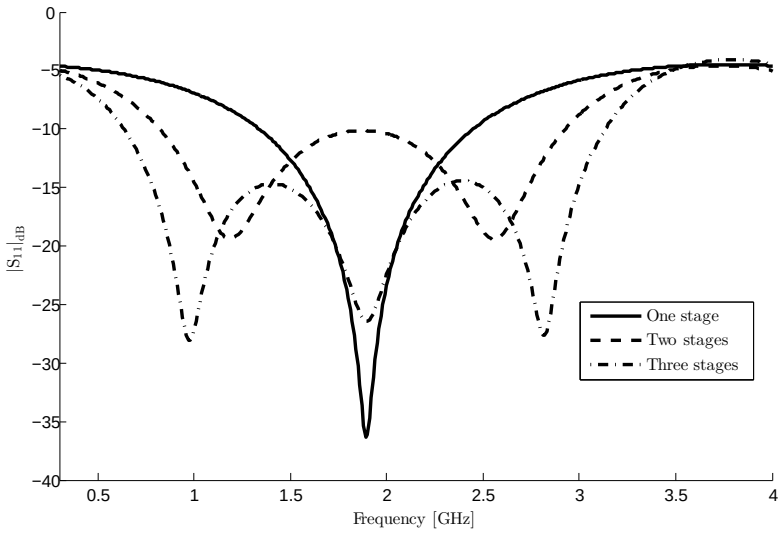

Figure 3.30: Comparison in return loss between a single, double and triple stage Wilkinson power divider. The result is based on circuit simulation in *AWR* and used to determine the required number of stages for the given bandwidth of 750 MHz to 3 GHz.

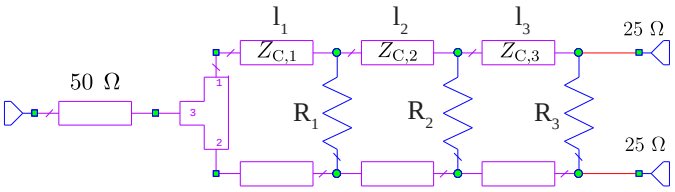

Figure 3.31: Closed-form simulation of a three stage Wilkinson power divider

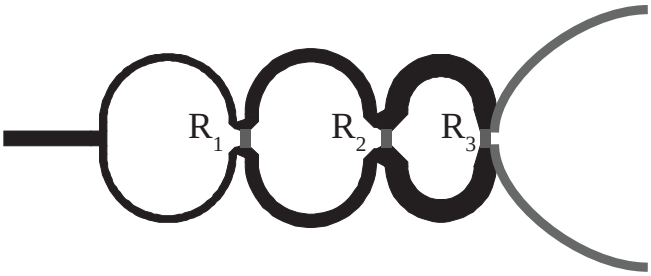

Figure 3.32: Final design of the three stage Winkinson power divider

Phase shifter Since the Wilkinson power divider will produce an in-phase output the great challenge with this setup is to achieve a broadband phase shift of 180° between the outputs over the band. The basics behind the 180° phase shifters that has been studied in this thesis is to use some

type of transmission line and switch ground to signal and signal to ground. In [27] two interesting designs of inverters are described. The first one is the one used in [26] where a coplanar waveguides is used as shown in Figure 3.33b. The phase inverter is achieved by a cross-section where the ground is connected to the signal and signal is connected to ground.

The other one is performed on a broadside waveguide where vias are used to switch the signals as illustrated in Figure 3.33a. None of these solutions are possible with the presence of a ground plane and since the rest of the amplifier will be designed upon a ground plane a more convenient solution has been developed using a coaxial cable as transmission line.

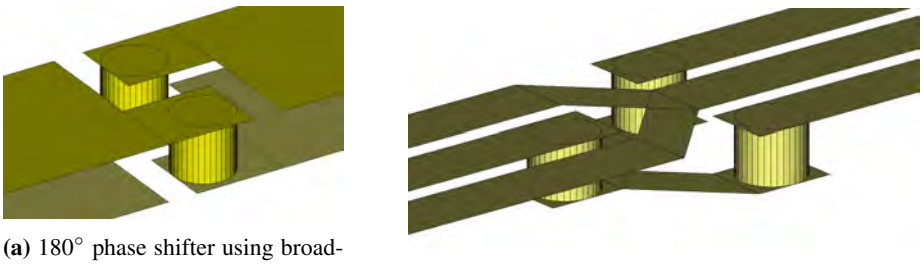

(a) 180° phase shifter using broadside transmission line

(b) 180° phase shifter using coplanar microstrips

Figure 3.33: Two different ways to accomplish a 180° phase shift

By using coaxial lines at the two outputs of the Wilkinson divider, a phase shift can be achieved by letting one of them switch ground to signal and signal to ground. The idea is the same as described above and the difference is the way the transmission lines are realised. Using coaxial cables there is no need to remove the ground plane which is a huge advantage.

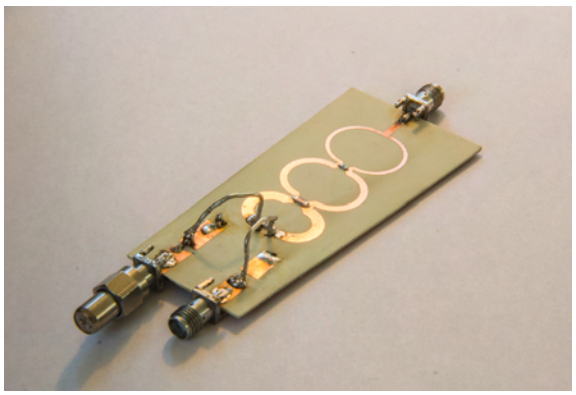

Figure 3.34: Wilkinson power divider together with coaxial phase shifter. The 3-port measurement was done on this device and S-parameters were extracted and implemented as a part of the whole amplifier design.

Date 2013-06-18 | Issue A | Document ID 87/03631-1/FCK11507
Issued by
OEGPU Viktor Hallman, Erik Sanford
Classification Company Confidentially
COMPANY UNCLASSIFIED
Classification Export Control
NOT EXPORT CONTROLLED
Classification Defence Secrecy
ÖPPEN/UNCLASSIFIED

Measurements of a 3-port network For measurements of the balun a 2-port network analyser has been used. The way to measure a 3-port network using a 2-port network analyzer is to do three 2-port measurements and combine the results into a 3-port measurement. While measuring on two ports, the third port must be terminated with standard impedance of 50 Ω in order to make the measurement equivalent to a 3-port measurement.

The way the results from each measurement are combined is explained in (3.3) where the matrices show the contribution of each 2-port measurement to the whole 3-port. The parameters S_{11}, S_{22} and S_{33} will be measured twice.

$$\begin{bmatrix} S_{11} & S_{12} & - \\ S_{21} & S_{21} & - \\ - & - & - \end{bmatrix} \quad \begin{bmatrix} S_{11} & - & S_{12} \\ - & - & - \\ S_{21} & - & S_{21} \end{bmatrix} \quad \begin{bmatrix} - & - & - \\ - & S_{11} & S_{12} \\ - & S_{21} & S_{21} \end{bmatrix} \tag{3.3}$$

Port 1 and port 2 Port 1 and port 3 Port 2 and port 3

Measured results In order to determine the performance of the balun, return loss, amplitude balance and phase balance have been measured. The balun was implemented using the technique described above and the resulting 3-port was imported into *AWR* as a 3-port element where the two output port impedances are set to 25 Ω. Measured return loss together with simulated return loss is shown in Figure 3.35. One reason to the difference between the simulated and measured results could be the coaxial phase inverter which is implemented in the final device but not in the simulations. The connection between the circuit and the coaxial cable is hard to implement in the simulation since the connection tend to be too ideal compared to reality.

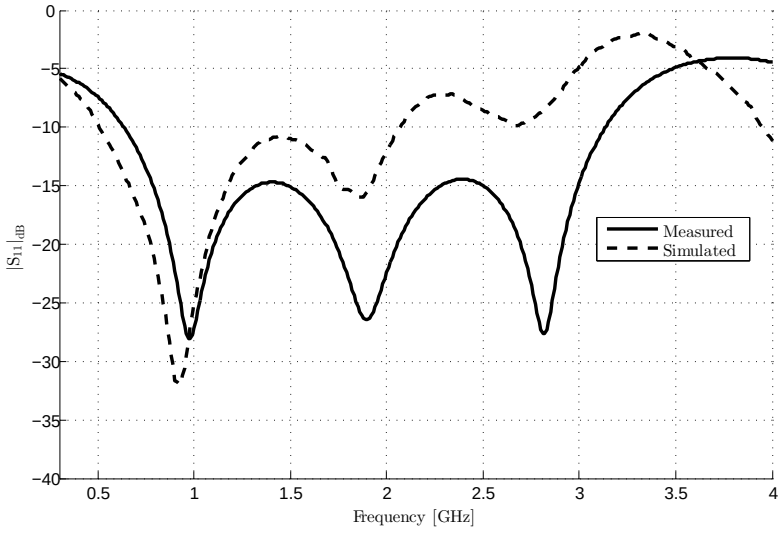

Figure 3.35: Measured return loss compared to simulated return loss

Date 2013-06-18 | Issue A | Document ID 87/03631-1/FCK11507
Issued by
OEGPU Viktor Hallman, Erik Sanford
Classification Company Confidentially
COMPANY UNCLASSIFIED
Classification Export Control
NOT EXPORT CONTROLLED
Classification Defence Secrecy
ÖPPEN/UNCLASSIFIED

Amplitude imbalance is calculated by taking $|S_{31}|_{dB} - |S_{21}|_{dB}$ and is shown in Figure 3.36. The reason why the amplitudes are not the same is because of the phase inverter. Without the phase inverter the circuit would be symmetrical and the output amplitudes would be identical at port 2 and 3. The phase imbalance is shown in Figure 3.37. No simulated data of the phase imbalance could be performed because difficulties to simulate the coaxial-circuit transition.

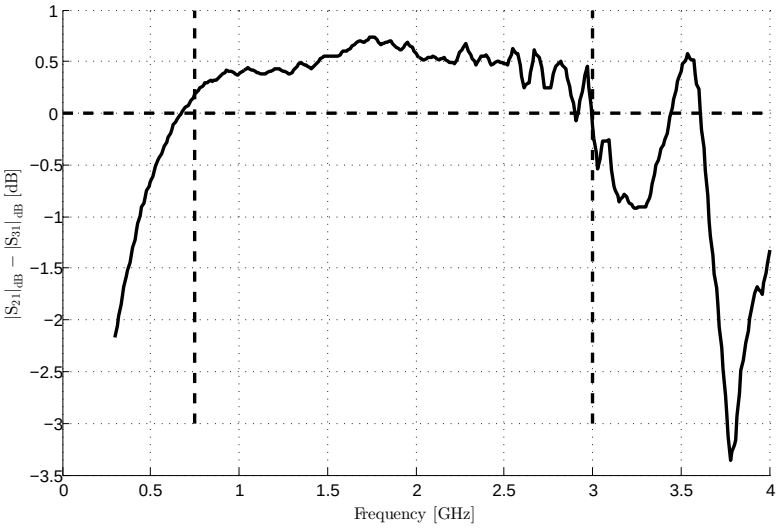

Figure 3.36: Amplitude imbalance at the two outputs

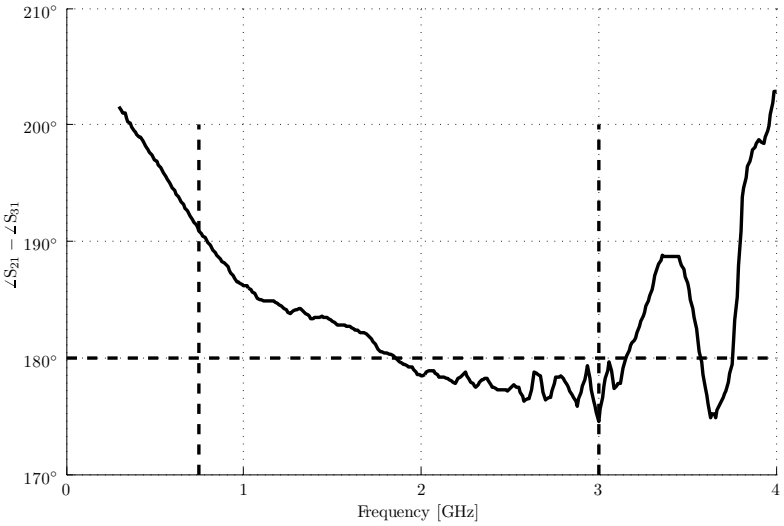

Figure 3.37: Phase imbalance at the two outputs

Date 2013-06-18 | Issue A | Document ID 87/03631-1/FCK11507
Issued by
OEGPU Viktor Hallman, Erik Sanford
Classification Company Confidentially
COMPANY UNCLASSIFIED
Classification Export Control
NOT EXPORT CONTROLLED
Classification Defence Secrecy
ÖPPEN/UNCLASSIFIED

3.2.2 Matching networks

Since the output impedance of the balun does not necessarily match the optimum in-impedance of the transistor and the antenna does not necessarily match the optimum out impedance of the transistor matching networks are required. For the amplifier in the frequency region 750 MHz to 3 GHz microstrip stubs are used as matching network. In this section techniques of how the optimum input and output impedances are retrieved will be explained together with some basic techniques about how the matching networks were designed.

3.2.2.1 Load pull The first stage in the design of the amplifier matching networks is to determine the optimum load in order to reach the highest output power and PAE. By using the model for the transistor this can be done by using a simple schematics shown in Figure 3.38 where a tuner is used to sweep all possible impedances at input and output. Load-pull measurements can be done for any specified measurements such as gain, PAE or return loss. Considering only the gain the optimal input and output impedance is shown in Figure 3.39 where the Smith Chart is normalised to 10 Ω. Load pull measurement considering the power added efficiency is shown in Figure 3.40a with a maximum of 74.2%. Load pull of total output power is shown in 3.40b having a maximum value of 47.6 dBm. Both load pull measurements are measured at the center frequency 1.5 GHz.

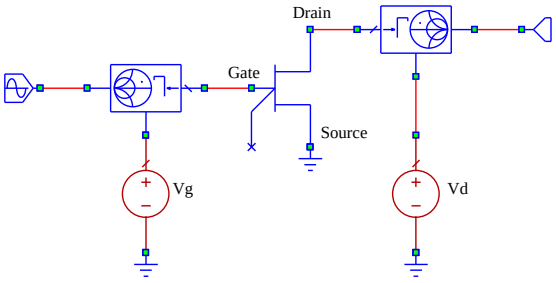

Figure 3.38: Setup used to simulate a load pull measurement where the all possible in and out impedances are swept in the gamma plane

The goal when designing the input matching network is to transform the 50 Ω impedance to the optimal impedance for the transistor. For a narrowband amplifier the matching becomes easy by just using an equivalent LC-network as an impedance transformation. This approach is not possible as a broadband solution since the values of L and C will only be valid for a single frequency.

Date 2013-06-18 | Issue A | Document ID 87/03631-1/FCK11507
Issued by
OEGPU Viktor Hallman, Erik Sanford
Classification Company Confidentially
COMPANY UNCLASSIFIED
Classification Export Control
NOT EXPORT CONTROLLED
Classification Defence Secrecy
ÖPPEN/UNCLASSIFIED

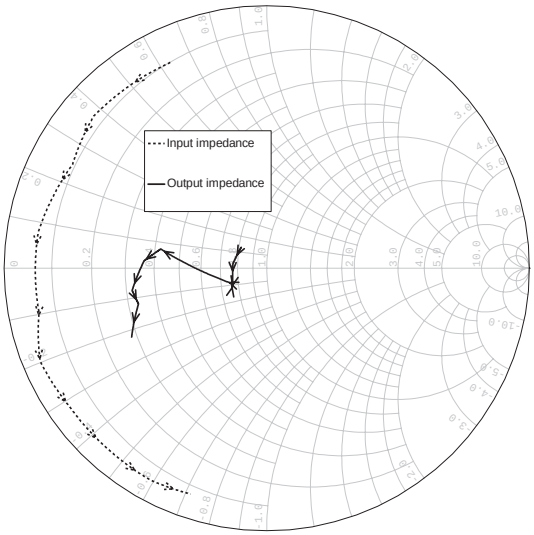

Figure 3.39: Optimal input and output impedance considering the gain. Smith chart is normalised to 10 Ω.

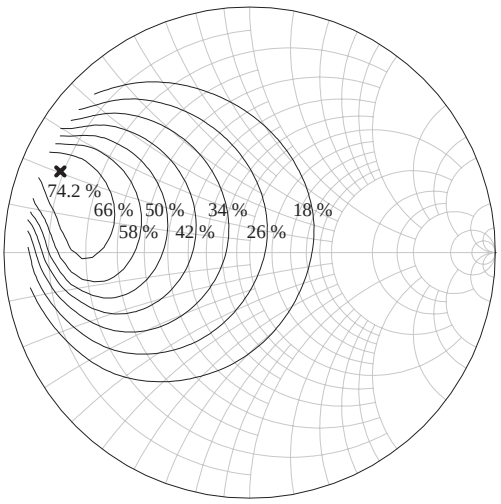

(a) Load pull measurement of PAE at 1.5 GHz where the contours start from 18% with a step of 8% units. The maximum PAE is 74.2%.

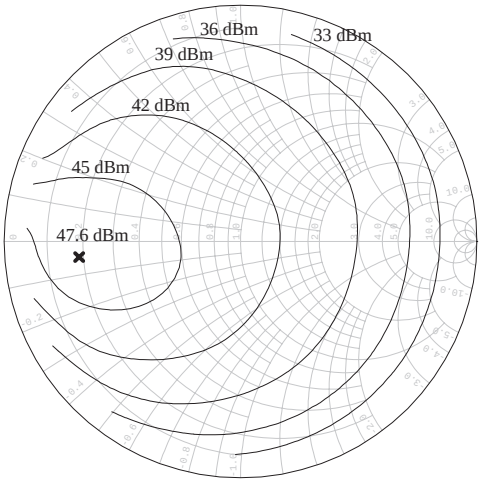

(b) Total output power feeding the transistor with an input power of 30 dBm where the contours are drawn starting from 30 dBm to 45 dBm with a step of 3 dBm. The maximum output power is 47.6 dBm.

Figure 3.40: Two load pull measurements calculated for the model of the transistor using the setup illustrated in Figure 3.38.

Date 2013-06-18 | Issue A | Document ID 87/03631-1/FCK11507
Issued by
OEGPU Viktor Hallman, Erik Sanford
Classification Company Confidentially
COMPANY UNCLASSIFIED
Classification Export Control
NOT EXPORT CONTROLLED
Classification Defence Secrecy
ÖPPEN/UNCLASSIFIED

3.2.2.2 Matching the antenna Next step after determining the optimal load for the transistor is to match the antenna to that load. Neither the antenna impedance or the optimum load impedance is fixed which makes the procedure complex. The differential mode impedance of the antenna is shown in Figure 3.41 together with the resulting matched impedance seen by the transistors.

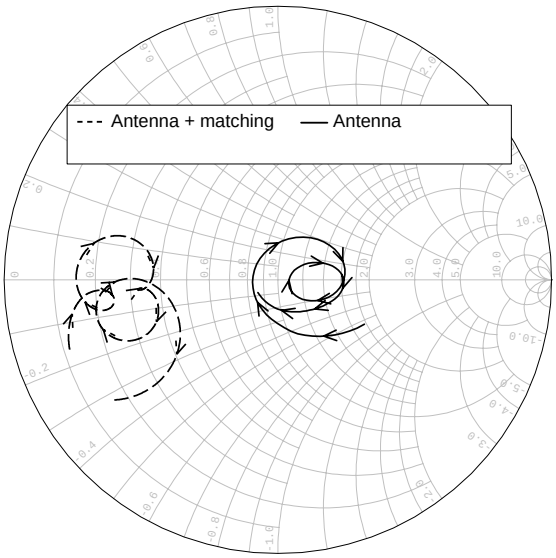

Figure 3.41: Differential mode impedance with and without output matching network

3.2.2.3 Broadband matching network Broadband matching networks can be achieved using many different techniques. The three main techniques are:

- Transformer matching
- Lumped component matching
- Transmission line matching

The 4:1 coaxial transformer investigated in [24] is an example of a transformer network. Matching networks constructed using transformers are usually broadband but hard to achieve for high frequencies.

The principles behind *Lumped component matching* and *Transmission line matching* are basically the same and the difference is the way components are realised. One way to achieve a wideband lumped component matching network is to connect multiple filters in cascade and transform the impedance in small steps each stage shown in Figure 3.42. The maximum possible bandwidth of the matching network is dependent on the number of stages used. By transforming the impedance in many small steps the bandwidth will increase. In practice problems will occur having small steps in impedance since that will require small component values which could be hard to realise.

Date 2013-06-18 | Issue A | Document ID 87/03631-1/FCK11507
Issued by
OEGPU Viktor Hallman, Erik Sanford
Classification Company Confidentially
COMPANY UNCLASSIFIED
Classification Export Control
NOT EXPORT CONTROLLED
Classification Defence Secrecy
ÖPPEN/UNCLASSIFIED

Other parasitic effects like coupling will also have a greater influence if component values are small.

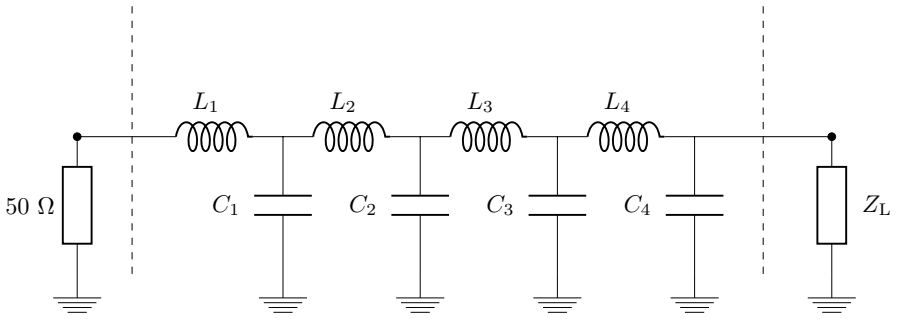

Figure 3.42: Four stages of low pass filter used to match a 50 Ω source to a load Z_L.

3.2.3 Feedback network

In [28] different designs of power amplifiers are presented and resistive feedback networks are used to increase the input impedance in order to simplify the input and output matchings. A resistive feedback network usually consists of a resistor and a capacitor in series connecting the drain and the gate of the transistor. The capacitor is used to separate the DC-bias voltages at each side of the feedback network and can also be used as a frequency selective component. Because of the extra path connecting gate and drain the total S-parameters of the amplifier will be changed and so will the stability of the amplifier.

The typical frequency response of a transistor is decreasing gain as frequency increases. In that case a frequency dependent feedback can improve the gain flatness by either decrease the gain for low frequencies or increase the gain for high frequencies. The physical length of the feedback network will introduce a phase shift which will affect the feedback. During the simulation it was shown that having a short feedback network was preferable in both stability and gain aspect. In the final layout the feedback network was therefore mounted on top of transistor in order to make the path as short as possible.

3.2.4 Bias network

The challenge of designing the bias network is to provide the right bias condition for the transistor without affecting the high frequencies. Therefore, low pass filters are often used to isolate the RF signal from the DC-supply.

High frequency isolation can be achieved in many different ways. For the gate bias the current level will be low and a broadband solution for isolation is to simply use a resistance. The extra

losses introduced by the resistance will be neglectable relative the total loss since the DC-current level at the gate is low.

At the drain bias the DC-current level will be a few amperes which means every extra resistance added in the drain bias network will affect the overall efficiency in terms of power loss in the resistors. A better way for the drain bias is to use an inductor to isolate the RF signal without introducing any loss. In reality the inductors will contain parasitic capacitances according to Figure 3.43. By using inductors there is a potential risk for self resonance because of the extra capacitance C_{p}, which makes the inductor behave like an LC-resonator. In a more accurate model, parasitic capacitances to ground may also be included.

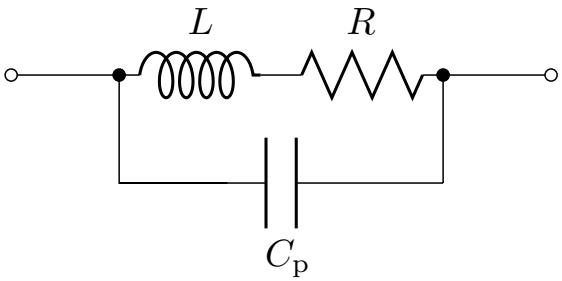

Figure 3.43: A model for an inductor which includes parasitic elements and losses in terms of capacitance and resistance

After trying different wires, different numbers of turns and different spacings between turns the final design of the inductors is shown in Figure 3.44. The wire used is a 0.25 mm copper wire wound two turns around a plastic core and the resulting impedance is shown as inductor 2 in Figure 3.45. Thin wire in the inductor is desirable since that will decrease the parasitic capacitance and increase the impedance which has been verified with simulations in *AWR*.

Figure 3.44: The final design of the drain bias inductors shown together with the head of a match. The thickness of the copper wire used is 0.25 mm.

The drawback having a thin wire is that the fusing current is decreased. Fusing current is the maximum amount of current a wire can handle placed in open air without melting. The fusing

Date 2013-06-18 | Issue A | Document ID 87/03631-1/FCK11507
Issued by
OEGPU Viktor Hallman, Erik Sanford
Classification Company Confidentially
COMPANY UNCLASSIFIED
Classification Export Control
NOT EXPORT CONTROLLED
Classification Defence Secrecy
ÖPPEN/UNCLASSIFIED

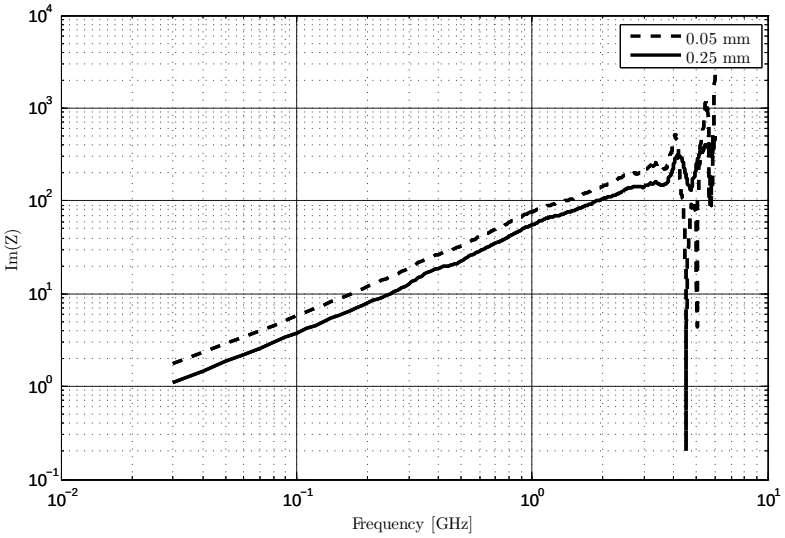

Figure 3.45: Inductor 1 is made using a 0.05 mm copper wire with a resulting inductance of 11 nH. Inductor 2 which is shown in Figure 3.44 is wound in the same way as inductor 1 but with 0.25 mm copper wire. The resulting inductance for inductor 2 is around 7 nH.

current can be approximated using *Onderdonk's equation* [29]:

$$I_{\text{fuse}} = 344A\sqrt{\frac{\log(1+(T_{\text{m}}-T_{\text{a}})/(234+T_{\text{a}}))}{s}},$$

where A is the area given in mm^2, T_{m} the melting point of the metal used, T_{a} the ambient temperature and s is the time in seconds. In the model $I_{\text{fuse}} \propto s^{-1}$ which means that any current will burn any wire as long as $s \to \infty$ which is not realistic since a steady state temperature will be reached. Therefore the model is recommended to use for $s < 10$ seconds. Using $s = 10$ for a copper wire of width 0.25 mm the resulting I_{fuse} is 6.8 A which is way beyond the necessarily level. Instead using a 0.05 mm wire I_{fuse} is 0.27 A.

3.2.5 Antenna representation

In the following section admittances will be used in order to simplify the calculations. The main goal of this thesis is to investigate the possibility to connect an antenna directly to the balanced output of a push-pull amplifier. For accurate simulations a good representation of the antenna is essential because the impedance at the output of the amplifier will affect the performance of the amplifier which has been illustrated earlier as a load pull measurement in Figure 3.39.

Since the antenna will show different input impedances for the even and odd mode the load can not be represented by just one frequency dependent impedance. By terminating the amplifier with

Date 2013-06-18 | Issue A | Document ID 87/03631-1/FCK11507
Issued by
OEGPU Viktor Hallman, Erik Sanford
Classification Company Confidentially
COMPANY UNCLASSIFIED
Classification Export Control
NOT EXPORT CONTROLLED
Classification Defence Secrecy
ÖPPEN/UNCLASSIFIED

a circuit shown in Figure 3.46a the circuit seen by the odd and the even mode will be different. The odd mode will see the same circuit and the even mode will see a circuit shown in Figure 3.46b

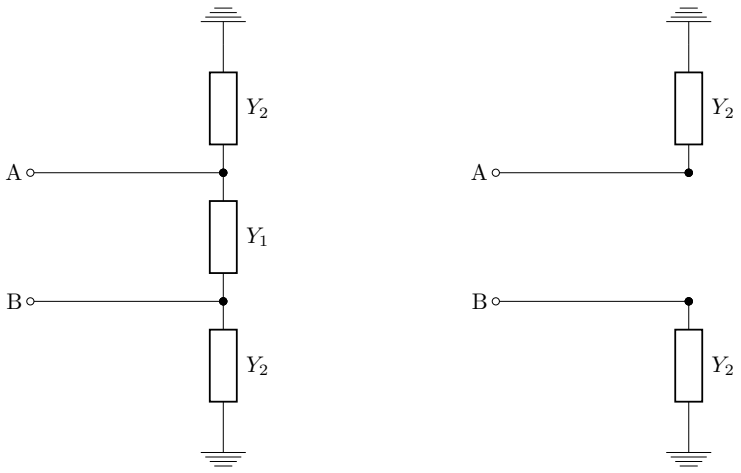

(a) Setup for representation the antenna taking both the even and odd mode under consideration. This is also the equivalent circuit seen by the odd mode.

(b) Equivalent circuit seen by the even mode. Since the potential difference of point A and B is 0, no current will go through the admittance Y_1 and therefore it has been removed.

Figure 3.46: Figures showing the equivalent circuit for even and odd mode

The total input admittance of the circuit in Figure 3.46b is

$$Y_{\text{even}} = \frac{1}{2}Y_2 \tag{3.4}$$

The total input admittance of the circuit in Figure 3.46a is

$$Y_{\text{odd}} = Y_1 + \frac{1}{2}Y_2 \tag{3.5}$$

Given the odd and even admittance for the antenna and using (3.4) and (3.5) the expression for Y_1 and Y_2 can derived and gives

$$\begin{aligned} Y_1 &= Y_{\text{odd}} - Y_{\text{even}} \\ Y_2 &= 2Y_{\text{even}} \end{aligned}$$

Distinguishing the power radiated at the common and differential mode will not be straightforward using this setup. Another equivalent setup which distinguish the common and differential power

Date 2013-06-18 | Issue A | Document ID 87/03631-1/FCK11507
Issued by
OEGPU Viktor Hallman, Erik Sanford
Classification Company Confidentially
COMPANY UNCLASSIFIED
Classification Export Control
NOT EXPORT CONTROLLED
Classification Defence Secrecy
ÖPPEN/UNCLASSIFIED

Table 2: Relates current to resulting temperature rise for different widths of microstrip of height 0.017 mm (RO4350)

	I [A]	ΔT [°C]		
		20	50	100
	0.5	0.86	1.3	1.8
	1	1.5	2.2	3.1
w [mm]	2	2.5	3.8	5.2
	3	3.36	5.1	7.0
	4	4.2	6.4	8.8

is shown in Figure 3.47, which has been implemented and used for simulations in *AWR*. The setup contains two ideal baluns which are connected in parallel having a 180° ideal phase shifter before the balun which is connected to the common mode impedance.

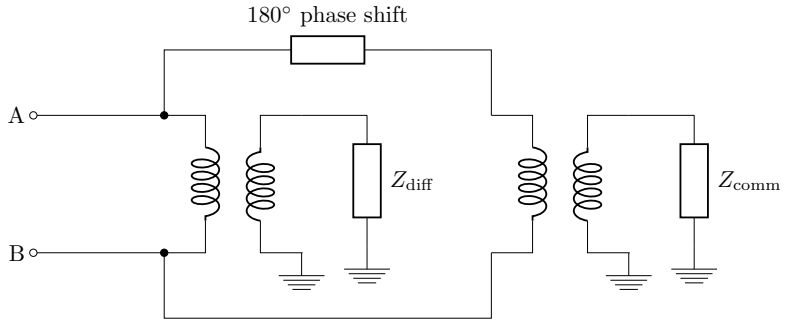

Figure 3.47: Setup of antenna representation where Z_{diff} and Z_{comm} are simulated values of differential and common mode impedance of the antenna extracted using *HFSS*.

3.2.6 Current limit of microstrip

One important thing to take under consideration when designing the output matching network is the risk of overheating the microstrip. The current flowing through a microstrip will generate heat and the amount of heat generated is related to the cross section of the conductor.

In [30] a model that relates the temperature rise in microstrips has been developed. The temperature rise is given for a certain current and cross section area. The cross section area is calculated by multiplying the width and height of the conductor. The substrate that will be used in the design is Rogers 4350B which has a conductor thickness of 0.017 mm. In Table 2 the model has been applied to some microstrip widths and some temperatures and the corresponding current is calculated. The data has been used to estimate the limit of conductor width based on the estimated current level.

Date 2013-06-18 | Issue A | Document ID 87/03631-1/FCK11507
Issued by
OEGPU Viktor Hallman, Erik Sanford
Classification Company Confidentially
COMPANY UNCLASSIFIED
Classification Export Control
NOT EXPORT CONTROLLED
Classification Defence Secrecy
ÖPPEN/UNCLASSIFIED

3.2.7 Final layout

The design process resulted in a layout shown in Figure 3.48. The layout includes the input Wilkinson balun, input matching network, bias network and output matching network. At the output the two output microstrips will be transformed into a broadside transmission line using another piece of substrate which is mounted perpendicular between the gap at the output.

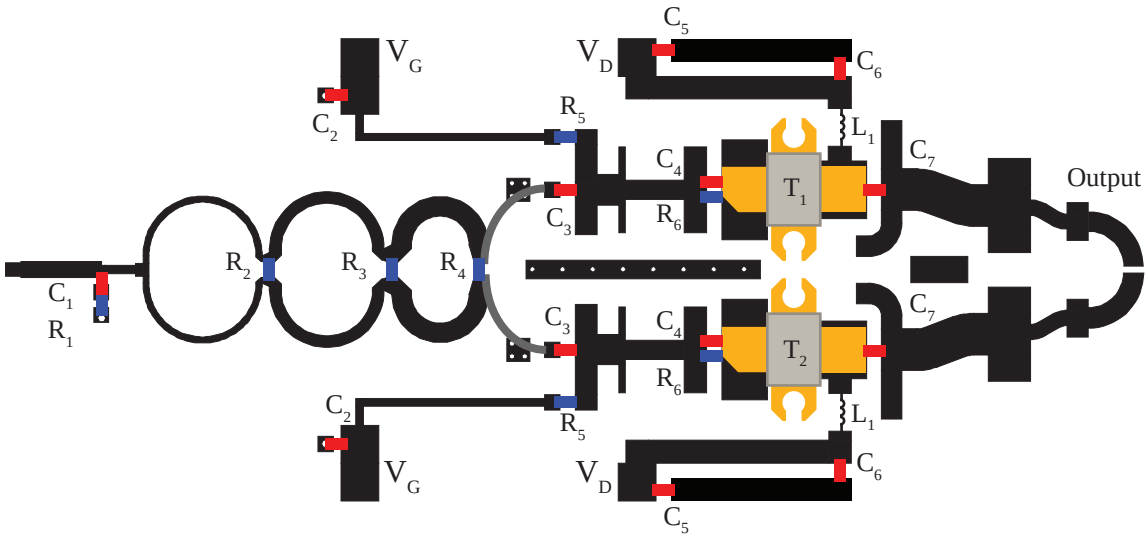

Figure 3.48: Complete layout where all components are marked and T_1 and T_2 are the two transistors, V_G and V_D gate respectively drain bias voltage. A list of the component values used are listed in the following table:

C_1	=	0.47 pF	L_1	=	8 nH
C_2	=	1000 pF	R_1	=	141 Ω
C_3	=	50 pF	R_2	=	116 Ω
C_4	=	3.0 pF	R_3	=	167 Ω
C_5	=	1000 pF	R_4	=	215 Ω
C_6	=	1000 pF	R_5	=	470 Ω
C_7	=	100 pF	R_6	=	14.7 Ω
C_8	=	3000 pF	R_7	=	87 Ω

4 Results

In this section the simulated and measured results from the antenna-amplifier system will be presented. Because of overheating problem with the amplifier no measurement having the amplifier and antenna mounted together were performed in the anechoic chamber. Measuring the system in the anechoic chamber is the only way to measure the system since that is the only reliable way to measure all radiating power from the antenna. Both the amplifier and the antenna has been measured separately but since the amplifier is designed for the impedance of the antenna the antenna is irreplaceable in order to reach to expected performance. Measurements of the amplifier was performed using a 50 Ω instead of using the antenna as a load.

4.1 Gain

Measurements of the amplifier are hard to perform for two reasons. First of all there is no output port included in the design since the amplifier is terminated with the antenna. Second of all the antenna is balanced, which means it will not be possible to, in a simple way, replace it with an unbalanced 50 Ω output port. Having an unbalanced 50 Ω output port is required for performing power measurements is a convenient way.

The gain of the amplifier has been measured by replacing the antenna with a 50 Ω power resistor shown in Figure 4.1a. By measuring the temperature of the resistor and relating the temperature to a power, the total gain has been calculated and is shown in Figure 4.2. The power and temperature relation has been measured by performing a DC measurement. For more details about the DC-measurement, see section C.3 on page 91.

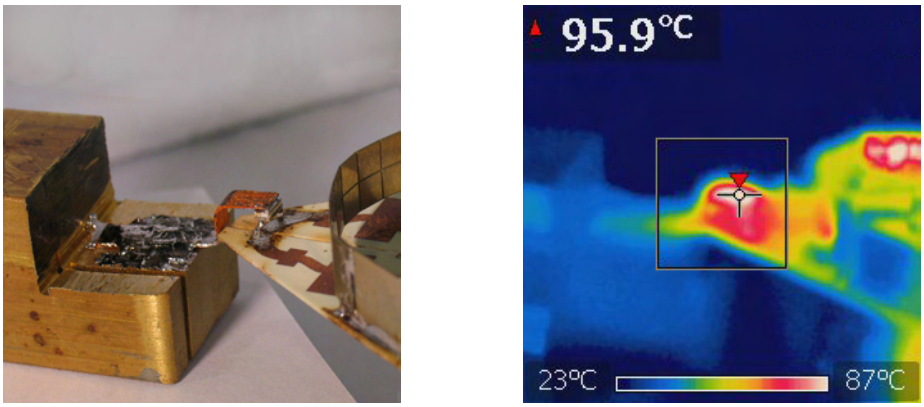

(a) **(b)**

Figure 4.1: (a) Setup for measuring the gain using a 50 Ω power resistor together with a heatsink. (b) An IR picture of the same setup used to measure the power dissipated in the load

Date 2013-06-18 | Issue A | Document ID 87/03631-1/FCK11507
Issued by
OEGPU Viktor Hallman, Erik Sanford
Classification Company Confidentially
COMPANY UNCLASSIFIED
Classification Export Control
NOT EXPORT CONTROLLED
Classification Defence Secrecy
ÖPPEN/UNCLASSIFIED

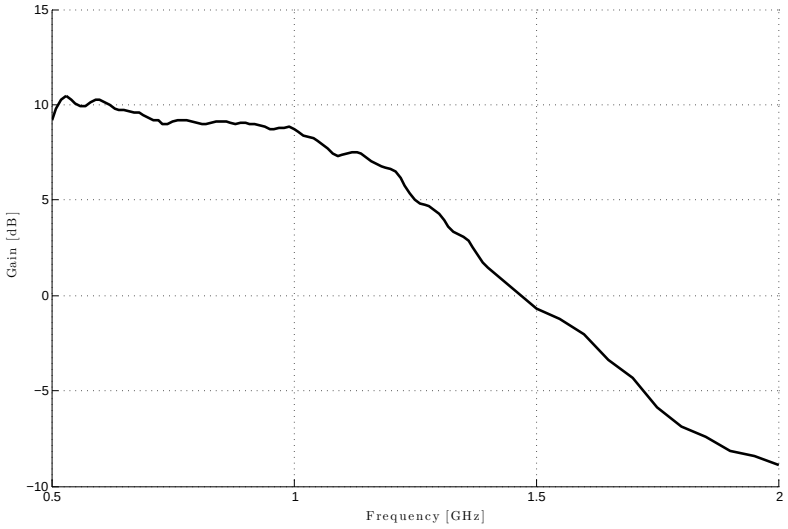

Figure 4.2: Gain measured having an input power of 28.4 dBm and load of 50 Ω

In the simulations the gain of the amplifier is defined as the ratio between the total power delivered at the differential mode and the total input power, shown in Figure 4.3. The variation in gain is quite large which is a result of the variation in the antenna impedance.

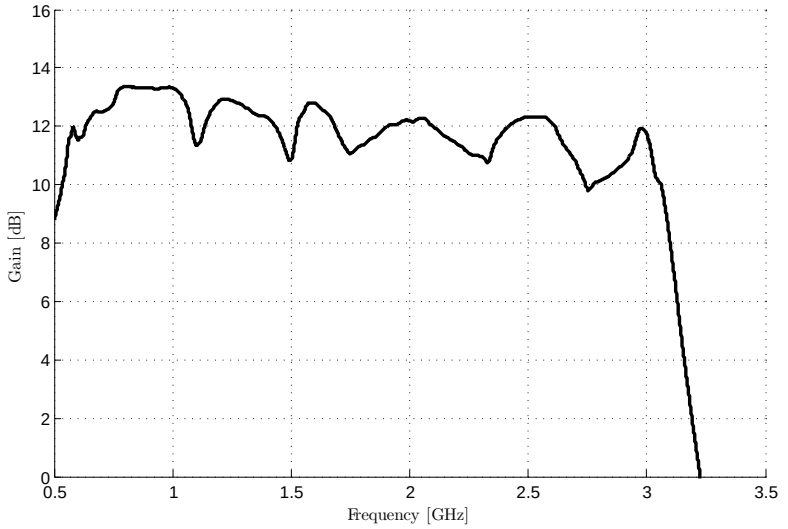

Figure 4.3: Gain simulated having an input power of 33 dBm.

Date 2013-06-18 | Issue A | Document ID 87/03631-1/FCK11507
Issued by
OEGPU Viktor Hallman, Erik Sanford
Classification Company Confidentially
COMPANY UNCLASSIFIED
Classification Export Control
NOT EXPORT CONTROLLED
Classification Defence Secrecy
ÖPPEN/UNCLASSIFIED

4.2 Output power

In the previous section the total gain was measured by measuring the output power dissipated in a 50 Ω load. The output power level in the measurement was far from the expected maximum output power, which is around 47 dBm. The load setup shown in Figure 4.1a would not be able to handle the expected maximum output power level because of overheating. In order to be able to measure the maximum output power a more power resistant load would be needed. A way to make the load more power resistant would be to use many resistors and distribute the power equally to each resistor. The drawback of doing so is the resulting parasitic components, which will be increased. Attempts were made to use four resistors but the resulting parasitic effects were too large to get any useful results. No more attempts were made to measure the maximum output power.

In the simulation, the antenna is represented by using two impedances, Z_{diff} and Z_{comm} discussed in previous sections. The impedance Z_{diff} corresponds to the impedance seen when the two inputs to the antenna have a phase shift of 180°. That is the way the antenna is supposed to be fed and therefore the output power is defined as the power radiating at the differential mode. In Figure 4.4 the power delivered to the antenna at the differential and the common mode are shown as a function of input power. The frequency for the simulation is 1.5 GHz and the resulting maximum output power is 47.4 dBm at an input power of 37.5 dBm.

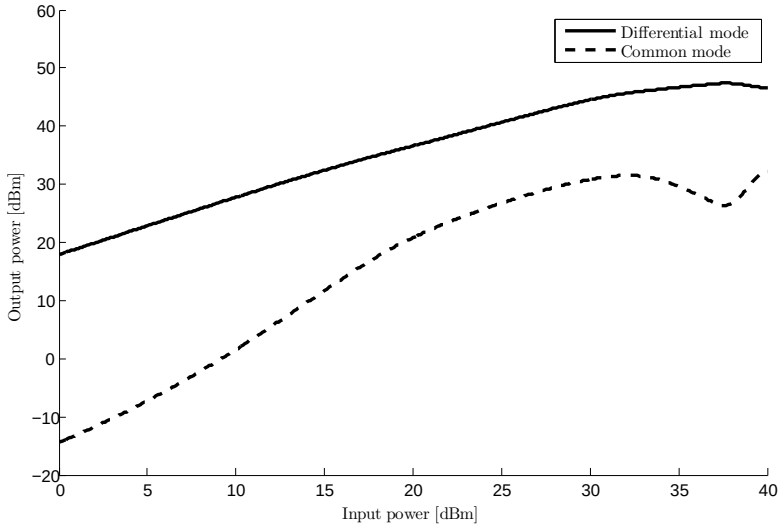

Figure 4.4: Simulation of power delivered to the antenna in both differential and common mode

4.3 PAE

In order to get the highest possible PAE, having a high output power is necessary. That is because the transistor will consume a certain amount of power that is independent of the output power.

That power will be relatively smaller if the output power is increased and therefore the efficiency will increase.

Because of the limitation in the maximum possible output power level, the required output for maximum PAE could not be reached. The data presented in Figure 4.5 is the simulated result of the PAE, having an input power of 36 dBm.

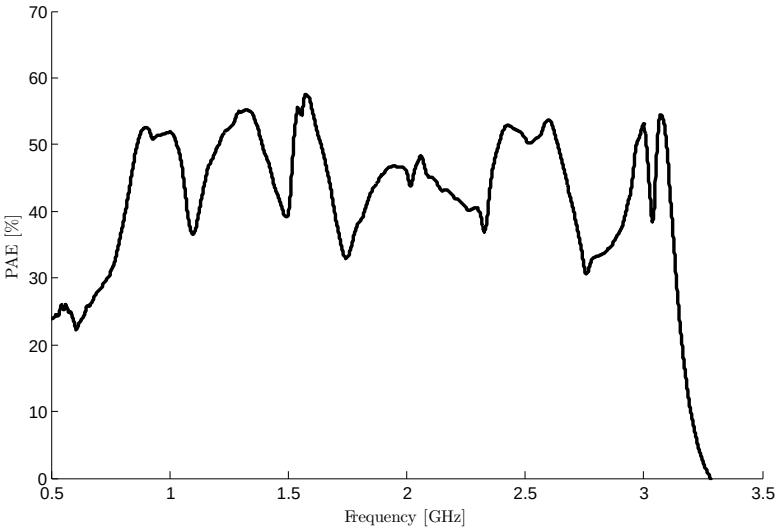

Figure 4.5: Power added efficiency for input power of 36 dBm.

4.4 Return loss

The return loss of the amplifier and the antenna was measured and the result is shown in Figure 4.6. A mismatch at high frequencies is obvious and the goal to have a return loss below -10 dB was not reached.

No measurements except return loss were made on the co-design because of the problems with overheating of the amplifier. In order to measure the return loss of the antenna, the input balun was connected directly to the antenna. The resulting measured and simulated return loss is shown in Figure 4.7. The simulated return loss for the balun-antenna configuration is achieved by using the model for the input balun with the model for the antenna together in *AWR*. As seen in Figure 4.7 the total model is good correlated to the measured data up to 750 MHz. At frequencies above 2 GHz the uncertainty between measured and simulated values is obvious. This result is interesting because it shows that there is a problem with the modeling of the balun, antenna or the connection between them. This uncertainty of the modeling might be the reason to the mismatch in the complete setup.

Date 2013-06-18 | Issue A | Document ID 87/03631-1/FCK11507
Issued by
OEGPU Viktor Hallman, Erik Sanford
Classification Company Confidentially
COMPANY UNCLASSIFIED
Classification Export Control
NOT EXPORT CONTROLLED
Classification Defence Secrecy
ÖPPEN/UNCLASSIFIED

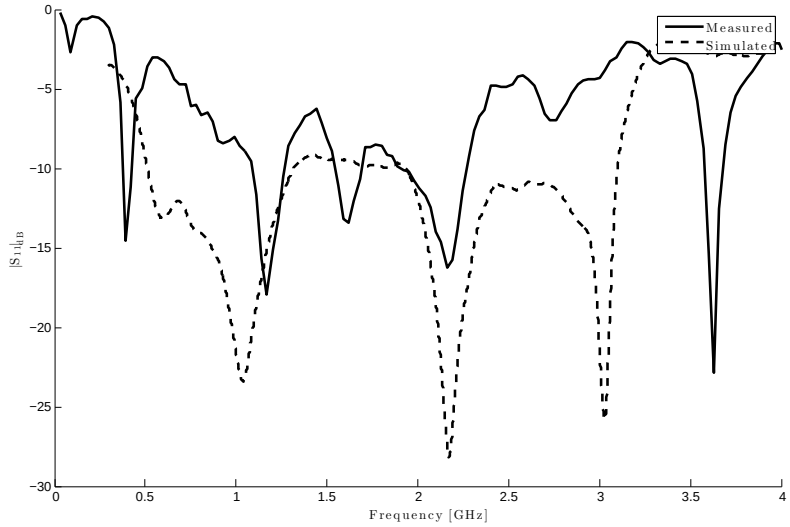

Figure 4.6: Measured and simulated values for S_{11} of amplifier with the antenna mounted at the output

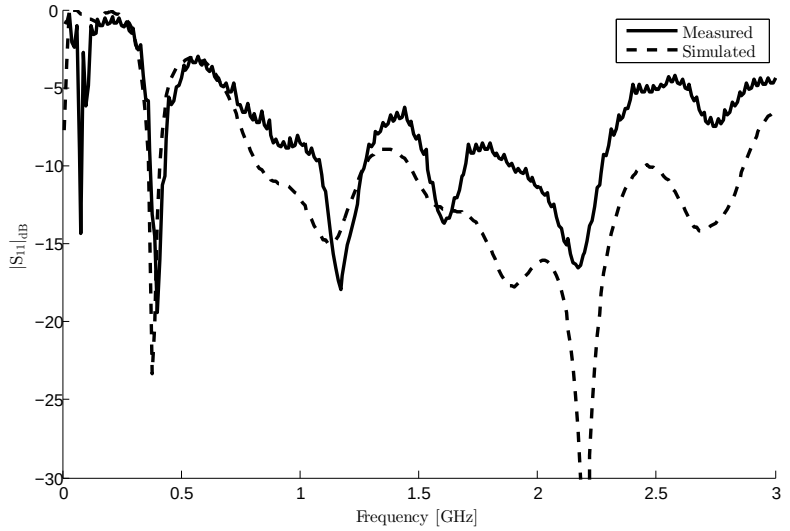

Figure 4.7: Measured values for S_{11} of balun with the antenna mounted at the output

4.5 Stability

Since oscillations are not restricted to the defined bandwidth of the amplifier it is of great importance to simulate the stability for frequencies from DC to $f_{\max}$ where $f_{\max}$ is the upper limit in frequency where oscillation may appear. The maximum possible frequency for oscillation is not a well defined frequency and during the design process the upper limit has been chosen to 6 GHz which is above the maximum operation frequency of the transistor (4 GHz). During the project

Date 2013-06-18 | Issue A | Document ID 87/03631-1/FCK11507
Issued by
OEGPU Viktor Hallman, Erik Sanford
Classification Company Confidentially
COMPANY UNCLASSIFIED
Classification Export Control
NOT EXPORT CONTROLLED
Classification Defence Secrecy
ÖPPEN/UNCLASSIFIED

discussions were held weather having the amplifier unconditionally stable is necessary. Since the load is fixed and supposed to be well defined, it might not be necessary to fulfill the stability criterion for all possible loads.

The simulation of the stability was performed by calculating the two parameters K and B1. According to the theory in section 2.3.1.4 on page 25 the stability was fulfilled by having K>1 and B1>0, see Figure 4.8.

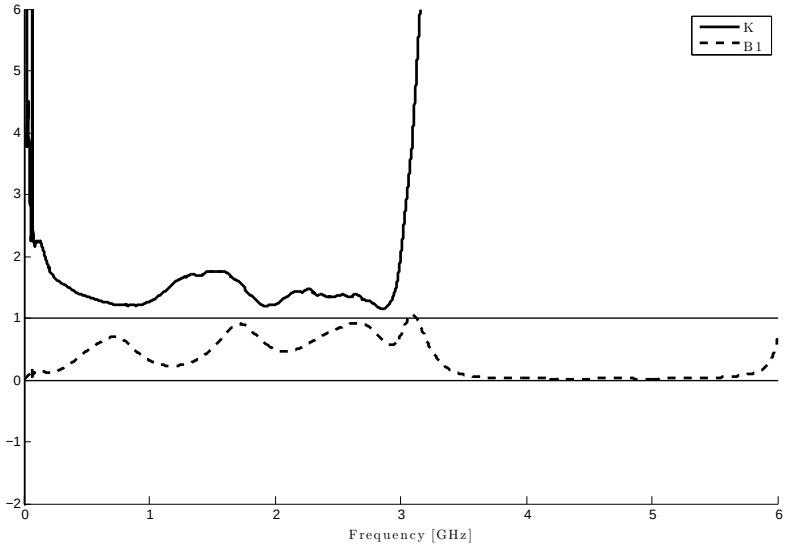

Figure 4.8: Stability simulation in order to ensure the amplifier to be unconditionally stable

4.6 Radiation pattern

As previously mentioned the radiation pattern of the antenna-amplifier system is to some extent affected by the presence of the amplifier and the shielding and cooling parts associated with it. In Figure 4.9 the simulated radiation pattern of the directivity is presented for a couple of frequencies in the range of interest, both in the azimuth plane and the elevation plane.

As can be seen in Figure 4.9, the directivity seems to be somewhat concentrated in the direction of the amplifier for lower frequencies. For higher frequencies however, the main concentration of the directivity seems to shift direction $180°$. This shift is also confirmed by the measurements made in the anechoic chamber, shown in Figure 4.10. In Figure 4.11 the antenna inside the anechoic chamber is shown. An anechoic chamber is chamber with absorbing material on the inner walls in order to mimic the case of free space radiation. The reason for that the maximum measured frequency in the chamber is 2.7 GHz is that this frequency was the closest measurable frequency to 3 GHz.

The presented measurements were not made with the actual amplifier present, but instead with a

Date 2013-06-18 | Issue A | Document ID 87/03631-1/FCK11507
Issued by
OEGPU Viktor Hallman, Erik Sanford
Classification Company Confidentially
COMPANY UNCLASSIFIED
Classification Export Control
NOT EXPORT CONTROLLED
Classification Defence Secrecy
ÖPPEN/UNCLASSIFIED

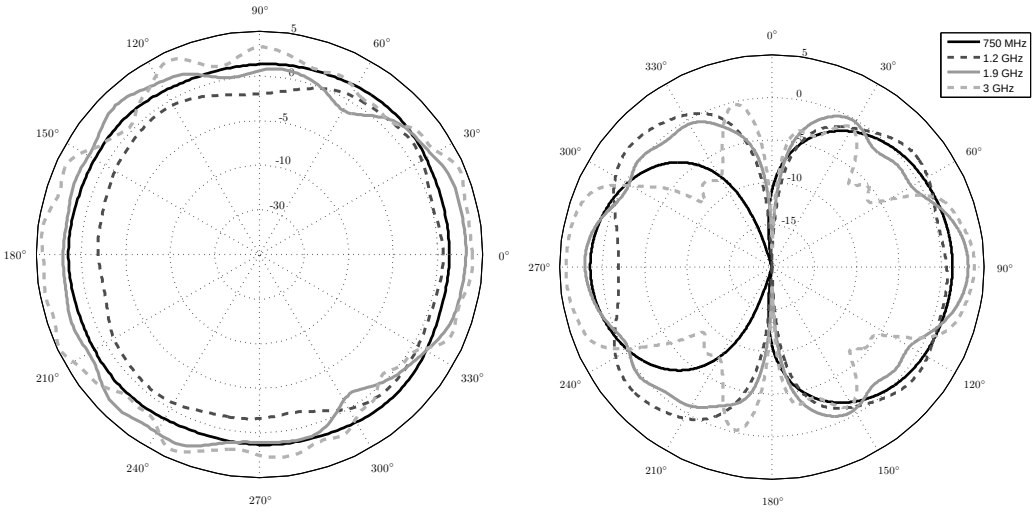

(a) $\theta = 90^\circ$ **(b)** $\varphi = 0^\circ$

Figure 4.9: The radiation pattern of the directivity in logarithmic scale shown in the azimuth plane ($\theta = 90^\circ$) (a) and in the elevation plane ($\varphi = 0^\circ$) (b). The amplifier is present in the direction $(\theta, \varphi) = (90^\circ, 0^\circ)$.

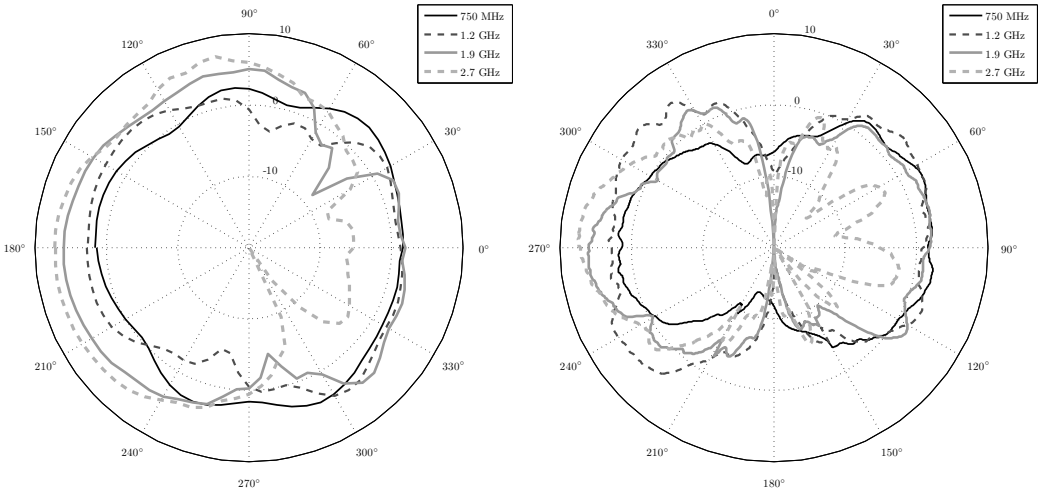

(a) $\theta = 90^\circ$ **(b)** $\varphi = 0^\circ$

Figure 4.10: The measured radiation pattern of the directivity in logarithmic scale shown in (a) the azimuth plane ($\theta = 90^\circ$) and in (b) the elevation plane ($\varphi = 0^\circ$). The feeding balun is present in the direction $(\theta, \varphi) = (90^\circ, 0^\circ)$.

feeding balun and a block of aluminium to represent the conditions of interest. The lack of time made it not feasible to measure the whole antenna-amplifier system. An explanation for the shifts in the radiation pattern could be that the metal structure close to the antenna acts as beam director

Date 2013-06-18 | Issue A | Document ID 87/03631-1/FCK11507
Issued by
OEGPU Viktor Hallman, Erik Sanford
Classification Company Confidentially
COMPANY UNCLASSIFIED
Classification Export Control
NOT EXPORT CONTROLLED
Classification Defence Secrecy
ÖPPEN/UNCLASSIFIED

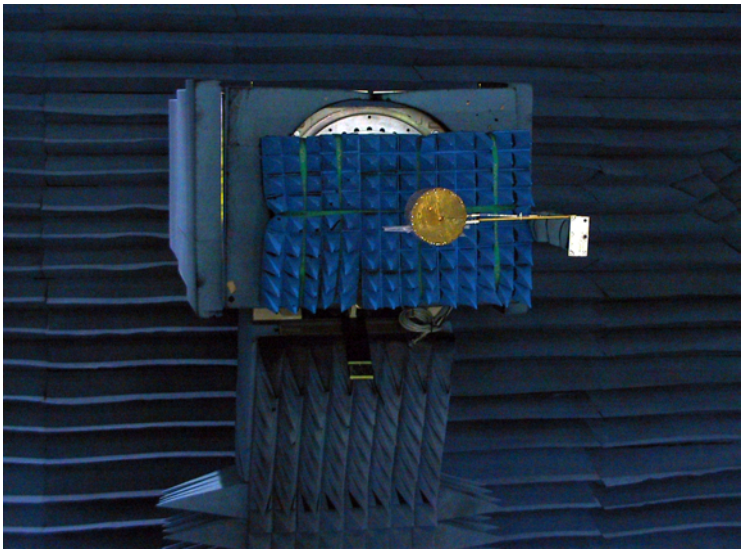

Figure 4.11: The antenna about to be measured in the anechoic chamber

for low frequencies and a beam reflector for high frequencies. Some support for this theory can be derived from the Yagi-Uda antenna [4, p. 578].

To verify that the presented shift was due to the amplifier cooling and shielding, simulations were made without them being present. The simulated data is plotted in Figure 4.12. As expected, the shifts of directivity are in all essentiality gone and the antenna behaves like a half-wave dipole.

The simulated 3D radiation pattern of the directivity is shown together with the complete model at a frequency of 750 MHz in Figure 4.13. In Figure 4.14, the 3D counterparts of the simulated directivity is presented and in Figure 4.15 the measured directivity is presented in 3D polar plots.

Date 2013-06-18 | Issue A | Document ID 87/03631-1/FCK11507
Issued by
OEGPU Viktor Hallman, Erik Sanford
Classification Company Confidentially
COMPANY UNCLASSIFIED
Classification Export Control
NOT EXPORT CONTROLLED
Classification Defence Secrecy
ÖPPEN/UNCLASSIFIED

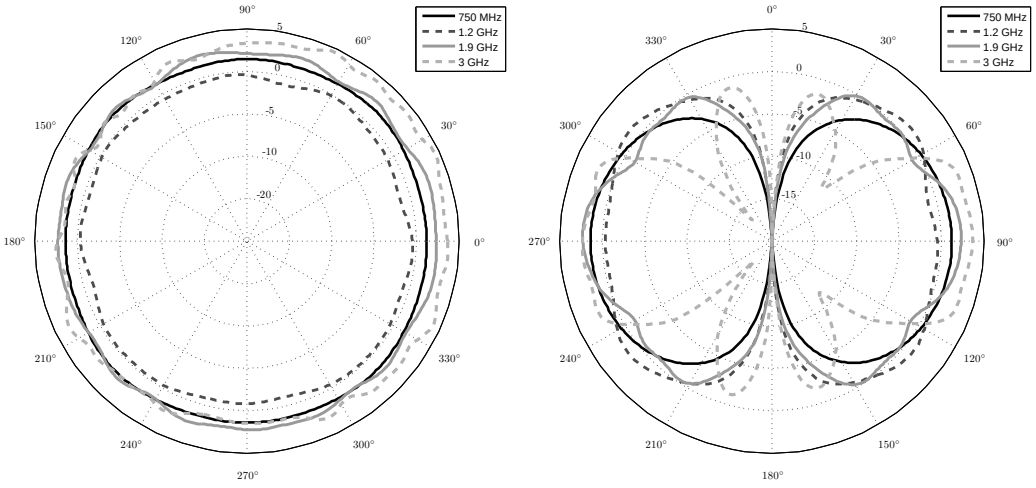

(a) $\theta = 90^\circ$ **(b)** $\varphi = 0^\circ$

Figure 4.12: The radiation pattern of the directivity in logarithmic scale shown in the (a) azimuth plane ($\theta = 90^\circ$) and in (b) the elevation plane ($\varphi = 0^\circ$). No amplifier box for shielding and cooling was present in the simulation.

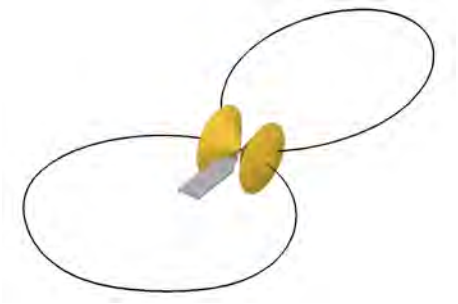

Figure 4.13: The simulated 3D radiation pattern of the directivity in linear scale together with the whole antenna-amplifier system at a solution frequency of 750 MHz

Date 2013-06-18 | Issue A | Document ID 87/03631-1/FCK11507
Issued by
OEGPU Viktor Hallman, Erik Sanford
Classification Company Confidentially
COMPANY UNCLASSIFIED
Classification Export Control
NOT EXPORT CONTROLLED
Classification Defence Secrecy
ÖPPEN/UNCLASSIFIED

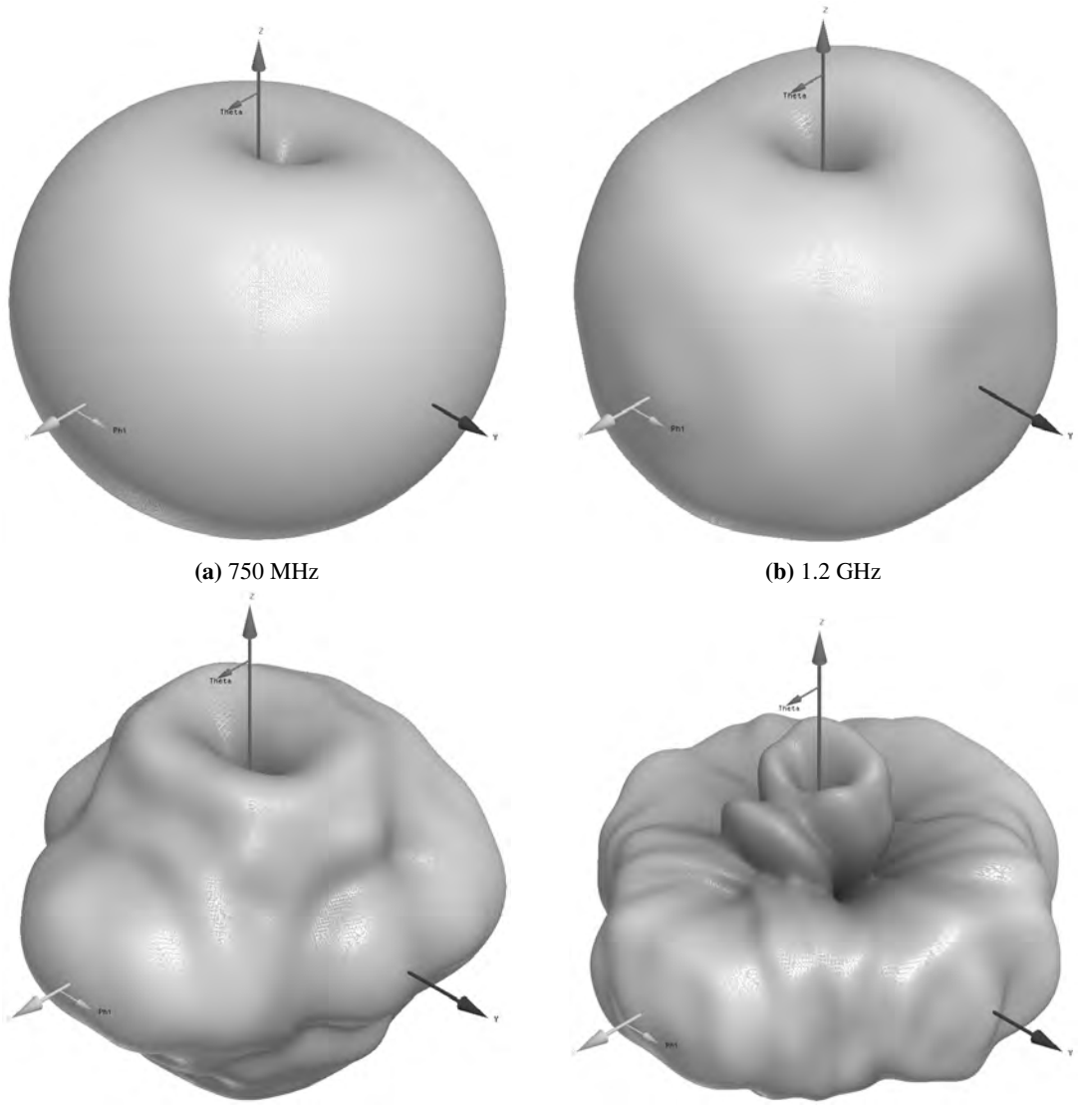

(a) 750 MHz

(b) 1.2 GHz

(c) 1.9 GHz

(d) 3 GHz

Figure 4.14: The simulated 3D radiation pattern of the directivity in linear scale for the whole antenna-amplifier system. The amplifier is present along the x axis, which is pointing to the left in the images.

Date 2013-06-18 | Issue A | Document ID 87/03631-1/FCK11507
Issued by
OEGPU Viktor Hallman, Erik Sanford
Classification Company Confidentially
COMPANY UNCLASSIFIED
Classification Export Control
NOT EXPORT CONTROLLED
Classification Defence Secrecy
ÖPPEN/UNCLASSIFIED

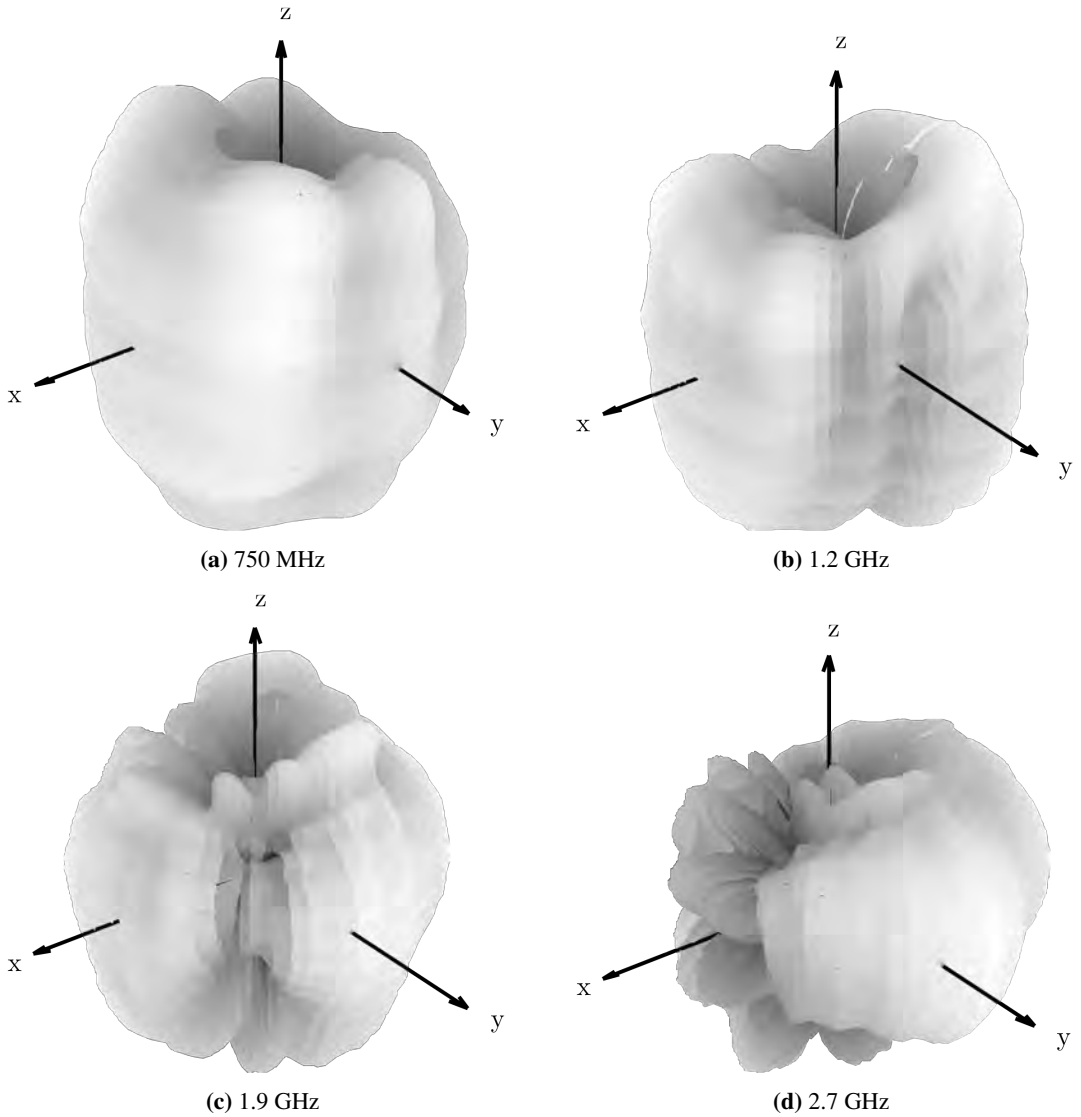

(a) 750 MHz **(b)** 1.2 GHz **(c)** 1.9 GHz **(d)** 2.7 GHz

Figure 4.15: The measured 3D radiation pattern of the directivity in logarithmic scale for the whole antenna-amplifier system. The balun and aluminium block is present along the x axis

5 Conclusions and Analysis

The main outcome of this project has been that the difficulties with co-designing an antenna-amplifier system has emerged to the surface. This has provided useful lessons about how to not conduct a co-design, but it has also given hints about how to proceed with future development within the subject. In this final section, the project conclusions will be stated along with some comments about possible approaches for future work.

5.1 Conclusions

First of all it should be said that the effort to separately model each part of an antenna-amplifier system is not very high. Concerning the antenna part, the only thing to do is roughly to simulate the antenna, aiming at as constant impedance as possible and deliver the result to the amplifier designer. The extra effort needed to then match a frequency dependent load instead of the comfortable 50 Ω at the amplifier output is of course not negligible, but with the computer aid of today it is certainly manageable.

The most difficult part with this project has by far been to measure. The in-process measurements has not been a problem per se, but the problem to measure the complete system and its different parts has overshadowed all possible benefits of the co-design. Typically, the gain of the amplifier is measured by connecting a standard network analyser to the input and output. In our case there is not even an output port, since the antenna should be directly mounted onto the amplifier output. Even if the two parts were separated, the possibilities to measure them individually and get meaningful results were almost non-existent due to that the intersection was balanced and not 50 Ω. As described, both the antenna and amplifier were measured individually, but the data is merely a hint of what the whole system would perform, since the very idea with the project is for the antenna and amplifier to be integrated. A way to measure the total system gain would be to put the whole construction into an anechoic chamber and measure the radiated power. From the power data obtained, a total gain could be calculated. The problem with this is that once the antenna-amplifier unit is in the chamber and measured, it is cumbersome to reverse the process and for example alter individual components in the amplifier to increase gain.

Even if the problems with the measurements were in the main focus of attention, other issues were also run into. As previously mentioned, the amplifier heatsink was heavily heated. In order for the substrate and components to endure the excessive heat, an even more bulky heatsink would have been needed. This would inevitably affect the antenna parameters and even the radiation pattern would be compromised since a big enough heatsink would act as a reflector for all frequencies. A bigger heatsink would also be more complex to mechanically integrate, a process that was already non-trivial.

5.2 Sources of errors

To make the co-design meaningful, accurate models for the devices used is important and has been one of the greatest challenges during this project . Inaccurate antenna parameters will lead to a more or less dysfunctional output matching network since the transistor will see another impedance than expected. In the same way, an inaccurate model for the input balun will cause problems for the input matching.

One possible source of error for the antenna parameters is the surroundings of the antenna. All objects, especially metallic ones, will affect the impedance of the antenna. Although the amplifier heatsink and the shielding box was simulated, it was not made with perfect resemblance with reality. The approximate nature of the mechanical structure fixating the antenna-amplifier unit also made the metallic objects approach the antenna more than foreseen, which most certainly did not work in the advantage of the antenna characteristics. During assembly of the unit, the antenna was somewhat deformed in the bottom area. This caused a permanent change of shape of the cone, which probably also resulted in some parametric changes in the same way as a different cone angle would do.

When the measurement in the anechoic chamber was made, the antenna could not be exactly centered on the axis of rotation, which inevitably would lead to some shift and misalignment in the radiation pattern of the antenna. Also the the fact that the fixation of the antenna was not completely rigid, in combination with fast movements of the measurement device due to low sample rate, probably introduced some unwanted artifacts in the radiation patterns.

For the balun a possible source of error was the transition between the microstrip and the coaxial cables used for the phase shifter. The resulting performance of the balun was shown to be highly dependent on the way that transition was made and small changes in the way the cables were mounted could affect the resulting parameters of the balun.

5.3 Future work

By having another approach to the project, most of the problems mentioned above could have been eliminated. A necessary improvement is to try to come up with a solution where the amplifier and antenna can be separated a greater distance by for example two cables. The cables could be connected to each of the two output branches of the amplifier and feed the antenna in a balanced way. In that way the interaction of the antenna caused by the amplifier would be minimised. The co-design part would more be about determining what characteristic impedance the cables should have, which is preferably as close to the antenna impedance as possible. An additional investigation that could be made is to find antennas and transistors that more or less match each other when it comes to desired load impedance of the transistor and input impedance of the antenna. By doing this it would be easier to find a suitable characteristic impedance of the connecting cable.

Date 2013-06-18 | Issue A | Document ID 87/03631-1/FCK11507
Issued by
OEGPU Viktor Hallman, Erik Sanford
Classification Company Confidentially
COMPANY UNCLASSIFIED
Classification Export Control
NOT EXPORT CONTROLLED
Classification Defence Secrecy
ÖPPEN/UNCLASSIFIED

References

[1] Balanis CA. Modern Antenna Handbook (v. 1). Wiley-Interscience; 2008.

[2] Beccari C. Typesetting mathematics for science and technology according to ISO 31/XI. TUGboat. 1997;18(1):39–48.

[3] Pozar DM. Microwave Engineering. Wiley; 2011.

[4] Balanis CA. Antenna Theory: Analysis and Design, 3rd Edition. Wiley-Interscience; 2005.

[5] IEEE Standard Definitions of Terms for Antennas. IEEE Std 145-1983. 1983;p. 1–31.

[6] IEEE Standard Definitions of Terms for Antennas. IEEE Std 145-1993. 2013;p. 1–32.

[7] Volakis J, Chen CC, Fujimoto K. Small Antennas:Miniaturization Techniques & Applications. McGraw-Hill Professional; 2010.

[8] Russer P. Electromagnetics, Microwave Circuit, And Antenna Design for Communications Engineering, Second Edition (Artech House Antennas and Propagation Library). Artech House; 2006.

[9] Mayes PE. Frequency-independent antennas and broad-band derivatives thereof. Proceedings of the IEEE. 1992;80(1):103–112.

[10] Kraus JD, Marhefka RJ. Antennas For All Applications. McGraw-Hill Science/Engineering/Math; 2001.

[11] Kai Z, Wanli L, Xiwei C. Study on the Biconical Antenna in the EMC Test Suitable for Engineering Machinery. In: Computer Science and Information Engineering, 2009 WRI World Congress on. vol. 1; 2009. p. 81–84.

[12] Kraus JD. Antennas. McGraw-Hill Companies; 1988.

[13] Raines BD, Obeidat KA, Rojas RG. Characteristic mode-based design and analysis of an electrically small planar spiral antenna with omnidirectional pattern. In: Antennas and Propagation Society International Symposium, 2008. AP-S 2008. IEEE; 2008. p. 1–4.

[14] R&S HK116 Biconical Antenna [Bicone datasheet]. Rohde & Schwarz; 2012. Available from: `http://cdn.rohde-schwarz.com/dl_downloads/dl_common_library/dl_brochures_and_datasheets/pdf_1/HK116_catalog_2013_84_84.pdf`.

[15] Schelkunoff SA. Electromagnetic waves,. D. Van Nostrand Company, inc; 1943.

[16] Brown GH, Woodward J O M. Experimentally Determined Impedance Characteristics of Cylindrical Antennas. Proceedings of the IRE. 1945;33(4):257–262.

[17] C E Smith CMB, Umashankar KR. Characteristics of Wire Biconical Antenna. Microwave Journal. 1979;p. 37–40.

[18] Warnagiris TJ. A Monopole with a Twist. Microwave Journal. 2001;44(9):120–137.

[19] Warnagiris TJ. A Monopole with a Twist Revisited. Microwave Journal. July 2005;p. 54–74.

[20] Warnagiris TJ, inventor; Southwest Research Institute, assignee. Wide bandwidth multi-mode antenna. ; 2002 Jan 7.

[21] Arnold O, Richter F, Fettweis G, Blume O. Power consumption modeling of different base station types in heterogeneous cellular networks. In: Future Network and Mobile Summit, 2010; 2010. p. 1–8.

[22] Gonzalez G. Microwave transistor amplifiers : analysis and design. Englewood Cliffs, N.J: Prentice-Hall; 1984.

[23] Kazimierczuk MK. RF Power Amplifiers. Wiley; 2008.

[24] Gentzler CG, Leong SK. Broadband VHF/UHF amplifier design using coaxial transformers. High Freq Design. 2003;2(3):42–51.

[25] J S Sun TLL. Design of a planar microstrip balun at S-band. Microwave Journal. 2001;44(8):132–136.

[26] Lim JS, Park UH, Oh S, Koo JJ, Jeong YC, Ahn D. A 800- to 3200-MHz Wideband CPW Balun Using Multistage Wilkinson Structure. In: Microwave Symposium Digest, 2006. IEEE MTT-S International; 2006. p. 1141–1144.

[27] Chang CY, Yang CC. A novel broad-band Chebyshev-response rat-race ring coupler. Microwave Theory and Techniques, IEEE Transactions on. 1999;47(4):455–462.

[28] Krishnamurthy K, Vetury R, Keller S, Mishra U, Rodwell MJW, Long SI. Broadband GaAs MESFET and GaN HEMT resistive feedback power amplifiers. Solid-State Circuits, IEEE Journal of. 2000;35(9):1285–1292.

[29] Brooks D. When Traces Melt Without a Trace. UltraCAD Design, Inc. 1998;.

[30] Brooks D. Temperature Rise in PCB Traces. Proceedings of the PCB Design Conference. 1998;.

[31] HFSS Online Help; 2011. Available from: `http://www.scribd.com/doc/82687895/Ansoft-HFSS-Online-Help`.

Date 2013-06-18 | Issue A | Document ID 87/03631-1/FCK11507
Issued by
OEGPU Viktor Hallman, Erik Sanford
Classification Company Confidentially
COMPANY UNCLASSIFIED
Classification Export Control
NOT EXPORT CONTROLLED
Classification Defence Secrecy
ÖPPEN/UNCLASSIFIED

A Guidelines for simulation in HFSS

The antenna simulations in this project have been carried out using *Ansys HFSS*. This appendix will cover some of the guidelines followed while simulating. The guidelines are written out of experience gained during the simulations as well as the different topics covered in the *HFSS Online Help* [31].

A.1 Modelling

When setting up a model in *HFSS* there is always the dilemma of accuracy versus computational time. In some cases, simplification of the reality can spare both size of the problem and modelling hours, but in some cases simplifications will do more harm than good. In this project for instance, the aim of the simulations was often to obtain an input impedance. If this is the case, a well modeled feeding of the structure is of high priority. As can be seen in Figure A.1, the modelling of an SMA connector in the system meant the difference between mediocre and good results.

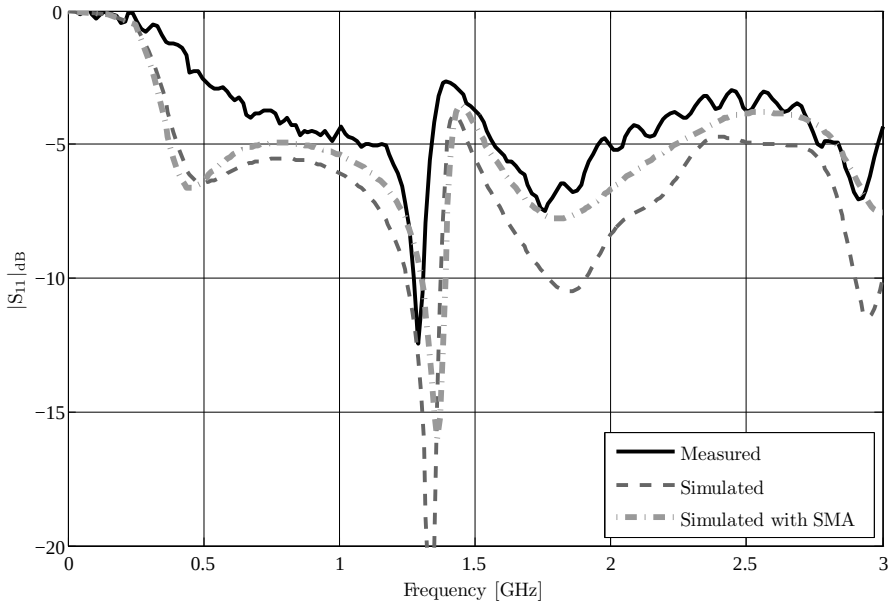

Figure A.1: $|S_{11}|$ function of frequency in the case of an SMA connector present in the simulation or not, compared with measured data.

Another subject that can cause hours of frustration is the case of intersecting parts. Sometimes *HFSS* has got no problem at all with the presence of intersecting parts, but at other times it will result in that none of the intersecting parts are created or that the execution of the simulation is aborted. One thing that usually solves this problem is to utilise the tools *Unite* and *Subtract*, available in the modelling environment, in order to make parts either stick together or to be apart.

Date 2013-06-18 | Issue A | Document ID 87/03631-1/FCK11507
Issued by
OEGPU Viktor Hallman, Erik Sanford
Classification Company Confidentially
COMPANY UNCLASSIFIED
Classification Export Control
NOT EXPORT CONTROLLED
Classification Defence Secrecy
ÖPPEN/UNCLASSIFIED

A.2 Boundaries

There are two types of boundaries that are of major importance when doing antenna simulations in *HFSS*. These are the *Radiation* boundary and the *Perfect E* boundary.

A.2.1 Radiation boundary

When an antenna simulation is to be made, the desire of putting the model into a free space environment will become significant at some point. The easiest way to realise this is by assigning the *Radiation* condition to the surface of the solution volume. A recommendation is to not put the radiation surface closer than $\lambda/4$ to the antenna at the lowest frequency of interest, which in practice means that a solution volume with a smaller extension than $\lambda/2$, in addition the largest antenna dimension, is not preferable. The radiation surface is supposed to prevent any reflections, and thereby act as free space, but this is not always achieved. Another way to go around the free space problem is the so called *Perfectly Matched Layer* (PML). The PML can be thought of as electromagnetic absorbers that are placed on the sides of the solution volume to prevent reflection. On one hand, the problem to solve becomes bigger, but the reflections decreases which results in a more accurate calculations. Another drawback with the PML is that it has got be assigned to a rectangular surface, whereas the radiation condition can be assigned to any surface.

A.2.2 Perfect E boundary

The *Perfect E* boundary indicates that a certain surface is perfectly conducting. Therefore, the Perfect E can be used when assigning the properties of for instance a strip line or a thin antenna. This boundary condition can also be used when the simulated model is symmetric and the electric polarisation is anti-symmetric with respect to a certain plane. By assigning Perfect E to the plane of symmetry, the problem size and computational time is essentially half of the original ones. The 3D counterpart to the Perfect E surface is a *Perfect Electric Conductor* (PEC).

A.3 Excitations

In order to do a simulation there has got to be an excitation of electromagnetic field somewhere in the model. There are different types of excitations available in *HFSS*. The ones used in this project will here be briefly explained.

A.3.1 Modal and Terminal solution type

There are two solution type in *HFSS* to chose from. In the *Modal* solution the results are calculated in terms of powers, whereas in the *Terminal* solution the calculations are made in terms of current

and voltages. In this project the modal solution type has been used most of the time. However, when including multi-conductor structures the terminal solution is preferable, since this allows the extraction of differential and common mode impedances.

A.3.2 Wave port and Lumped port

When a solution type is chosen, the next thing to do is to assign one or several ports. The most frequently used ports in this project has been the *Wave port* and the *Lumped port*. The two ports resembles each other but there are some differences. The lumped port is to be placed at a location where the field distribution would be as it is defined at the port, whereas the wave port excites a wave that is let to propagate and stabilise after a certain distance from the port. The wave port should also be placed outside the solution volume as some kind of window to the outer world, but the lumped can be place inside the solution volume. There is however a way to circumvent the restriction of external wave ports. This is done by capping the wave port surface with a PEC object.

A.3.3 Differential pairs

If multiple excitations are present in the model it can sometimes be of interest to find out the differential and common mode impedances and S parameters. To do this one can define *Differential pairs*. *HFSS* will then excite signals that are completely in phase and signals that are completely out of phase separately. If visualising of the present fields in the solution is desired, it is important to note that by default only one source will be excited in *Field overlays*. By editing the sources any kind of excitation can be realised. The change in source excitation will also affect other instances, such as the radiation pattern.

A.3.4 Deembedding

If the impedance and S-parameters of interest is not where the port is placed but rather a distance l away from the port, there is a function in *HFSS* called *Deembed* that can be helpful. The way deembed works is that it takes the S-matrix at the port and then add a desired propagating length according to

$$[\mathrm{S}^{\mathrm{desired}}] = [\mathrm{e}^{\gamma l}][\mathrm{S}^{\mathrm{port}}][\mathrm{e}^{\gamma l}] \tag{A.1}$$

where $[\mathrm{S}^{\mathrm{desired}}]$ is the S-matrix at the desired position, $[\mathrm{S}^{\mathrm{port}}]$ the S-matrix at the port and $[\mathrm{e}^{\gamma l}]$ is a diagonal matrix on the form of

$$\begin{bmatrix} \mathrm{e}^{\gamma_1 l_1} & 0 \\ 0 & \mathrm{e}^{\gamma_2 l_2} \end{bmatrix}, \tag{A.2}$$

if a 2-port is of interest. In the matrix, γ_i is the complex propagation constant of the uniform transmission line between the port i and its desired position, which has got a length of l_i.

Date 2013-06-18 | Issue A | Document ID 87/03631-1/FCK11507
Issued by
OEGPU Viktor Hallman, Erik Sanford
Classification Company Confidentially
COMPANY UNCLASSIFIED
Classification Export Control
NOT EXPORT CONTROLLED
Classification Defence Secrecy
ÖPPEN/UNCLASSIFIED

A.4 Analysis

When setting up a solution for analysis there are a quite some alternatives. If it for instance only is the radiation pattern at one frequency that is of interest, a simple *Solution setup* at the specific frequency along with an infinite sphere is sufficient enough. Often a sweep over a frequency range is essential, which calls for a *Frequency sweep* setup. In the frequency sweep dialog there are three different solution types to chose from. The *Fast sweep* is suited for models with resonances that are behaving in an abrupt way or fast change of the characteristics in the frequency band. The Fast sweep gives an accurate description of the model near the resonance frequency. The *Discrete sweep* will generate an accurate solution at specific frequency point. This sweep type is best used as a verifier of the simulated data at certain frequencies. The default sweep in *HFSS* is *Interpolating sweep* and will give an interpolated simulation result for a specified frequency range. The Interpolating sweep is best suited for wide frequency ranges and when the frequency response is smooth. One option that is available for the Interpolating sweep is *Enforce passivity*. This option enables the user to specify the degree of passivity in the system for the interpolated data points.

A.5 *HFSS* scripting

A feature of *HFSS* that can really come in handy when doing repetitive tasks is the *HFSS scripting*. A script can either be recorded or ran from the command window of *HFSS*, which makes it easy to repeat a cumbersome command as many times as necessary without too much work. When a script is recorded it is saved as a Visual Basic script file, which can be reviewed in any text editor. By analysing the text written in the file it is easy to reproduce the script using for instance *MATLAB*. During the course of this project, *MATLAB* has been used to create a single script containing the creation of the model simulated, the material used, the boundaries set and so on. When using *MATLAB*, or any other software of choice, it is easy to generate a script that takes care of the whole solution of interest. It is then easy to modify the script by altering predefined variables in the software code.

B Guidelines for simulation in AWR

Amplifier simulations in this thesis has been performed using *AWR Microwave Office*. The purpose of this section is to share some experiences acquired during the design process.

B.1 Reliability

Having a simulation which produces result of high reliability is always desirable. It is also desirable with a low time consumption. Some different methods that will improve the reliability will be discussed in this section.

B.1.1 Simulation method

Layout simulations can be performed in two different ways. One way is to represent each piece of conductor as a closed form component where no coupling between conductors are taken into account. Another way is to draw the layout and define ports and perform an electromagnetic field (EM-field) simulation. An EM-field simulation calculates parameters for a component by calculating the corresponding electromagnetic fields. All possible couplings are therefore taken into account which is a great benefit of using the EM-field simulation. On the other hand the time consumption will be much higher compared to closed form simulation.

A possible method is to combine both EM and closed form simulation in the same layout, shown in Figure B.1. Objects that should be simulated using EM-simulation are components that in some way, intentionally or unintentionally, are influenced by coupling. The time consumption is highly dependent on the area and by using this technique the time consumption will be reduced. In case the layout in one block is changed only that block needs to be re-calculated which is another benefit of dividing the EM-simulation into blocks.

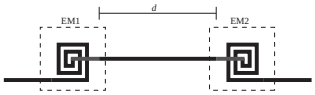

Figure B.1: A constructed layout with the purpose to illustrate the benefit of combining both EM- and closed form simulation. The length l of the conductor joining the two inductors can be changed without recalculating the EM-solution of the two inductors which improves the time consumption.

Each block will assume an empty surrounding when solving the EM-solution which requires space between each block in order to perform reliability simulations.

Date 2013-06-18 | Issue A | Document ID 87/03631-1/FCK11507
Issued by
OEGPU Viktor Hallman, Erik Sanford
Classification Company Confidentially
COMPANY UNCLASSIFIED
Classification Export Control
NOT EXPORT CONTROLLED
Classification Defence Secrecy
ÖPPEN/UNCLASSIFIED

B.1.2 Layout simulation techniques

Both input and output matching networks for the amplifier has been constructed using stubs. For closed form simulation stubs can be constructed in at least two different ways. To evaluate which method that gives the most accurate result the simulations has been compared to an EM-simulation performed in Axiem which is one of the EM-simulations included in *AWR*. In this chapter the EM-simulation will be treated as the correct result and the two different closed form result will be compared to the EM-simulation.

The two different methods of closed form simulation that has been investigated are illustrated in Figure B.2. In the first method the stubs are realised by changing the width of the conductor. Method number two is realised by connecting stubs to a cross section element.

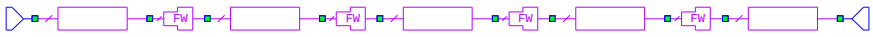

(a) Method 1 where stubs are realised using striplines of different width.

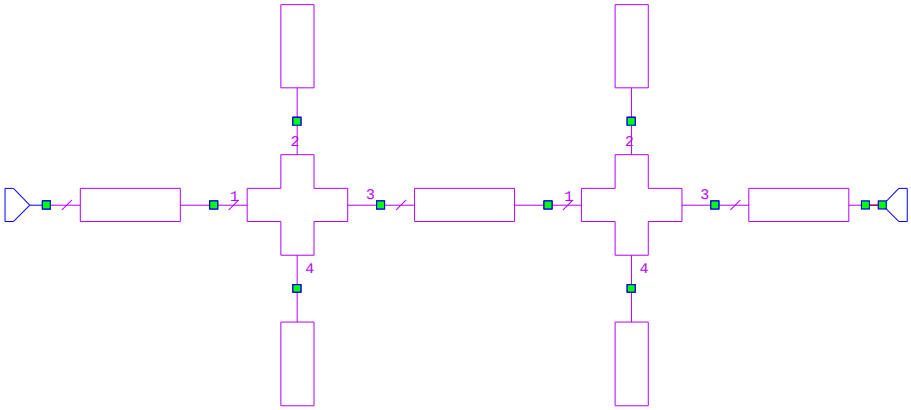

(b) Method 2 where stubs are realised using open stubs connected using a cross section.

Figure B.2: Two different ways to realise a section of two double stubs.

To investigate the differences in accuracy the following layout, see Figure B.3, has been drawn and simulated using the two methods. In order to compare the methods the return loss S_{11} has been simulated and the result is shown in Figure B.4. Result extracted using method 2 with the cross section elements is showing best agreement to EM-simulation. Method 1 is less accurate especially for high frequency.

The next layout that has been investigated is shown in Figure B.5. Same type of simulation has been applied to this layout and the result is shown in Figure B.6

These results shows the importance of knowing when to use different types of methods to construct a layout. In general method 1, where the width of the conductor is changed, should only be used

Date 2013-06-18 | Issue A | Document ID 87/03631-1/FCK11507
Issued by
OEGPU Viktor Hallman, Erik Sanford
Classification Company Confidentially
COMPANY UNCLASSIFIED
Classification Export Control
NOT EXPORT CONTROLLED
Classification Defence Secrecy
ÖPPEN/UNCLASSIFIED

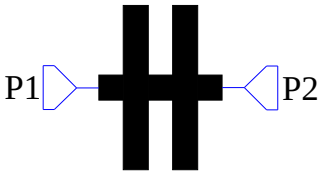

Figure B.3: First layout that has been used to test methods 1 and 2.

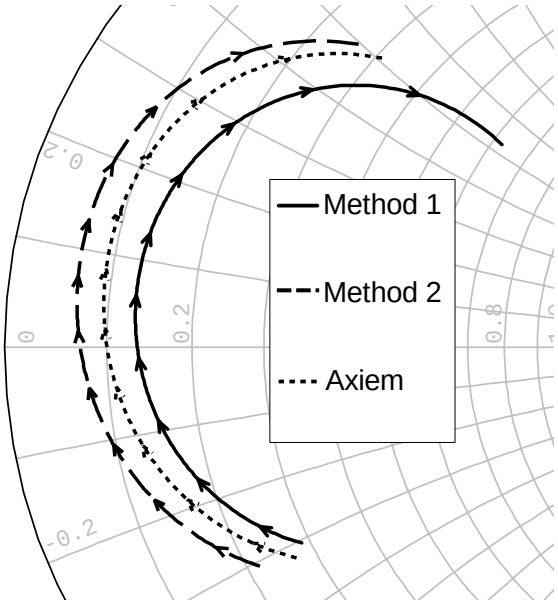

Figure B.4: Simulated result for S_{11} of layout shown in Figure B.3. Method 2 which is based on stub connected to a cross section is showing the best agreement for this layout. Simulation is done for frequencies from 750 MHz to 3 GHz.

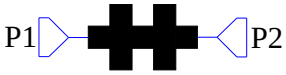

Figure B.5: Layout with short stubs.

for small step in width. *AWR* will display a warning if the ratio $W_2/W_1 > 10$ which should be considered.

For short stubs on the other hand the change in width showed a more accurate result than using the cross section element. In *AWR* no warning is displayed when using too short stub so an extra attention here is required.

Date 2013-06-18 | Issue A | Document ID 87/03631-1/FCK11507
Issued by
OEGPU Viktor Hallman, Erik Sanford
Classification Company Confidentially
COMPANY UNCLASSIFIED
Classification Export Control
NOT EXPORT CONTROLLED
Classification Defence Secrecy
ÖPPEN/UNCLASSIFIED

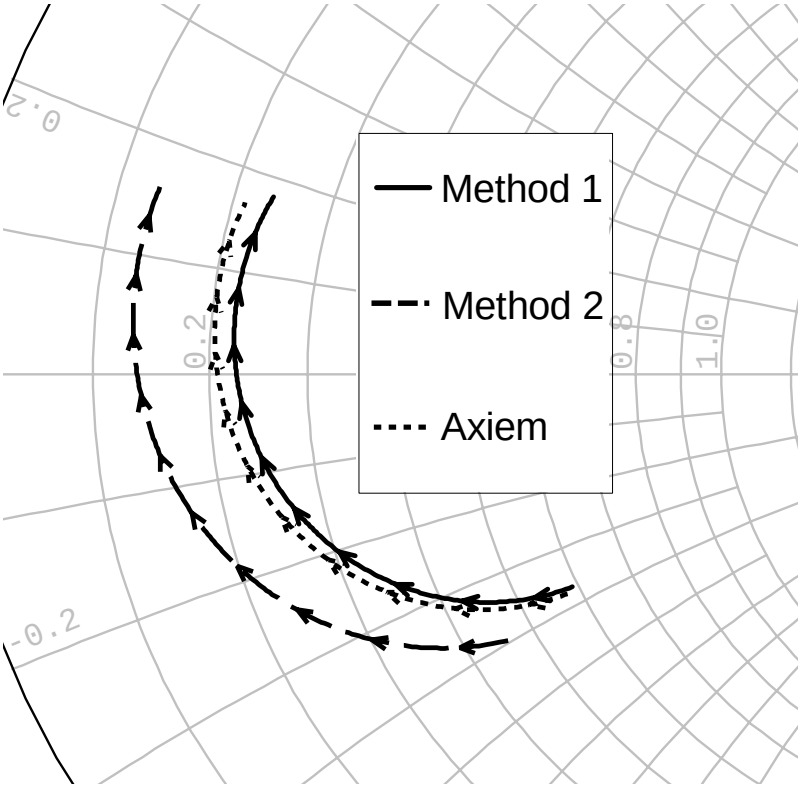

Figure B.6: Simulated result for S_{11} of layout shown in Figure B.5. Compared to the long stub method 1 is having the best agreement to EM-simulation. Simulation is done for frequencies from 750 MHz to 3 GHz.

Date 2013-06-18 | Issue A | Document ID 87/03631-1/FCK11507
Issued by
OEGPU Viktor Hallman, Erik Sanford
Classification Company Confidentially
COMPANY UNCLASSIFIED
Classification Export Control
NOT EXPORT CONTROLLED
Classification Defence Secrecy
ÖPPEN/UNCLASSIFIED

C In report not presented data

In this appendix, some of the data and information that could not fit in the main report will be presented.

C.1 Design of the biconical antenna

The choice of the cone angle α_{cone} to be $110°$ and the top cone angle α_{top} to be $140°$, is presented previously in the report. The factors of decision are stated to primarily be Λ, ς and $\overline{|\Gamma_{\text{A}}|}$. However, other parameters also showed it favourable to chose the stated angles. In Figure C.1, the standard deviation of $|\Gamma_{\text{A}}|$ is shown as a function of α_{cone}. From the graph it is clear that a cone angle around $100°$ is a suitable choice.

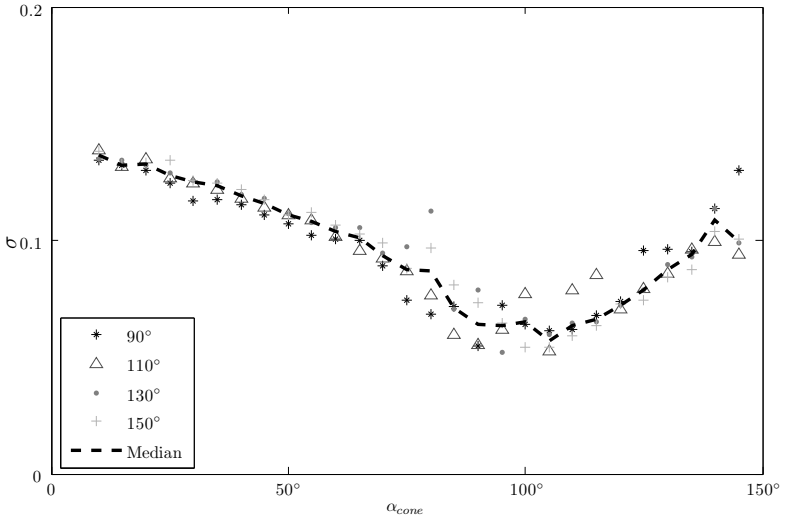

Figure C.1: The standard deviation σ of $|\Gamma_{\text{A}}|$ as a function of α_{cone}

All parameters to determine the goodness of a certain cone angle are inevitably dependent on the behaviour of the impedance. As can be seen in Figure C.2 and C.3, the standard deviation of the impedance decreases when α_{cone} increases.

To determine the top cone angle α_{top}, simulations were made keeping α_{cone} constant at $110°$. As a measure of goodness the spreading ς, as previously defined, was observed. As can be seen in Figure C.4, the spreading is kept on a relatively low level compare to when α_{cone} was swept. Though the data is quite noisy, it is observable that according to ς, α_{top} should be chosen to be between $130°$ and $150°$. In order to keep size down and not to be close to the edge of this interval, a top cone angle of $140°$ was chosen.

Date 2013-06-18 | Issue A | Document ID 87/03631-1/FCK11507
Issued by
OEGPU Viktor Hallman, Erik Sanford
Classification Company Confidentially
COMPANY UNCLASSIFIED
Classification Export Control
NOT EXPORT CONTROLLED
Classification Defence Secrecy
ÖPPEN/UNCLASSIFIED

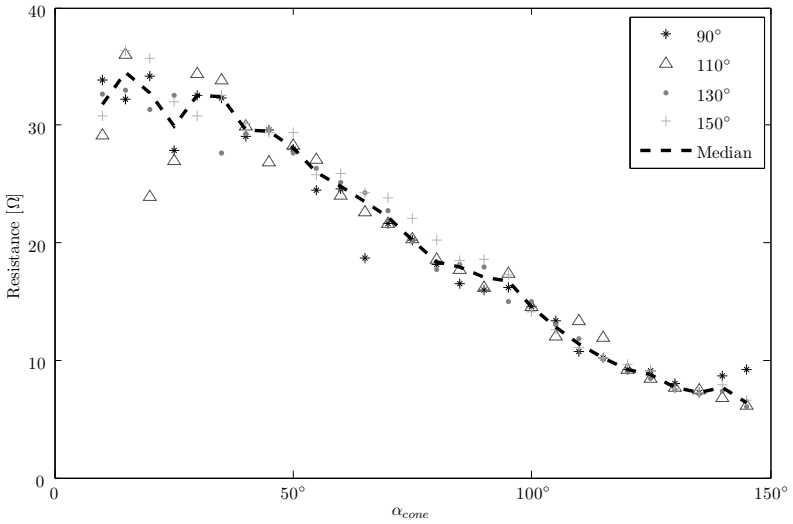

Figure C.2: The standard deviation of the antenna resistance as a function of α_{cone}

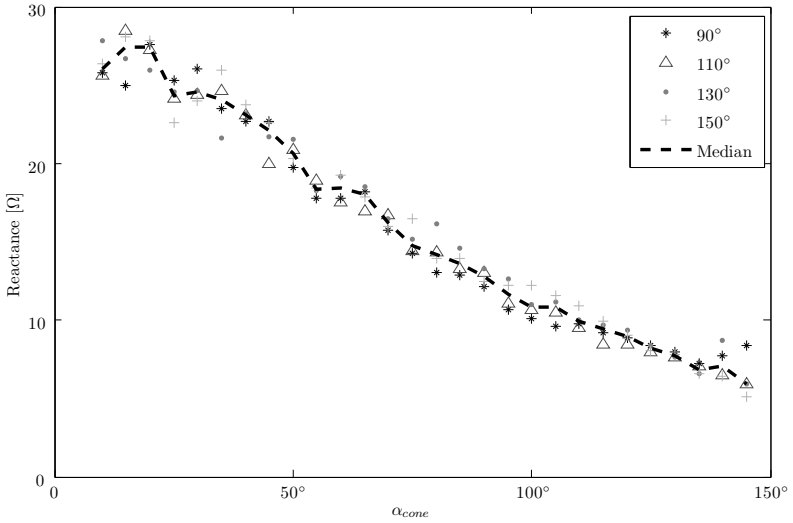

Figure C.3: The standard deviation of the antenna reactance as a function of α_{cone}

Date 2013-06-18 | Issue A | Document ID 87/03631-1/FCK11507
Issued by
OEGPU Viktor Hallman, Erik Sanford
Classification Company Confidentially
COMPANY UNCLASSIFIED
Classification Export Control
NOT EXPORT CONTROLLED
Classification Defence Secrecy
ÖPPEN/UNCLASSIFIED

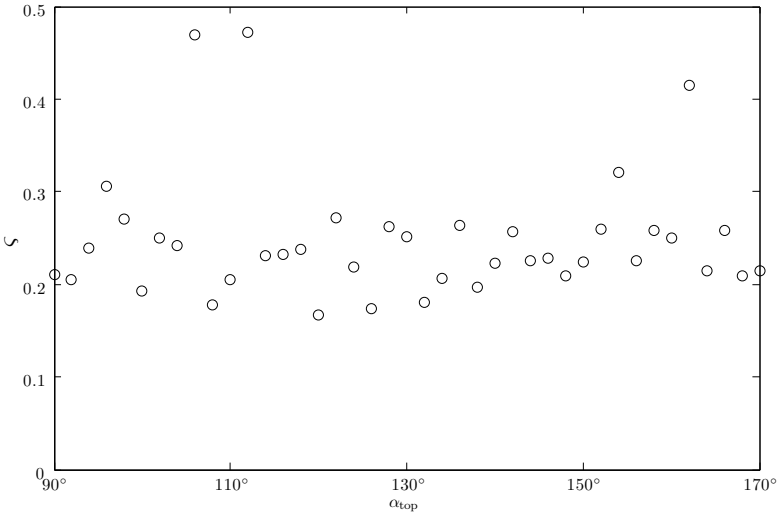

Figure C.4: The spreading ς, as previously defined, as a function of the top cone angle α_{top}

Date 2013-06-18 | Issue A | Document ID 87/03631-1/FCK11507
Issued by
OEGPU Viktor Hallman, Erik Sanford
Classification Company Confidentially
COMPANY UNCLASSIFIED
Classification Export Control
NOT EXPORT CONTROLLED
Classification Defence Secrecy
ÖPPEN/UNCLASSIFIED

C.2 Model and result for coax transformer

The complete model for the coaxial transformer is shown in Figure C.5. The parasitic components were derived by choosing the values in order to make the simulated return loss fit the measured return loss. The values of the parasitic capacitances are probably results of coupling between the coaxial cables and then highly dependent on the way the coaxial cables are mounted. Therefore the values could be verified before the model is used.

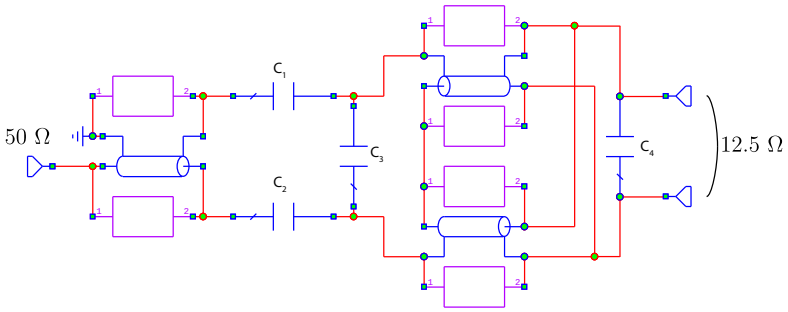

Figure C.5: Complete model for the coaxial transformer. The capacitances $C_{1...4}$ represents parasitic capacitances. C_1 and C_2 are 540 pF, C_3 is 1 pF and C_4 is 9 pF.

Date 2013-06-18 | Issue A | Document ID 87/03631-1/FCK11507
Issued by
OEGPU Viktor Hallman, Erik Sanford
Classification Company Confidentially
COMPANY UNCLASSIFIED
Classification Export Control
NOT EXPORT CONTROLLED
Classification Defence Secrecy
ÖPPEN/UNCLASSIFIED

C.3 DC calibration of the load

In order to measure the power dissipated in the load, a DC calibration was performed by applying a known power to the load and measure the resulting temperature, see Figure C.6. At first the temperature was shown not to be stable enough and the reason to that was probably because of air currents in the surrounding. That was solved by shielding the amplifier using a cardboard box. A fan was also mounted to the box in order to create a stationary flow of air through the box. Having a stationary flow around the amplifier made the temperature more stable since the fan made other air flows neglectable.

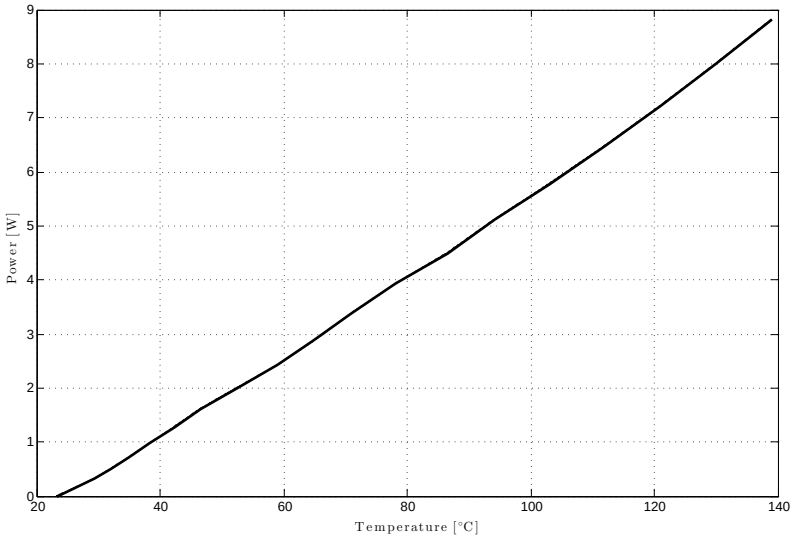

Figure C.6: Temperature related to power dissipated in the load. The relation was used to relate output power of the amplifier by measuring the temperature of the load.